

INVESTIGATION OF THE THERMAL GRADIENT HISTORY OF THE  
THRACE BASIN, NW TURKEY, BY USING A MODIFIED EASY%Ro  
MATURITY MODEL

A THESIS SUBMITTED TO  
THE GRADUATE SCHOOL OF NATURAL AND APPLIED SCIENCES  
OF  
MIDDLE EAST TECHNICAL UNIVERSITY

BY

ÖZKAN HUVAZ

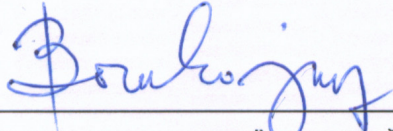
IN PARTIAL FULFILLMENT OF THE REQUIREMENTS  
FOR  
THE DEGREE OF DOCTOR OF PHILOSOPHY  
IN  
GEOLOGICAL ENGINEERING

JULY 2005

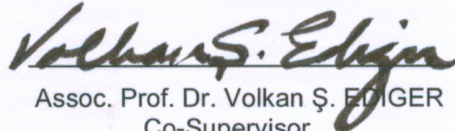
Approval of the Graduate School of Natural and Applied Sciences

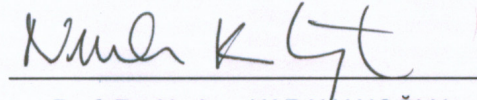
Prof. Dr. Canan ÖZGEN  
Director

I certify that this thesis satisfies all the requirements as a thesis for the degree of Doctor of Philosophy.

  
Prof. Dr. Asuman G. TÜRKMENOĞLU  
Head of Department

This is to certify that we have read this thesis and that in our opinion it is fully adequate, in scope and quality, as a thesis for the degree of Doctor of Philosophy.

  
Assoc. Prof. Dr. Volkan Ş. EDİGER  
Co-Supervisor

  
Prof. Dr. Nurkan KARAHANOĞLU  
Supervisor

**Examining Committee Members**

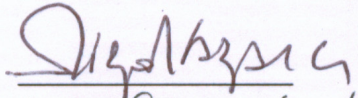
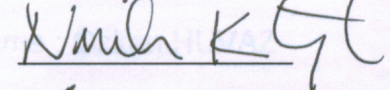
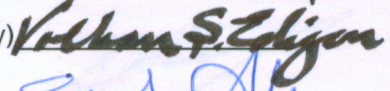
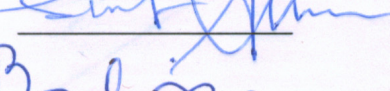
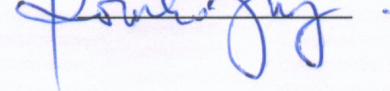
Prof. Dr. Nizamettin Kazancı (Ankara Univ., GEOE)

Prof. Dr. Nurkan Karahanoğlu (METU, GEOE)

Assoc. Prof. Dr. Volkan Ş. Ediger (Presidency of Rep. of Turkey)

Assoc. Prof. Dr. Serhat Akın (METU, PETE)

Assoc. Prof. Dr. Bora Rojay (METU, GEOE)

**I hereby declare that all information in this document has been obtained and presented in accordance with academic rules and ethical conduct. I also declare that, as required by these rules and conduct, I have fully cited and referenced all material and results that are not original to this work.**

Name, Last name : Özkan HUVAZ

Signature :

A handwritten signature in dark ink, appearing to read 'Özkan HUVAZ', written in a cursive style.

## ABSTRACT

### INVESTIGATION OF THE THERMAL GRADIENT HISTORY OF THE THRACE BASIN, NW TURKEY, BY USING A MODIFIED EASY%RO MATURITY MODEL

HUVAZ, Özkan

Ph.D., Department of Geological Engineering

Supervisor : Prof. Dr. Nurkan KARAHANOĞLU

Co-Supervisor: Assoc. Prof. Dr. Volkan Ş. EDİGER

July 2005, 106 pages

Thermal maturity modeling is widely used in basin modeling. Of the available models, Easy%Ro has gained acceptance. Thermal gradients (TG) at seventy wells in the Thrace Basin are calibrated against vitrinite reflectance (%Ro) using the “Modified Easy%Ro” model. Mean squared residual (MSR) is used for measuring mismatch between the modeled and observed %Ro. A 90% confidence interval is used to assess the uncertainty. Best paleo-TG are obtained from the MSR curves. Comparison of the paleo-TG with the actual ones showed that thermal regime of the Thrace Basin did not dramatically change during geologic history. A correlation between geological and thermal properties of the basin is established. Thermal regime of the Thrace basin is controlled by 1) basement edge affect; 2) crustal thickness variations and basement heat flow; 3) lateral thermal conductivity variations within the stratigraphic column; 4) transient heat flow affect; and 5) influence of the tectonic features. Basement edge effect is traced at the steep northern margin. Central part of the basin demonstrates lower TG. The Eocene Ceylan Formation with relatively lower thermal conductivity plays a thermal reducing role. Areas of high sediment influx are associated with low TG due to the transient effect of the immature sediments. Fault systems of the Thrace Basin do not possibly have influence on paleo-thermal gradients.

Keywords: Thrace Basin, thermal gradient, Easy%Ro, uncertainty

## ÖZ

### TRAKYA HAVZASI'NIN, KD TÜRKİYE, TERMAL GRADYAN TARİHÇESİNİN UYARLANMIŞ EASY%RO OLGUNLUK MODELİYLE ARAŞTIRILMASI

HUVAZ, Özkan

Doktora, Jeoloji Mühendisliği Bölümü

Tez Yöneticisi : Prof. Dr. Nurkan KARAHANOĞLU

Ortak Tez Yöneticisi: Doç. Dr. Volkan Ş. EDİGER

Temmuz 2005, 106 sayfa

Isıl olgunluk modelleri havza modellemesinde sıkça kullanılmaktadır. Var olan modellerden Easy%Ro kabul görmüştür. Trakya Havzası'ndaki yetmiş kuyuya ait ısı gradyanlar (IG) "Uyarlanmış Easy%Ro" modelinin kullanılmasıyla vitrinit refleksiyon (%Ro) ile kalibre edilmiştir. Artan en küçük kareler (MSR), modellenen ve ölçülen %Ro değerleri arasındaki farkı ölçmek için kullanılmıştır. Belirsizliği değerlendirilmek için %90 güvenlik aralığı kullanılmıştır. En iyi paleo-TG MSR eğrilerinden elde edilmiştir. Paleo-TG ile günümüzdeki değerlerin karşılaştırılması sonucu Trakya Baseni'nin ısı rejiminde jeolojik tarihçe boyunca kayda değer bir değişim olmadığı sonucuna varılmıştır. Basenin jeolojisi ile ısı özellikleri arasında ilişki kurulmuştur. Trakya Baseni'nin ısı rejimi; 1) temel kenar etkisi; 2) kabuk kalınlığı değişimi ve temel ısı akısı; 3) yanal ısı iletkenlik değişimi; 4) süreksiz ısı akısı etkisi; ve 5) tektonik özelliklerin etkisi tarafından kontrol edilmektedir. Temel kenar etkisi havzanın kuzey kenarında izlenmektedir. Havza ortasında, düşük IG gözlenmektedir. Görelî olarak düşük ısı iletkenliğe sahip Eosen Ceylan Formasyonu ısı azaltma etkisi yaratmaktadır. Yüksek çökelme hızına sahip alanlar ısı olgunluğa ulaşmamış çösellerin yarattığı süreksiz ısı akısı etkisi nedeniyle düşük ısı gradyanına sahiptir. Basenin fay sistemlerinin paleo-ısı gradyanlara etkisi muhtemelen yoktur.

Anahtar kelimeler: Trakya Havzası, ısı gradyan, Easy%Ro, belirsizlik

## ACKNOWLEDGEMENTS

The author wishes to express his deepest gratitude to Turkiye Petrolleir A.O. (TPAO) for giving permission to use well and seismic data, Prof. Dr. Nurkan Karahanođlu, Assoc. Prof. Dr. Volkan Ő. Ediger, Assoc. Prof. Dr. Bora Rojay, Assoc. Prof. Dr. Serhat Akın for their guidance, advice, criticism, encouragements and insight throughout the research, Prof. Dr. Nizamettin Kazancı for participating to the PhD exemining commitee, Mehmet Sünnetçiođlu and A. Kadir Yılmaz for their help in interpretation of the seismic section, Prof. Dr. N.V. Lopatin for his further consultancy in development of the methodology, Taner IŐık, YaŐar Akçay and Levent Kırpe for testing the constructed models.

The author would also like to thank Dr. Jerry Sweeney, Dr. James Ilifee and Hasan Sarikaya for their editorial comments on the manuscript of the thesis.

Very special thanks to Muzaffer Siyako for interpretation of the thermal gradient data and his further consultansy in any issue associated to the geological and tectonic setting of the Thrace Basin.

The encouragement, motivation and patience provided by Elif Batur Huvaz is gratefully acknowledged.

## TABLE OF CONTENTS

PLAGIARISM.....	iii
ABSTRACT.....	iv
ÖZ.....	v
ACKNOWLEDGEMENTS.....	vi
TABLE OF CONTENTS	vii
LIST OF TABLES.....	ix
LIST OF FIGURES.....	x
CHAPTER	
I. INTRODUCTION.....	1
<b>1.1. Previous Studies</b> .....	4
<b>1.2. Technical Background</b> .....	8
1.2.1. Vitrinite Reflectance.....	8
1.2.2. Source of the Heat Flux in the Earth.....	10
1.2.3. Thermal History Modeling.....	12
1.2.3.1. Maturity Models .....	14
1.2.4. A First Order Kinetic Model.....	15
1.2.4.1. Easy%Ro.....	15
<b>1.3. Methodology</b> .....	18
II. GEOLOGY OF THE THRACE BASIN.....	29
<b>2.1. Regional Geology and Burial History</b> .....	29
<b>2.2. Stratigraphy</b> .....	31
<b>2.3. Tectonics</b> .....	35
III. THERMAL GRADIENT HISTORY OF THRACE BASIN.....	38
<b>3.1. Determination of the Thermal Gradient from MSR Curves</b> .....	38
<b>3.2. Statistical Assessment of Sensitivity, Resolution and Uncertainty on Thermal Gradients and MSR Curves</b> .....	43

<b>3.3. Geological Interpretation of the Thermal Gradients in Thrace Basin</b> .....	44
3.3.1. Basement Edge Affect.....	46
3.3.2. Crustal Thickness Variations and Basement Heat Flow.....	49
3.3.3. Lateral Thermal Conductivity Variations.....	51
3.3.4. Transient Heat Flow Affect.....	52
3.3.5. Influence of the Tectonic Features.....	54
IV. DISCUSSION AND CONCLUSIONS.....	56
<b>4.1. Discussion</b> .....	56
<b>4.2. Conclusions</b> .....	57
REFERENCES.....	59
APPENDICES	
A. GENERAL FLOW CHART OF THE MODIFIED EASY%RO CODE.....	70
B. LIST OF THE 70 STUDIED WELLS.....	77
C. MSR DATA AND GRAPHS.....	79
D. PREDICTED AND CALCULATED MSR VALUES.....	103
E.THERMAL CONDUCTIVITY MEASUREMENT WITH QTM-D3.....	105
CIRRICULUM VITAE.....	106



## LIST OF TABLES

### TABLES

Table 1	Average surface heat flow, reduced heat flow and characteristic depths for several continental heat flow provinces <sup>A</sup> (Sass, et al., 1981). <sup>A</sup> Data from Rao and Jessop (1975); Rao et al. (1976); Sass and Lachenbruch (1979); <sup>B</sup> Depth assumed for calculation of reduced heat flow.....	12
Table 2	Calculation of MSR values for different thermal gradients ranging from 5 to 50 for the Ballı-1 well (Ro <sub>m</sub> : measured %Ro values from the core samples gathered from the Ballı-1 well; Tg: thermal gradient).....	26
Table 3	Thermal conductivity of various lithologies and rocks (Brigaud and Vasseur, 1989) (TC: thermal conductivity).....	51
Table 4	Arithmetic average of various thermal conductivity measurements performed on cores (Appendix E) taken from different wells and formations in the Thrace Basin (Engin, 1999).....	52
Table B.1.....		77
Table D.1.....		103

## LIST OF FIGURES

### FIGURES

Figure 1	Activation energy distributions for the vitrinite maturation model of Burnham and Sweeney (1989). The overall range of 38 to 74 kcal/mole of the activation energies provides the foundation for the distribution of activation energies of the Easy%Ro model. The pre-exponential factor (A) is $10^{13}$ /sec.....	16
Figure 2	Flow diagram presenting the methodology of the study (Modified from Huvaz et al., 2005).....	21
Figure 3	90% confidence interval constructed on the determined mean (mean squared residual) for a synthetic data set....	23
Figure 4	Application of the confidence interval approach on a synthetic data set (C/: confidence interval).....	24
Figure 5	Exponential model for perfect data set and the MSR curves representing the 0.00035 and 0.0005 values of the exponential function.....	25
Figure 6	Thermal gradient versus MSR and the misfit function for Ballı-1 well.....	27
Figure 7	Descriptive statistics and the calculated 90% confidence interval on the mean (C/: confidence interval; Sigma: standard deviation; N: number of samples).....	28
Figure 8	Geology map of the Thrace Basin (Modified from Huvaz et al., in press).....	30
Figure 9	Burial history diagram and the isotherms constructed by using transient heat flow model. Tectonic subsidence curve is shown with dash line.....	31
Figure 10	Generalized stratigraphy of the Thrace Basin showing the depositional environment and thickness of formations, petrophysical properties of the reservoirs, type and average total organic carbon (%TOC) of the source rocks, producing fields versus formations and summary of the tectonic history ( $\phi$ : porosity; K: permeability; HC: hydrocarbon). (Modified from Kasar et al., 1983; Siyako, 2005 and Huvaz et al., in press).....	32

Figure 11	Average paleo-thermal gradients of the Thrace Basin which are obtained from the MSR curves.....	39
Figure 12	Measured BHT from Kaynarca-1 (a) and Ergene-1 (b) wells and the predicted temperature trend versus depth...	41
Figure 13	Average paleo-thermal gradients created using the bestfit values which are obtained from the MSR curves. Thermal gradients are ranked using the value windows...	45
Figure 14	Concentration of heat to the edge of the graben margin due to the heat that is preferred to be retrained in the highly conductive basement rock rather than being transferred into the relatively low conductive sediments (Q: Heat flow) (Modified from Yu et. al, 1995).....	46
Figure 15	Uninterpreted and interpreted seismic sections from the northern Thrace Basin. Sedimentary pile truncates and pinches out through north where the basement edge is bound by the Strandja Mountains. Heat flow paths are shown by white dash lines and arrows and the abnormally heated areas are painted to transparent dark gray. Heat flow paths, simulating heat transfer directions within the basement, are controlled by the geometry of the basement-sediment contact geometry. Heat prefers to be retrained in the basement which has higher thermal conductivity than the sediments. Location of the seismic section and the wells (K-1 and K-2) are shown on Figure 8.....	47
Figure 16	Total sediment thickness map of the Thrace Basin and basin margins overlain by thermal gradient windows.....	48
Figure 17	Crustal thickness model created using gravity and magnetic data. Basement heat flow parameters for calculation of heat generated by radiogenic minerals within the upper crust are demonstrated in tables (Personal communication: Yüksel, 2005).....	50
Figure 18	Regional seismic section from SE to NW showing thickness variation of the Ceylan Formation from the depocentre through the margin of the basin. Location of the seismic section is shown on Figure 8 (from Huvaz et al., in press).....	53
Figure 19	Miocene structures of the Thrace Basin (Modified from Perinçek, 1991).....	55

Figure A.1.....	70
Figure C.1.....	79

## CHAPTER I

### INTRODUCTION

The necessity of assessing maturity of a source rock and other features related to temperature, such as hydrocarbon generation and expulsion makes thermal gradient history a central theme in petroleum exploration studies (Thomsen, 1998). For evaluating the petroleum system of a basin, thermal gradient history must be well understood.

The objective of this study is to investigate thermal gradient history of the Thrace Basin, which is the second most important hydrocarbon province of Turkey. This is done by predicting average paleo-thermal gradients and evaluating variation of thermal gradients in association with the geological properties, such as thermal conductivity, sediment thickness, sedimentation rate and tectonic features using seventy wells from the Thrace Basin (Appendix B). Thus, the role of the geological features of the basin on the thermal gradient properties are evaluated and discussed. Validity of estimated thermal gradients is assessed by comparing them with the results of previous studies performed in the basin. Besides discussing the thermal properties of the Thrace Basin in association with the geological features, two newly discovered unconformity surfaces; one between Soğucak/Ceylan and Hamitabat Formations and the other within the Hamitabat Formation are demonstrated under the light of seismic and well data. Also, a modification in the chronostratigraphy of the basin is suggested (Siyako, 2005; Huvaz et al., in press).

Thermal gradient history comprises all of the paleo-temperature variations with depth in a basin. Since the present day thermal gradients are determined using bottom hole temperature (BHT) which represents only the present day thermal state, robust methods for evaluating thermal gradient history of a basin, such as geodynamic methods (Mc Kenzie, 1978) and thermal indicator methods (Lerche et al., 1984), are developed.

Accuracy in determining paleo-thermal gradient is a must because, a difference of 5 °C over a few million years can be critical in prediction of hydrocarbon generation (Nielsen, 1993). In most cases, geodynamic models are not suitable for thermal history reconstruction of this accuracy. However, models which are applied by calibrating the constructed models against thermal indicators give much more accurate results. In these models, vitrinite reflectance (%Ro) is the most widely used thermal indicator as a quantitative measure of the thermal maturity. It refers to the degree of heat that has been applied to a given potential hydrocarbon source rock over geological time.

Several models using thermal indicators which calculate systematic increase of vitrinite reflectance with increasing thermal maturity have been proposed in the past (Lerche et al., 1984; Lerche, 1988; Van, 1989; Sweeney and Burnham, 1990; He and Lerche, 1992). Among these models, chemical kinetic model, Easy%Ro, developed by Sweeney and Burnham (1990), has gained broad acceptance as the industrial standard. The Easy%Ro model and its application principles have been discussed in detail in the section 1.2.4.1 of this chapter. Unfortunately, reconstruction of the thermal gradient history using the Easy%Ro model brings some uncertainties, which arise from the quality and high scatter of the calibration data.

The objective of the study is met through three phases of development; developing and applying an inverse scheme in order to calibrate thermal gradients against measured vitrinite reflectance data from the Thrace wells using the Modified Easy%Ro model; providing a method for assessing the uncertainty associated with thermal history determined from vitrinite reflectance data; discussing the reliability of the determined thermal gradient and establishing the relation between thermal gradients and the geology of the Thrace Basin. The %Ro data from 70 wells are measured by the Geochemistry Department of the Research Center of TPAO.

The modified version of the Easy%Ro carries an implanted inverse scheme which enables a quick sensitivity, uncertainty, resolution and data quality assessment which could not be performed using the original Easy%Ro algorithm. While Easy%Ro is applied, modeler usually modifies the model input parameters such as time and temperature for providing a

reasonable fit between measured and modeled values. The use of this model is an extremely time consuming process and is trial and error based. Experience is essential in performing calibration and detailed geological knowledge of the study area is a must. Using this model, the best quantitative output, such as thermal gradient, may not necessarily be determined because there are no criteria for assessing the uncertainty on either the applied model or any input parameter. Also, with this kind of modeling scheme, it is almost impossible to perform sensitivity analysis on the applied model. These are all because, there is no measure of goodness of fit and no link to uncertainty assessment. The user, no matter what software is used, usually uses his/her own personal assessment in deciding if the fit is good enough to honor the calibration data. However, our challenge by implanting an inverse scheme to the traditional Easy%Ro algorithm is;

- to reduce time and effort spent in calibration,
- to provide consistency in calibration,
- to generate reproducible results which are independent of user,
- to statistically evaluate confidence in the predicted thermal gradients,
- to provide a measure of goodness of fit,
- to assess uncertainty in the calibration process.

On the other hand, by using the inverse scheme, sensitivity, uncertainty and resolution analysis could be performed on the model results which would give highly valuable information about the particular basin. Uncertainty is important, because it is a measure of accuracy of the model results and validity of the constructed model. Sensitivity assessment enables determination of the most sensitive parameters in the model. Also, measuring resolution of the calibration data within the model is significant in measuring the reliability of the model and model results.

The Modified Easy%Ro model, which have been introduced in this PhD thesis study, have been applied to five wells from the Danish Central Trough, North Sea by Huvaz et al. (2005).

## 1.1. Previous Studies

The tectonics and stratigraphy of the Thrace basin has been studied in more detail compared to its thermal history. Previous studies could be classified under four major periods; (1) 1947-1961 period, comprising studies about general geology and stratigraphy; (2) 1961-1974 period, consisting of first studies performed from hydrocarbon potential and exploration point of view which are carried out by N.V. Turkse Shell and TPAO; (3) 1974-1980 period, comprising studies of TPAO which enabled development of the basin from a frontier hydrocarbon exploration area into the second most prolific hydrocarbon producing basins of Turkey; and (4) 1980-present period, when most of the commercial hydrocarbon fields of the basin are totally developed under the light of new exploration tools such as high resolution 3D seismic, sequence stratigraphy and basin modeling.

In the 1947-1961 period, Pamir and Baykal (1947) indicated that the basement of the Thrace Basin is formed by the Strandja Massif and is composed of metamorphics. Akartuna (1953) and Arıç (1955) created the first detailed local geological map of the southern Thrace Basin. Holmes (1961) is the first scientist who presented the type localities and carried out geological mapping of the Thrace Basin sediments at a basin scale. Most of the names of the formations which are actually in use are suggested by him. Holmes (1961) analyzed the Tertiary sedimentary package under two subgroups; basinal and platform deposits. He also differentiated the transgressive and regressive sections using surface observations. Kemper (1961) worked on the evolution of the Early Eocene period of the Kırklareli region and presented detailed depositional and petrophysical properties of the Kırklareli Limestone. Druitt (1961) is one of the first prospect oriented workers of the basin who evaluated petroleum prospects of the basin. He emphasized the importance of the fault related structures which have turned into discoveries in the recent years (e.g. Hamitabat and Umurca Fields).

The 1961-1974 period starts with the exploration studies of N.V. Turkse Shell (1969 and 1972) that took place since the late 80's until this company completely abandoned the basin (N.V. Turkse Shell, 1986, 1988 and 1989). In this period, Keskin (1971 and 1974) constructed the



stratigraphy of the Thrace Basin by reorganizing the Keşan, Yenimuhacır and Ergene Groups and their formations. Keskin (1974)'s work is significant because it was the first attempt in constructing the detailed geological and depositional model of the basin. Gökçen (1971 and 1973) constructed the Paleogene stratigraphy of the basin and gave detailed lithological and sedimentological properties of the Karaağaç, Fıçitepe and Gaziköy Formations. Studies related to petroleum prospectivity of the basin is accelerated after the Second Petroleum Congress of Turkey held in 1974 (e.g. Doust and Arıkan, 1974; Aydın, 1974) which enabled transition from 1961-1974 to 1974-1980 periods. During this congress, the importance of the Thrace Basin from hydrocarbon exploration point of view was well understood.

Despite the others, a sharp boundary between 1974-1980 and 1980-present periods could not be observed. This smooth transition is represented by the studies of Aydın (1982), Saltık (1975), Sonel (1981), Kasar et al. (1983), Umut et al. (1983), Turgut et al. (1983 and 1987), Siyako and Kasar (1985), Kasar and Eren (1986) and Ediger (1982). In these studies, new approaches to the hydrocarbon potential and exploration strategies of the northern Thrace was developed under the light of stratigraphical, structural and paleo-environmental studies performed along the NW-SE trending Thrace Fault System and at the Kuleli-Babaeski High. Gerhard and Alişan (1986) studied palynostratigraphy, paleo-ecology and organic chemistry using data from three wells drilled in the basin. This study provided construction of detailed chronostratigraphy of the Thrace Basin. Detailed stratigraphical, sedimentological and palinological investigation of the Hamitabat-25 well by Ediger and Batı (1987) helped understanding most of the paleoenvironmental, stratigraphical and geological aspects related to the Tertiary section of the basin. Thus, source rock and reservoir rocks and their depositional systems have been identified. Later in the same year, Ediger et al. (1988) performed cluster and PCA analysis of the polymorphs using samples gathered from the Northern Thrace wells. These comprehensive studies aiming at investigation of the paleoecology and dating of the sedimentary packages had been of extreme importance in development of

the recent chronostratigraphy of the basin. Perinçek (1991) presented the affect and implications of the North Anatolian Fault System on the tectonic evolution of the Thrace Basin and presented three major fault systems of the Thrace region. This study is significant due to the importance of these fault systems in trapping commercial amount of hydrocarbons. Bürkan (1991) evaluated organic geochemical characteristics of the Tertiary deposits and demonstrated the petroleum generation potential of each source rock unit. He also ranked these source rocks according to their generation potential and maturity. Turgut et al. (1991) suggested a stratigraphic correlation chart based on well log and seismic data which is very useful in performing regional scale correlations. Tugut (1997) studied the depositional sequences and hydrocarbon potential of the basin based on sequence stratigraphic concepts and constructed sequence stratigraphy of the Eastern Thrace. This was the first study performed from sequence stratigraphy point of view which was suggesting classification of the deposits and stacking patterns based on identified systems tracts. Coşkun (2000) suggested that Thrace Basin is developed as an intermontane basin and discussed influence of the Stradja-Rhodope Massifs and the North Anatolian Fault System on oil potential of the basin. However, Görür and Okay (1996)'s fore-arc suggestion gained much more support compared to the other basin origins. Yaltırak and Alpar (2002) suggested a new kinematical model and discussed evolution of the Northern Branch of the North Anatolian Fault System between the Sea of Marmara and the Gulf of Saros which helped understanding the neotectonic features of the Thrace Basin. Ediger et al. (2003) discussed paleo-climate conditions of the basin by presenting the Dicolpopollis which is a commonly observed palynomorph in the Tertiary rocks mostly related to Oligocene and indicates a subtropical climate.

Thermal properties of the Thrace Basin are poorly understood due to the relatively few number of studies performed in the basin from maturity and petroleum potential point of views. None of the studies directly aimed at investigation of the thermal properties of the basin and its sedimentary deposits. The first attempt of analyzing the thermal properties of the Thace basin interlinked with thermal maturity have been done by İlleez (1984) and

Harput et al. (1991). These studies showed that the Hamitabat and Ceylan Formations reached to sufficient maturity for generating hydrocarbons in the central part of the basin. Present day thermal gradients of the Thrace Basin have been evaluated by Siyako (1984) using Bottom Hole Temperature (BHT) measurements from the wells (Appendix D) which demonstrated that the present day thermal gradients of the basin are above the world's average. İlleez (1985) presented and discussed timing of hydrocarbon generation in the basin by constructing the thermal history and evaluating the applied thermal model. Later, many 1D basin modeling studies are performed for the wells drilled in the Thrace Basin by the Basin Analysis Department of TPAO (Yükler, 1988a, 1988b, 1988c). Yükler et al. (1989) presented burial and temperature history and discussed lateral variation of heat flux within the Tertiary section. This study can be viewed as the first regional basin modeling study performed in this basin. They presented thermal stress, maturity and generation maps. Most of the organic geochemistry studies carried out in the Thrace Basin also gives many clues about thermal properties (Uğur, 1990; İztan, 1994). Karahanoğlu et al. (1995) performed one of the significant studies regarding the paleo-thermal development and construction at a basin scale in the Thrace Basin. They modeled the thermal stress and maturity using the mathematical approach of Lopatin (1971). Engin (1999) presented measured thermal conductivity values of some of the formations belonging to the Tertiary section. Gürgey (1999) discussed thermal properties of the Thrace basin while comparing geochemical characteristics of the Thrace and Türkmenistan oils. The recent basin scale modeling study is performed by Uğur (2002). They presented temperature and maturity maps for various formations and evaluated petroleum generation and expulsion in the kitchen areas accompanied by hydrocarbon volume calculations.

## 1.2. Technical Background

Technical details are highlighted in this section for providing better understanding of the applied methods which are presented in the 'Methodology' chapter.

### 1.2.1. Vitrinite Reflectance

The ability to predict thermal maturity is essential for assessing the petroleum potential of a basin or a particular source rock and the systematic variation of vitrinite reflectance with depth has long been in common use in the oil industry as a measure of the thermal maturity of sediments in a basin (Armagnac et al., 1988). Vitrinite reflectance, to some degree of accuracy, is said to record the effective maximum paleotemperature and is often referred to as a paleogeothermometer. Vitrinite reflectance or %Ro is a measure of the proportion of normal incident light reflected by a plane polished surface of vitrinite. The reflectance of vitrinite systematically increases with increasing thermal stress (Huvaz, 2003). It is a powerful recorder of thermal history and can in addition be used for purposes of identifying various geological phenomena such as faulting, thrusting, intrusion and unconformity (Dow, 1977). Typically only the mean %Ro at each depth of a distribution of individual vitrinite reflectance measurements is used as a measure of maturity (Huvaz et al., 2000).

The use of Vitrinite reflectance as a generic maturity indicator quickly gained acceptance for a variety of reasons. The presence of vitrinite or similar macerals in almost every organic-lean and organic-rich sedimentary or metasedimentary rock makes it an easy task to obtain vitrinite samples in almost any rock. Vitrinite or vitrinite-like macerals appear homogenous when viewed under the incident light microscope (in most cases, vitrinite grains are large enough for maturity determination) and vitrinite shows uniform physical and chemical changes under increasing thermal stress and other geological conditions.

The principles of using measured vitrinite reflection as an indicator of maturity of the level of thermal stress were developed by coal petrographers

and later widely applied to disperse organic matter. The method provides a universally applicable system for characterizing thermal maturity of sedimentary rocks, and for inferring their thermal history (Houseknecht et al., 1993). Stach (1968) developed the initial idea about the implications of the reflectance of various macerals in coal.

The physical laws of reflection and refraction show that when monochromatic optical light is shone normally onto a solid surface, the fractional intensity  $R$  of monochromatic light of angular frequency ( $\omega$ ), which normally is reflected from a plane interface of vitrinite of refractive index  $n$ , surrounded by immersion oil of refractive index  $n_0$ , is given by the following formula:

$$R = \frac{(n - n_0)^2}{(n + n_0)^2} \quad (1)$$

The beginning of the modern method of vitrinite reflectance measurements is marked by Stach (1968) who first used a single cell photo multiplier to measure vitrinite reflectance.

The earliest known reflectance measurement on dispersed vitrinite in other sedimentary rocks is derived from the work of Teichmüller and Durand (1983). The development of the technology used at the present day for measuring vitrinite reflectance on kerogen concentrate began during the middle of the 1960's by organic petrographers simultaneously in various oil company laboratories and other research organizations in Europe and USA (Castano et al., 1974). One of the earliest attempts to relate vitrinite reflectance to thermal maturity was by Lopatin (1971), who developed a basic kinetic model. He assumed that the change in the time temperature index was caused by doubling the reaction rate in every 10 °C increase in paleotemperature. Bostick et al. (1989) is known as the first scientist who used the vitrinite reflectance as a basin modeling tool by Lopatin's time-temperature curves which correlate temperature, duration of heating and coal rank parameters. Later, Waples (1980) popularized Lopatin's method and associated vitrinite reflectance to a time temperature integral (TTI), considered appropriate, in many cases, for hydrocarbon generation.

There are different ways of modeling vitrinite reflectance as a maturity parameter in basin modeling. The simplest model uses either temperature or time/temperature index as a maturation index with little consideration of kinetic variations (Mukhopadhyay, 1994). Adding a level of model complexity vitrinite reflectance can be modeled using a single channel first order reaction scheme. The single reaction chemical kinetic approach assumes that the behavior of vitrinite reflectance under increasing thermal stress can be modeled by first order chemical reaction with a single activation energy and Arrhenius constant. The third and complex model assumes that vitrinite maturation can be modeled using a number of parallel first order chemical reactions with a distribution of activation energies. The Easy%Ro model (Sweeney and Burnham, 1990), investigated in this study, falls in this category. First order reaction kinetics generally have stronger influence of temperature than time and general increase of the vitrinite reflectance with increasing temperature is believed to record the maximum temperature to which host strata have been exposed, although many additional variables (e.g. thermal conductivity, uplifting, subsidence) may have impact on vitrinite reflectance (Teichmüller and Durand, 1983). When measured in polarized light, vitrinite reflectance is characterized by increasing anisotropy with increasing maturity (Kilby, 1988).

#### 1.2.2. Source of the Heat Flux in the Earth

Surface heat flow is the sum of basal heat flow from the mantle plus radioactive heat flow from the upper crust and sediments. However, the major source of the heat flux affecting the sediments in a basin is the radiogenic heat associated with the upper crust. Radiogenic heat is defined as the heat given off by the decay of radioactive elements. Radioactive decay turns mass into energy, which is converted to heat. Attempts to describe basement heat flow include averaging heat flow data from available data measured from continental crust, (Haack, 1983), ductile zones (Taylor, 1982), crust and mantle studies based on meteorites (Gopel et al., 1985), measurements on vertical sections through the crust (Nicolaysen et al., 1981)

and estimates from heat flow data (Sclater et al., 1980). Currently, most estimates of heat production are based on an empirical linear relationship discovered by Birch et al. (1968) between heat flow and heat production of granites in the New England region of the USA. The concept of reduced heat flow assumes that at depths of approximately 7-10 km, the variation in radiogenic heat generation diminishes to a minimal amount. Below this depth there is a uniform background or “reduced heat flow”. By plotting the heat flow measured at many places in a region against the radioactive heat production of rocks (term “A” in the equation below) at each place of measurement, radiogenic heat and reduced heat flow can be determined. The linear heat flow-heat production relationship is expressed as:

$$Q_0 = Q_r + (D * A) \quad (2)$$

where:

$Q_0$  = Surface Heat Flow (mW/m<sup>2</sup>)

$Q_r$  = Reduced Heat Flow originating in deeper basement and underlying mantle

$D$  = Slope of line representing rate of reduction of A to baseline heat flow ( $Q_r$ )

$A$  = Radiogenic heat production

A simpler form of this expression can be created by assigning the term “D” to the equation as the thickness of a layer with constant radioactivity. In reality, “A” is a widely used variable but the net result at the surface is an average of rocks with high and low levels of radioactivity. The linear heat flow relation serves as a basis for defining heat flow provinces over which regional characteristic values for “D” and “ $Q_r$ ” have been observed. “ $Q_r$ ” values range from 10-60 mW/m<sup>2</sup> with values most commonly ranging from 30-40 mW/m<sup>2</sup> (Table 1).

Table 1. Average surface heat flow, reduced heat flow and characteristic depths for several continental heat flow provinces<sup>A</sup> (Sass, et al., 1981). <sup>A</sup>Data from Rao and Jessop (1975); Rao et al. (1976); Sass and Lachenbruch (1979); <sup>B</sup>Depth assumed for calculation of reduced heat flow.

Continent province	Surface heat flow (mWm <sup>-2</sup> )	Reduced heat flow (mWm <sup>-2</sup> )	Characteristic depth (km)
<b>North America</b>			
Basin and Range	92	59	9.4
Sierra Nevada	39	17	10.1
Eastern USA	57	33	7.5
Canadian Shield	39	22	12.3
		34	7.1
<b>Europe</b>			
Baltic Shield	36	22	8.5
Ukrainian Shield	36	25	7.1
<b>Africa</b>			
Niger	20	11	8
Zambia	67	40	(11) <sup>B</sup>
<b>Asia</b>			
Indian Shield	64	39	14.8
		33	7.5
<b>Australia</b>			
Western Shield	39	26	4.5
Central Shield	83	27	11.1
Eastern Australia	72	57	(11.1) <sup>B</sup>

### 1.2.3. Thermal History Modeling

A thermal history model ideally predicts the temperature variations of each sedimentary layer with time and depth (He and Lerche, 1992). A thermal history model typically consists of two interlinked models: a burial history model, providing the position and physical properties of the sedimentary rocks, and a thermal model providing the flux of heat from the basement for calculating the temperature field at any time during geologic history.

The burial history model used in this study is a one dimensional fluid-flow/compaction model. Once the burial history is properly calibrated, the heat flux model can be calibrated. In a heat flow model, paleoheat flux variation through time can be described by linear or non-linear models. A simple linear paleoheat flux variation with time can be expressed in the form:



$$Q(t) = Q_0(1 + \beta t) \quad (3)$$

where,

$Q(t)$  : Heat flux (mW/m<sup>2</sup>) at time,  $t$ .

$Q_0$  : Present day heat flux (mW/m<sup>2</sup>).

$\beta$  : Rate of change of heat flow (ratio).

The linear heat flux description can be viewed as a 1<sup>st</sup> order analysis of heat flux variation with time. The simplest case occurs when  $\beta$  equals 0, giving constant paleoheat flux through time. The ability to resolve higher order (non-linear) variation depends in part on the quality of the data and in part on the thermal history itself.

Lerche et al. (1984) presented and tested a time-temperature integral based on pseudo-first-order kinetics in order to determine paleoheat flux from vitrinite reflectance from wells. To test the method, they determined heat-flow history for the North Sea basin and the National Petroleum Reserve of Alaska and quantitatively observed increase and/or decrease of heat flux with time.

Lerche (1988) suggested a method based on inversion of multiple thermal indicators. He intended to determine paleoheat flux as well as other geological parameters such as amount of erosion and timing of unconformities, paleo-overpressuring, stratigraphic age, timing and temperature of an igneous intrusion over-thrust timing and frictional heating, fault and slump timing. Also, effects due to emplacement of a radioactive layer, and salt emplacement and dissolution timing could be predicted. Thus, inversion of present-day down-hole thermal indicator enables both the assessment of the paleoheat flux recorded by individual thermal indicators, and determination of geological burial history parameters that effect thermal indicators. He applied the inversion scheme on some of the thermal indicators; vitrinite reflectance, sterane and hopane isomers, sterane aromatization, pollen translucency, and apatite fission tracks. Nielsen (1996) applied a transient thermal model combined with least squares inversion and stochastic simulation on borehole temperatures, vitrinite reflectances, and

fluid inclusion temperatures to resolve paleo-thermal parameters. He suggested that when sediments are at their maximum temperature at present, maturity indicators which are less sensitive to resetting by increasing temperatures must be applied. Nielsen's argument was that the organic maturity indicators have limited thermal memory prior to the maximum sediment temperature and therefore, work best in cases where the general cooling of the basin more than outpaces the heating due to burial. Corrigan and Bergman (1996) applied apatite fission track for solving thermal reconstruction problem and argued that the method is not the ultimate solution to the thermal reconstruction because, even with a perfect predictive fission track model, the part of the paleotemperature history to which the fission track distribution is most sensitive to, is not likely to be resolved better than within a 10 °C window, and that resolution over most of the thermal history generally is much poorer. Gallagher and Sambridge (1992) applied a steady state thermal model and a least squares inverse method, which seeks smooth solutions satisfying different types of noise free borehole data. They concluded that the paleoheat flow, and therefore the paleo-thermal structure, could not easily be resolved back past the timing of maximum temperatures.

In summary, automatic model optimization procedures have previously been applied to the determination of paleoheat flow in thermal reconstruction with various levels of success. Application of inversion procedures clearly have the strength of being able to reveal the resolution of paleo-thermal parameters in the available control data and provide means of assessing the uncertainty on determined parameters.

#### 1.2.3.1. Maturity Models

In the past, several models have been suggested for modeling of vitrinite reflectance with time and temperature e.g. Easy%Ro (Sweeney and Burnham, 1990), Tissot and Espitalie (1975), Lerche et al. (1984), Tissot and Welte (1985), Van (1989) and He and Lerche (1992). A number of these models are available in a variety of basin modeling packages using well-constrained algorithms and kinetic parameters. Of the available models,

Easy%Ro has gained acceptance as the industry standard for modeling vitrinite reflectance. The primary objective of vitrinite reflection modeling is to aid in determining paleoheat flow for reconstructing the thermal history necessary for modeling hydrocarbon generation. At the same time vitrinite reflectance modeling can assist in estimating the time and duration of uplift and erosion in order to compare the timing of uplift with the timing of hydrocarbon generation.

Independent of the method used for modeling vitrinite reflectance, the uncertainty on the determined parameters such as thermal gradient is closely related to the quality of the control data (number of observations and the scatter in the data).

#### 1.2.4. A First Order Kinetic Model

Modeling vitrinite reflectance constitutes a highly non-linear problem and it has been argued that vitrinite reflectance behavior over a wide range of geological heating rates can be effectively modeled using a first order chemical kinetic model involving 20 parallel reactions (Larter, 1989; Burnham and Sweney, 1989).

##### 1.2.4.1. Easy%Ro

With the objective to predict the vitrinite reflectance value for a sedimentary unit buried in a sedimentary basin given the geologic age and heating rate, Sweeney and Burnham (1990) developed the Easy%Ro chemical kinetic model for modeling vitrinite reflection behavior with increasing thermal stress. The model is based on first-order kinetics (Arrhenius reaction) and the kinetics of H/C ratios in non-suppressed telocollinite and calculates the systematic variation of vitrinite reflectance with time and temperature. The reaction is modeled using a distribution of 20 parallel reactions that range from 34 to 72 kcal/mole (Figure 1) with a common frequency factor and an exponential relation between the extent of the reaction and the value of maximum %Ro.

For the distribution of these parallel reactions with equal stoichiometric factors, the extent of the reaction is linear in temperature for a given heating rate (Sweeney and Burnham, 1990). By tracing the temperature of any given layer at any point in time, a time-temperature integral is used to compute the modeled vitrinite reflectance for this layer through geologic time.

The classic formulation of first-order kinetics is presented in equation 4 which simply states that the rate of change in amount of organic matter remaining in the rock is described as the product of reaction rate ( $k$ ) and amount of unreacted component ( $w$ ) in mass.

$$\frac{dw_i}{dt} = -w_i * k_i \quad (4)$$

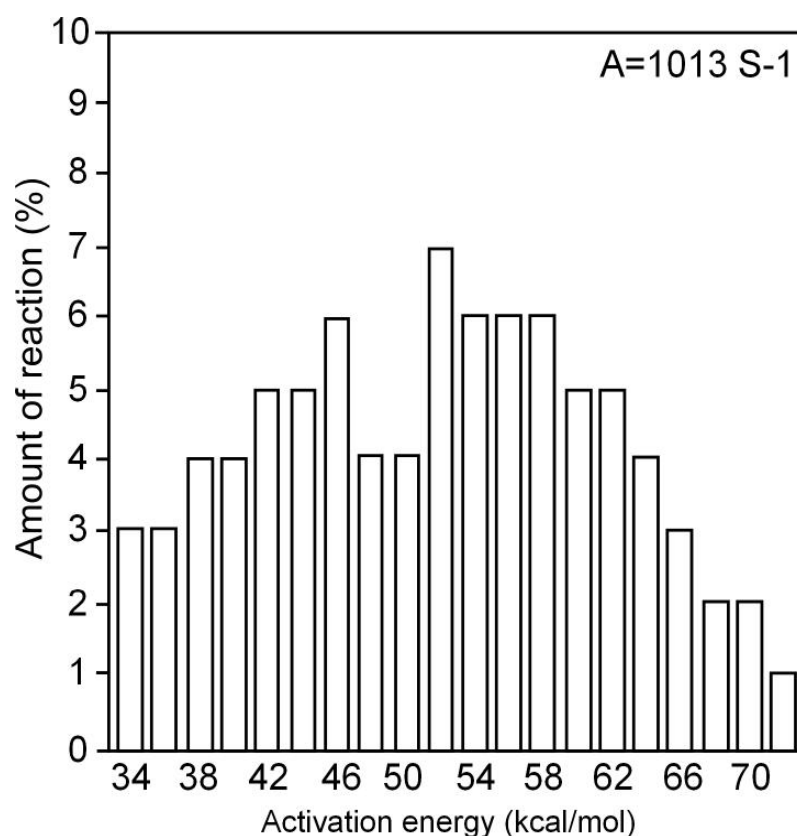


Figure 1. Activation energy distributions for the vitrinite maturation model of Burnham and Sweeney (1989). The overall range of 38 to 74 kcal/mole of the activation energies provides the foundation for the distribution of activation energies of the Easy%Ro model. The pre-exponential factor ( $A$ ) is  $10^{13}$  / sec.

The reaction rate can be calculated using equation below:

$$k = A * \exp\left[-\frac{E}{R * T(t)}\right] \quad (5)$$

where  $k$  is the reaction rate,  $A$  is the pre-exponential or frequency factor,  $E$  is the activation energy (kcal/mol),  $R$  is the universal gas constant and  $T$  is the temperature (°C).

When the reaction rate ( $k$ ) is expanded for reaction of the  $i^{th}$  component, the equation can be rearranged for a time-dependent temperature  $T(t)$  (Equation 6).

$$\frac{dw_i}{dt} = -w_i * A * \exp\left[-\frac{E_i}{R * T(t)}\right] \quad (6)$$

The amount of unconverted organic matter remaining in the  $i^{th}$  reaction of the distribution is described using equation 7, based on the change of the amount of the organic matter remained,

$$w_i = w_{0i} - \int_0^t \left[\frac{dw_i}{dt}\right] dt \quad (7)$$

and fraction of reactant converted is calculated using equation 8,

$$F = 1 - \frac{w}{w_0} = 1 - \sum_i f_i \left[\frac{w_i}{w_{0i}}\right] \quad (8)$$

where,

$w_0$  : Initial concentration of the total reactant (mass).

$w_{0i}$  : Initial concentration for component I (mass).

$f_i$  : Stoichiometric (weighting) factors which are obtained from chemical kinetics for the parallel reactions.

When the extent of reaction  $F$  has been calculated, vitrinite reflectance ( $\%Ro$ ) can be determined from the equation below which refers to the “calculated” or “modeled  $\%Ro$ ” in the Methodology section (Chapter 1.3) of the thesis.

$$\%Ro = \exp(-1.6 + 3.7 * F) \quad (9)$$

### 1.3. Methodology

Basin modeling methods and the Modified Easy $\%Ro$  algorithm in conjunction with a chosen measured maturity indicator (vitrinite reflectance) and statistical methods were used for investigating the thermal gradient history of the Thrace Basin.

The development of inverse methods and use of high speed computers gave momentum to the sensitivity and uncertainty analyses in basin modeling and made it possible to directly determine the resolution limits of any calibration parameter in a model, either a single parameter or in association with the other parameters (Thomsen, 1998). The sensitivity of model results to the choice of input parameters and constants could be analyzed not only as a response function from changes in the parameters but as a misfit to or departure from observed control information such as  $\%Ro$ , formation pressure, porosity and formation thickness.

In order to determine unknown parameters from indirect observations, an inverse scheme is applied. The logic of the inversion is explained by He and Lerche (1992). First, the present day values of a suite of vitrinite reflection samples ( $\%Ro_0, \%Ro_1, \%Ro_2, \dots, \%Ro_n$ ) are measured with increasing depth ( $z_1, z_2, z_3, \dots, z_n$ ). Theoretical considerations related to the underlying physical-chemical laws describing the evolution of the thermal indicator allow us to derive an expression for a predicted value at the present day,  $\%Ro(t)$ , of the vitrinite reflectance, of age “ $t$ ”. The predicted (calculated) value depends on the evolution of the temperature field and, on the burial path. Hence, it is possible to determine unknown variables influencing vitrinite reflectance by demanding agreement between the predicted and measured values of vitrinite reflectance. Briefly, the inverse scheme consists

of two steps. First, a criterion must be established for evaluating the goodness of fit of the predicted (calculated) to measured values. Then, an algorithm must be established to automatically improve the goodness of fit (to reduce the mismatch) by driving the parameters to their optimal values.

As a measure of the degree of agreement between the observations and the theoretical predictions normalized least squares are used (Noeth et al., 2002). The sum of the squares normalized with respect to the number of data points, the mean squared residual or MSR (equation 10), thus gives as a measure of the overall goodness of fit.

In this case, the task is to find the thermal gradient, which gives the minimum mismatch (smallest mean squared residual) between observations (measured vitrinite reflectance) and predictions (modeled vitrinite reflectance) using the MSR (Huvaz et al., 2005).

The MSR is given by:

$$MSR = \frac{1}{n} \sum_{i=1}^n (Ro_m - Ro_c)^2 \quad (10)$$

where,

$n$  : Number of measurements.

$Ro_m$  : Measured vitrinite reflection values.

$Ro_c$  : Calculated vitrinite reflection values.

In the inverse scheme, the investigated parameter is updated until either a preassigned goodness of fit or a minimum on the misfit function (smallest MSR) is obtained between observed and predicted vitrinite reflections or the limit of the search range is reached. This is done by updating the thermal gradient values controlling the evolution of the temperature field through the search range and determining the gradient at which the MSR value is at a minimum. In consequence, with this method, the thermal gradient that gives the best fit of the modeled vitrinite reflectance to the observed vitrinite reflectance would be established quantitatively.

The inverse scheme used here is a simple single parameter, linear, search scheme. This method does not require a complex inverse scheme

such as non-linear tomography but is applied by letting a single parameter, such as, thermal gradient varying linearly within pre-set boundaries and recording the MSR for each iteration. The recorded MSR provides a continuous mapping of the goodness of fit within the search range and the minimum, if present, can easily be determined.

In this study, paleo-thermal gradients are calibrated against vitrinite reflectance using the Easy%Ro model and the MSR function obtained from the inverse scheme is used to investigate the sensitivity and assess the uncertainty on the particular model.

The model investigates thermal gradients ranging from 5 to 50 °C/km by systematically varying the thermal gradient and at each instance calculating vitrinite reflectance using the Easy%Ro algorithm. The misfit (MSR) is calculated at each instance and the minimum MSR is determined. In order to determine the uncertainty on the best thermal gradient, the distribution of the squared residuals for each observation for the best thermal gradient is analyzed. The uncertainty can be assessed using a given confidence interval around the mean of the squared residuals. Using confidence interval around the determined mean (best fit), the range within which the variation in thermal gradient cannot be said on the given level of confidence, to be statistically significant, can be assessed. This approach provides the effective limits of resolution of paleo-thermal gradients in the control data. The extreme values of the thermal gradient such as 5 °C/km and 45 °C/km are calculated as well as the best fit in order to illustrate the influence of variation in the thermal gradient on the resulting modeled vitrinite reflectance. The resolution limits of the Easy%Ro and there by its ability to resolve paleoheat flow efficiently is intimately connected to the uncertainty associated with scatter in the data. A flow chart of the methodology of the model is presented in Figure 2. A more detailed flowchart showing the methodology and the developed and applied model algorithm where the Easy%Ro code coupled with the inverse scheme is presented in Appendix A.



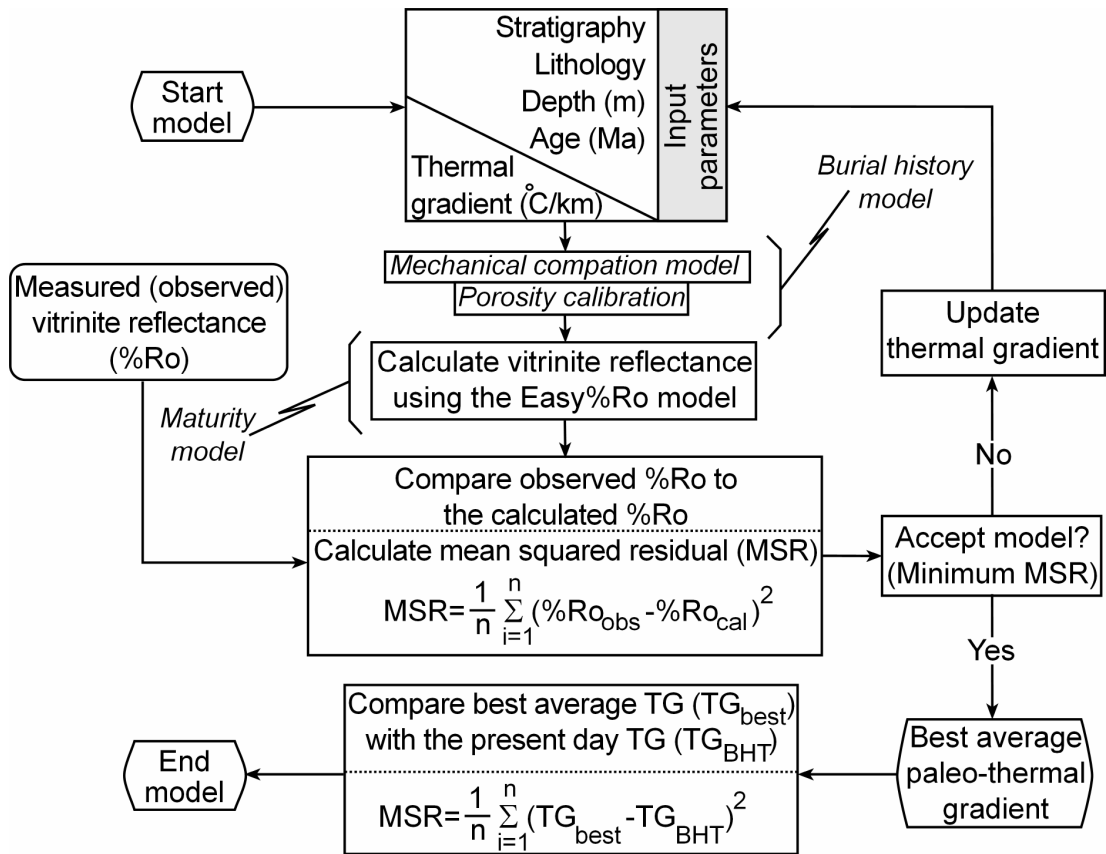


Figure 2. Flow diagram presenting the methodology of the study (Modified from Huvaz et al., 2005).

Inversion can be applied to any quantitative model by systematically changing the parameter in question and comparing the modeled parameter with its measured counterpart (Huvaz et al., 2005). In this way, we can determine the best value of the parameter (minimum mismatch) for a particular area and/or condition. Also we can assess the limits of resolution of the particular parameter and observe the impact of variations of this parameter on the model results. As stated above, the objective is to find the paleo-thermal gradient that gives the best modeled %Ro using Easy%Ro by investigating a range of gradients.

Results of the inverse method can be interpreted by analyzing the misfit function showing the variations of MSR values versus the parameter value here the thermal gradient. Thus, we can determine the thermal gradient that provides the best fit between the measured and modeled maturity

profiles in each well across the area. At the same time, an overall interpretation of the thermal gradients in an area can be performed.

In order to determine and discuss the resolution limits of the constructed model and its sensitivity within the variations of the thermal gradient quantitatively, a confidence interval on the determined mean (mean squared residual) representing the acceptable uncertainty range can be determined. The confidence interval on the mean is necessary in order to determine uncertainty ranges in terms of statistical significance (Huvaz et al., 2005). The confidence interval represents an interval such that a specified random variable will fall within that interval with the given level of confidence.

Suppose, measured %Ro is a random variable, then a 90% confidence interval would consist of an interval such that there is a 90% probability that measured %Ro values will fall within that interval. Thus, we can assess a statistical measure of the uncertainty for a particular model output.

By analyzing distribution of the squared residuals, the confidence level on the estimate of the mean (lowest MSR) can be evaluated. The upper limit of the confidence interval used in conjunction with the MSR curve provides a quantitative measure of the acceptable range of uncertainty on the determined thermal gradients. An example of a 90% confidence interval determined for the mean (lowest MSR) for a synthetic data set is shown in Figure 3. A 90% confidence interval is preferred to be applied rather than a 60 or 40%, because it is associated to a 10% uncertainty range. This range can be evaluated as the highest uncertainty range in a calibration process that can be tolerated within a basin modeling study at this scale.

Application of two different confidence intervals on a synthetic data set is presented in Figure 4. Here, the assumption is that, vitrinite reflectance does follow an exponential function.

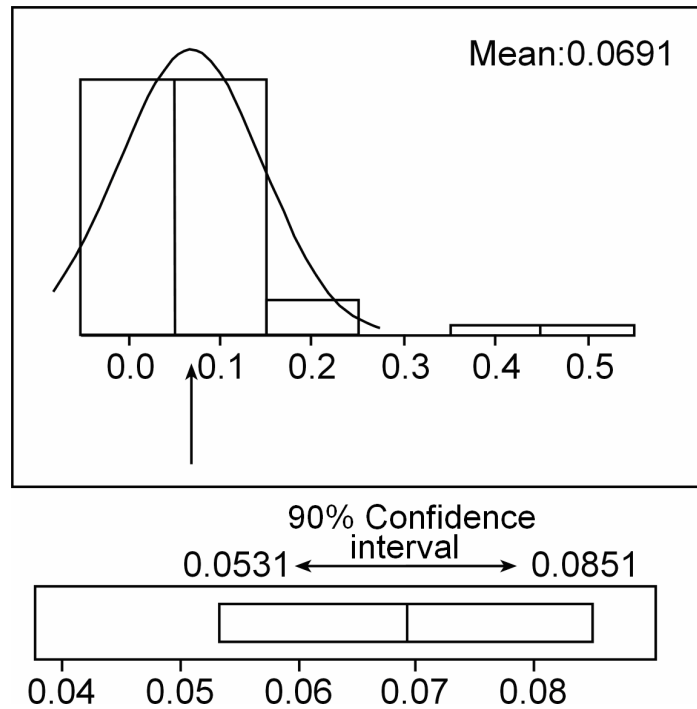


Figure 3. 90% confidence interval constructed on the determined mean (mean squared residual) for a synthetic data set.

The best model represents the best fit to the data set. 90% and 84% confidence intervals are constructed on the mean which is associated with the lowest mean squared residuals calculated using the MSR analysis from the MSR curves. This example shows how the limits of the confidence interval behave on a scattered data set and does depart from the best model (the lowest MSR). The use of the level of confidence on the best answer helps to define the uncertainty.

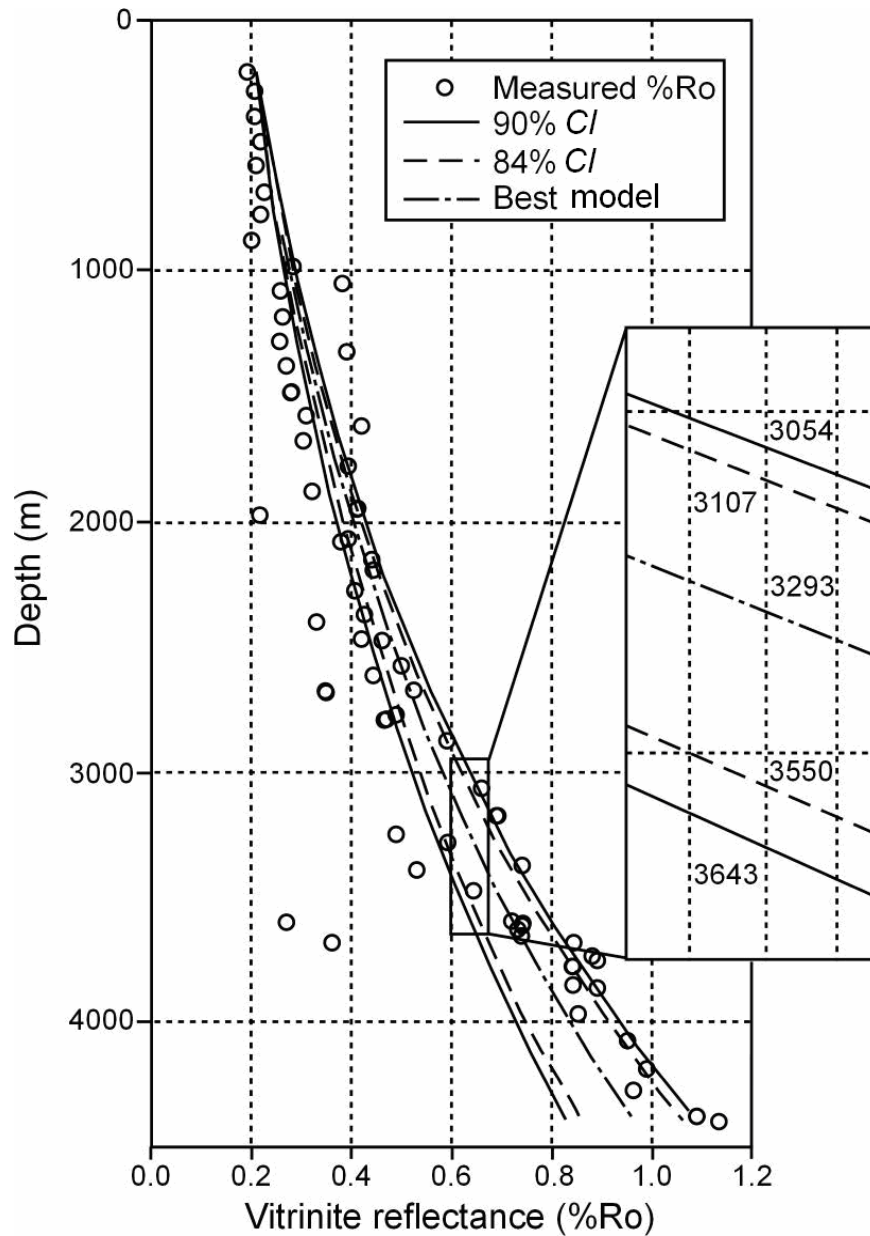


Figure 4. Application of the confidence interval approach on a synthetic data set (*CI*: confidence interval).

To evaluate the use of the inverse scheme, we can perform the sensitivity and uncertainty analysis on a perfect data set with no scatter in order. A simple exponential model is used to model the data and for investigating quality and resolution of parameters related to the modeled data (Figure 5).

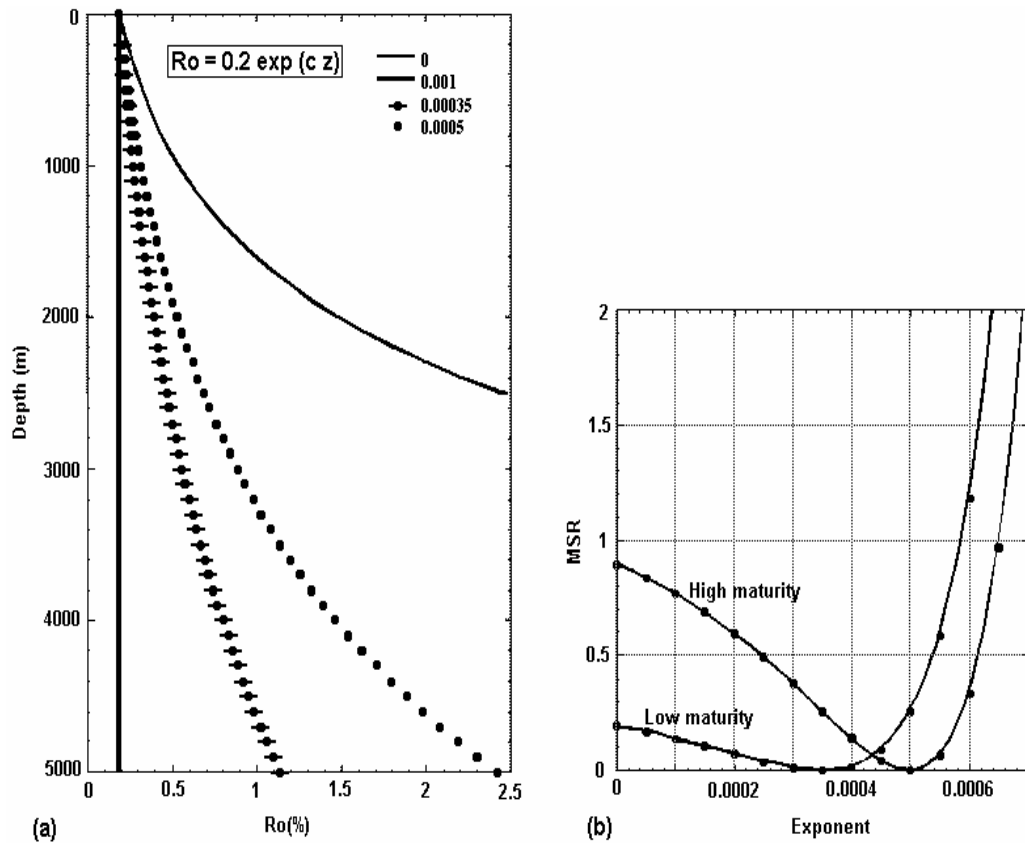


Figure 5. Exponential model for perfect data set and the MSR curves representing the 0.00035 and 0.0005 values of the exponential function.

Two sets of perfect data mimicking two different trends of vitrinite reflectance with depth are modeled and sketched in Figure 5a. The shape of the misfit function (MSR curves) is established for the two data sets recovering the exponents 0.00035 and 0.0005 used to model the data (Figure 5b).

The analysis of the MSR curves gives an assessment of the expected resolution limits and uncertainty for real data. The perfect data has no uncertainty and the lowest MSR is zero. It is clearly seen in Figure 6b that high maturity trend (large dynamic range of %Ro) have higher resolution than the lower trend for the same basic scatter in the data. Scatter in the data will result in a non-zero lowest MSR value. The shape of the MSR curve for the data modeled with an exponent of 0.00035 has a broader trough than the MSR curve for the data modeled with an exponent of 0.0005. This indicates

that an increase in the dynamic range of the control data will result in increased resolution of parameters in the data.

When the procedure is applied on real data (Table 2, Figures 6 and 7), the MSR curve indicates fair resolution, some inherent uncertainty is observed from the scatter in the data (elevated from the zero base-line).

Table 2. Calculation of MSR values for different thermal gradients ranging from 5 to 50 for the Ballı-1 well (Ro<sub>m</sub>: measured %Ro values from the core samples gathered from the Ballı-1 well; Tg: thermal gradient).

Depth	Ro <sub>m</sub>	Calculated %Ro for different thermal gradients using the Easy%Ro Model									
		Tg5	Tg10	Tg15	Tg20	Tg25	Tg30	Tg35	Tg40	Tg45	Tg50
1451	0.57	0.35	0.36	0.36	0.4	0.44	0.51	0.59	0.66	0.75	0.85
1660	0.62	0.36	0.37	0.38	0.41	0.47	0.54	0.63	0.70	0.81	0.94
1863	0.64	0.38	0.38	0.39	0.43	0.50	0.58	0.66	0.75	0.89	1.08
2066	0.7	0.40	0.40	0.41	0.46	0.52	0.62	0.70	0.80	0.99	1.20
2459	0.78	0.42	0.42	0.43	0.48	0.58	0.68	0.78	0.93	1.22	1.50
2505	0.81	0.42	0.43	0.43	0.49	0.59	0.68	0.79	0.95	1.24	1.53
MSR		0.093	0.097	0.086	0.061	0.030	0.008	0.0002	0.0131	0.099	0.277

Figure 6 presents the calculated MSR values for the search range of thermal gradients and the 10% uncertainty range (90% confidence interval) for the Ballı-1 Well. The upper limit of the constructed confidence interval (e.g. 0.0784 for the Ballı-1 well) (Figure 6 and 7) is calculated by using a PC based statistical software (Minitab). This calculation is done by inputting the MSR values versus thermal gradients and assuming a mean which is the best thermal gradient value obtained from the MSR curve (35 °C/km for the Ballı-1 well) (Figure 6 and 7).

The descriptive statistics and the calculated 90% uncertainty range are given in Figure 7. The quality of the fit is given by the absolute value of the lowest MSR. This time because of the modeled and observed values do not overlay each other, the MSR is not 0 on the best fit.

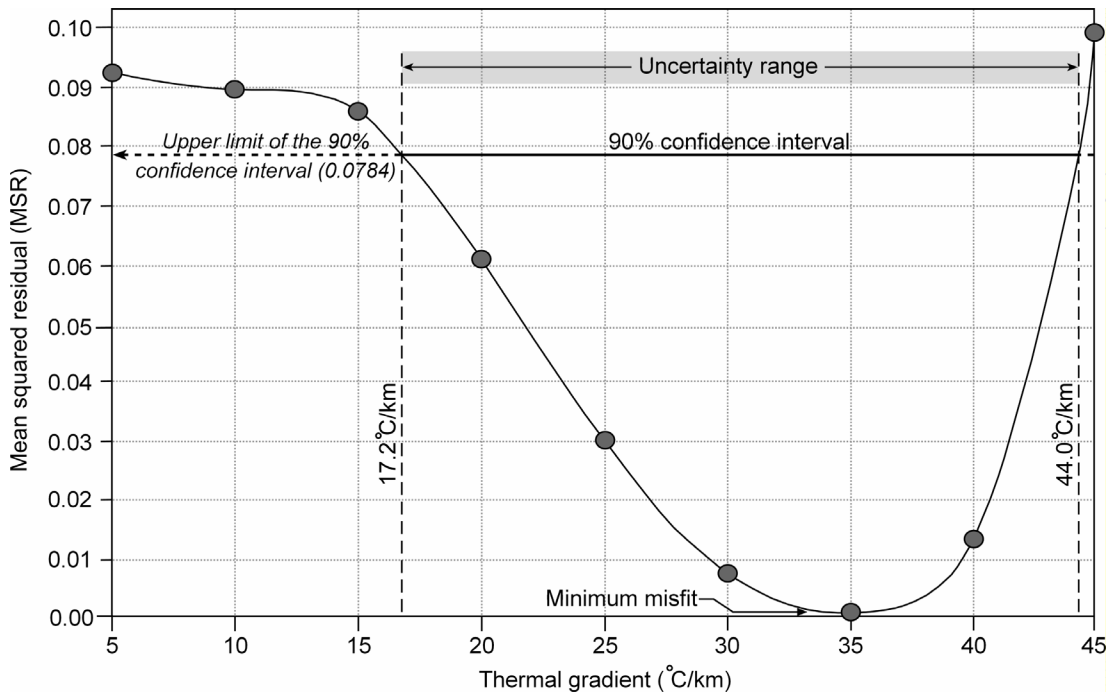


Figure 6. Thermal gradient versus MSR and the misfit function for Balli-1 well.

The shape of the misfit function enables us to make a quantitative evaluation of the acceptable range of thermal gradients. This means, values of thermal gradients within this range are equally acceptable for the particular model when calibrated against vitrinite reflectance using the Easy%Ro algorithm. Now, we can evaluate the sensitivity, applicability and success of the calibration. Besides, it enables us to perform sensitivity, uncertainty and resolution analysis using the MSR function and the level of the confidence constructed on the best answer. Shape of the MSR curve is an indicator of sensitivity based on the misfit between modeled and measured values. For vitrinite reflectance, the right flank (higher thermal gradients) of the function show higher sensitivity to changes in the thermal gradient (steeper than the left flank, the upper limit of curve). Acceptable thermal gradients are therefore better determined than the lower limit and departure of the modeled %Ro from the “best fit” is more dramatic for  $TG_{best} + \Delta T$  than  $TG_{best} - \Delta T$ . In such a case, it is generally expected that the lower uncertainty range to be wider

than the upper limit of the uncertainty range (e.g. Ballı-1 well,  $TG_{best}=35$  °C/km,  $TG_{upper}=44$  °C/km,  $TG_{lower}=17.2$  °C/km).

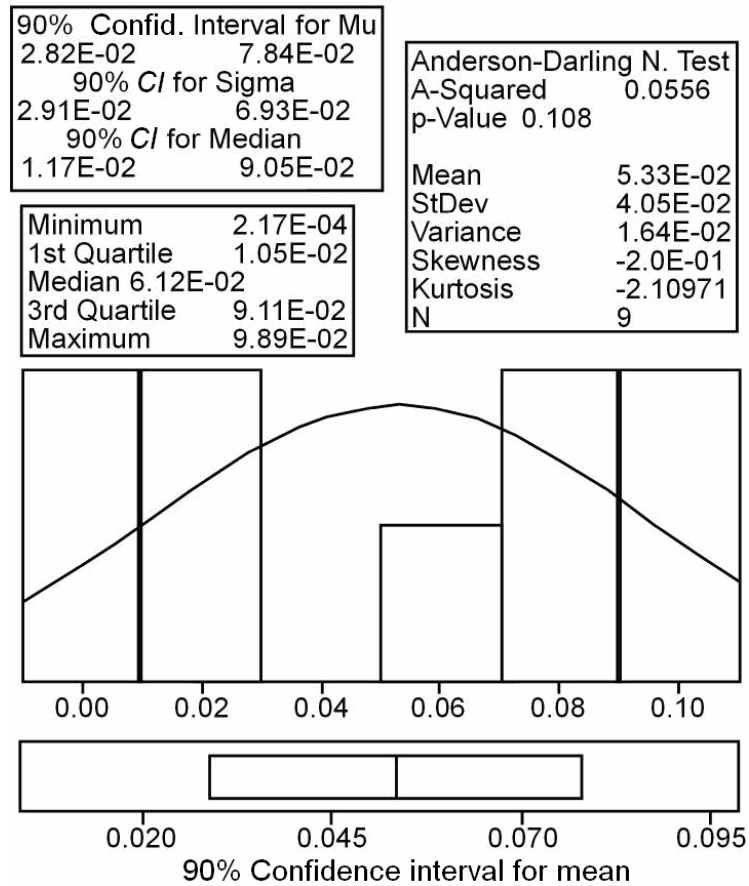


Figure 7. Descriptive statistics and the calculated 90% confidence interval on the mean (CI: confidence interval; Sigma: standard deviation; N: number of samples).



## CHAPTER II

### GEOLOGY OF THE THRACE BASIN

Thrace is a triangular shaped Tertiary basin located on the northwest of Turkey, bordered by the Rhodope Massif from west, crystalline Strandja mountain belt from north and Ganos Mountain complex from south (Figure 8). Many authors who have been cited in the section 1.1 (Previous studies) studied geological and tectonic setting of the basin. The basin is surrounded by metamorphic massifs on all three sides (Perinçek, 1991). Sedimentary thickness reaches up to 9,000 meters in the central part.

#### **2.1. Regional Geology and Burial History**

The basin is interpreted as a fore-arc basin by Görür and Okay (1996) which was affected from a plate convergence during the Upper Cretaceous (Maastrichtian), while Keskin (1974) and Perinçek (1991) agreed on an intermontane origin. During the Late Cretaceous and Paleocene, plate collision occurred causing intense compressional stress and over-thrusting. After the completion of the convergence during the Eocene, the Menderes-Tauride Platform and Sakarya Continent are clamped. At the northern side, rather than welding together, Pontide and Sakarya plates moved with respect to each other causing intense shear stress which is resulted in development of the North Anatolian Fault System (NAFS) from Miocene to early Pliocene (Şengör, 1979; Şengör and Yılmaz, 1981). However, the first sedimentation and development of the Thrace Basin began with an extension over the Pontide Plate in Early Eocene and is affected by the period of intense compressional tectonics afterwards.

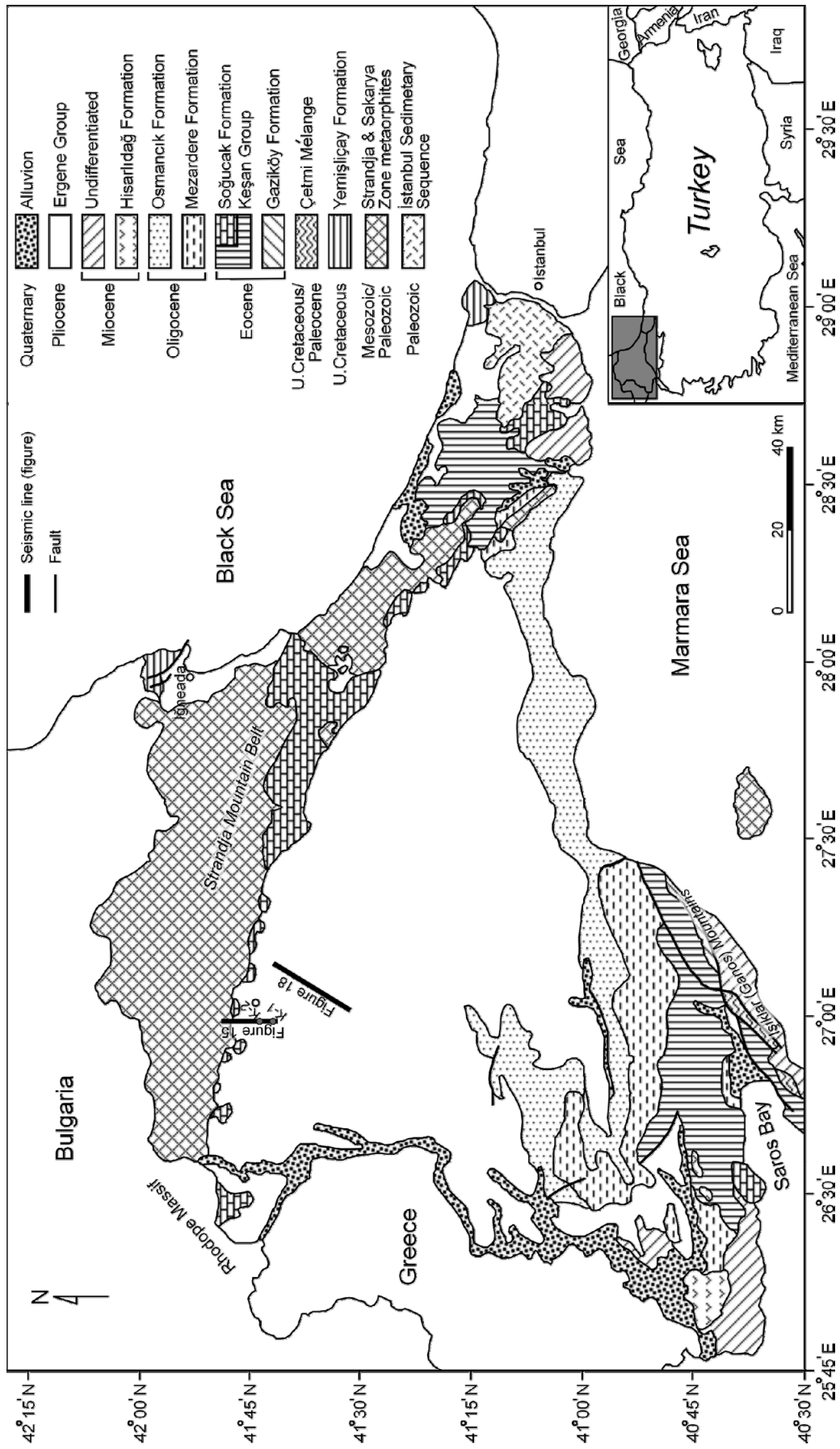


Figure 8. Geology map of the Thrace Basin (Modified from Huvaz et al., in press)

The early extensional phase caused a NE-SW transgression resulted in rapid subsidence of the Thrace Basin and triggered deposition of thick interbedded sandstone, conglomerate and shale sequences starting from Eocene time until the end of Early Miocene. These sediments over 8,000 meters thick are mostly turbidites. By the Late Miocene, central part of the basin was over pressured and the uplifting (Figure 9) of the south side of the basin (uplifted in response to NAFS) appear to have caused northward tilting of the basin. This enabled creation of a number of low angle thrusts.

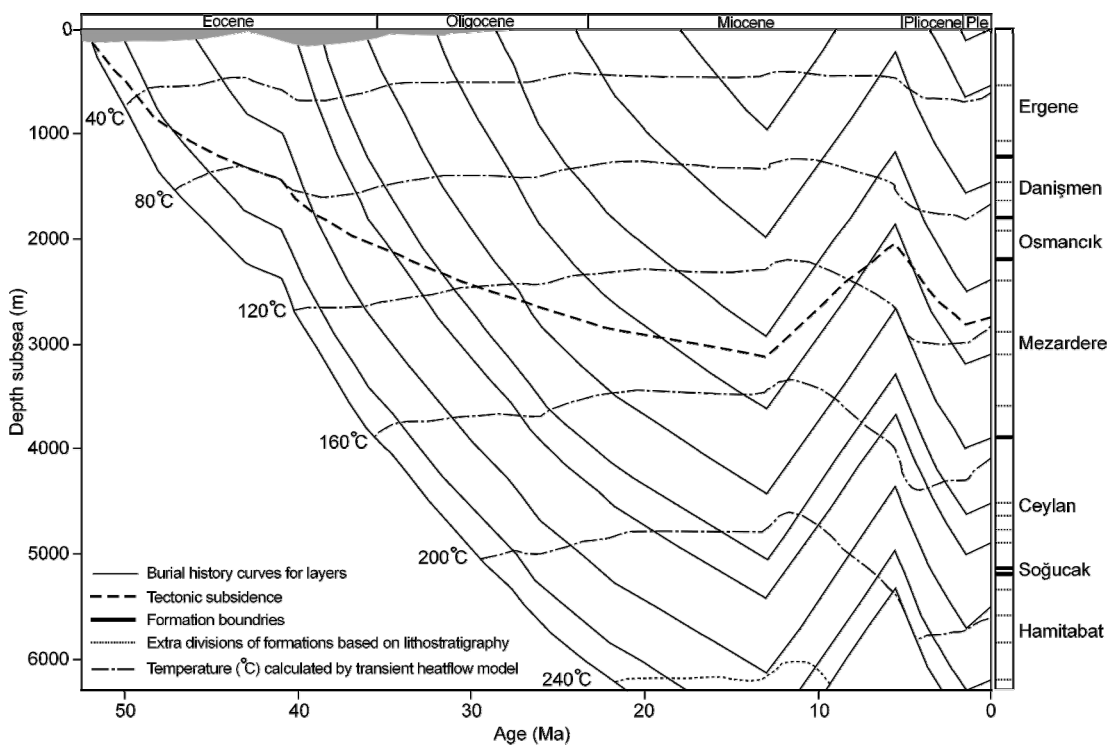


Figure 9. Burial history diagram and the isotherms constructed by using transient heat flow model. Tectonic subsidence curve is shown with dash line.

## 2.2. Stratigraphy

Tertiary sedimentary sequence of the Thrace Basin consists of interbedded clastics (e.g. sandstones and conglomerates), tuffs, coal stringers and carbonates (reefal or basinal limestones) and tuffs. The Tertiary

stratigraphic column resting on the basement is divided into three groups (Keşan Group, Yenimuhacir Group and Ergene Group) and a formation (Hisarlıdağ Formation) (Figure 10).

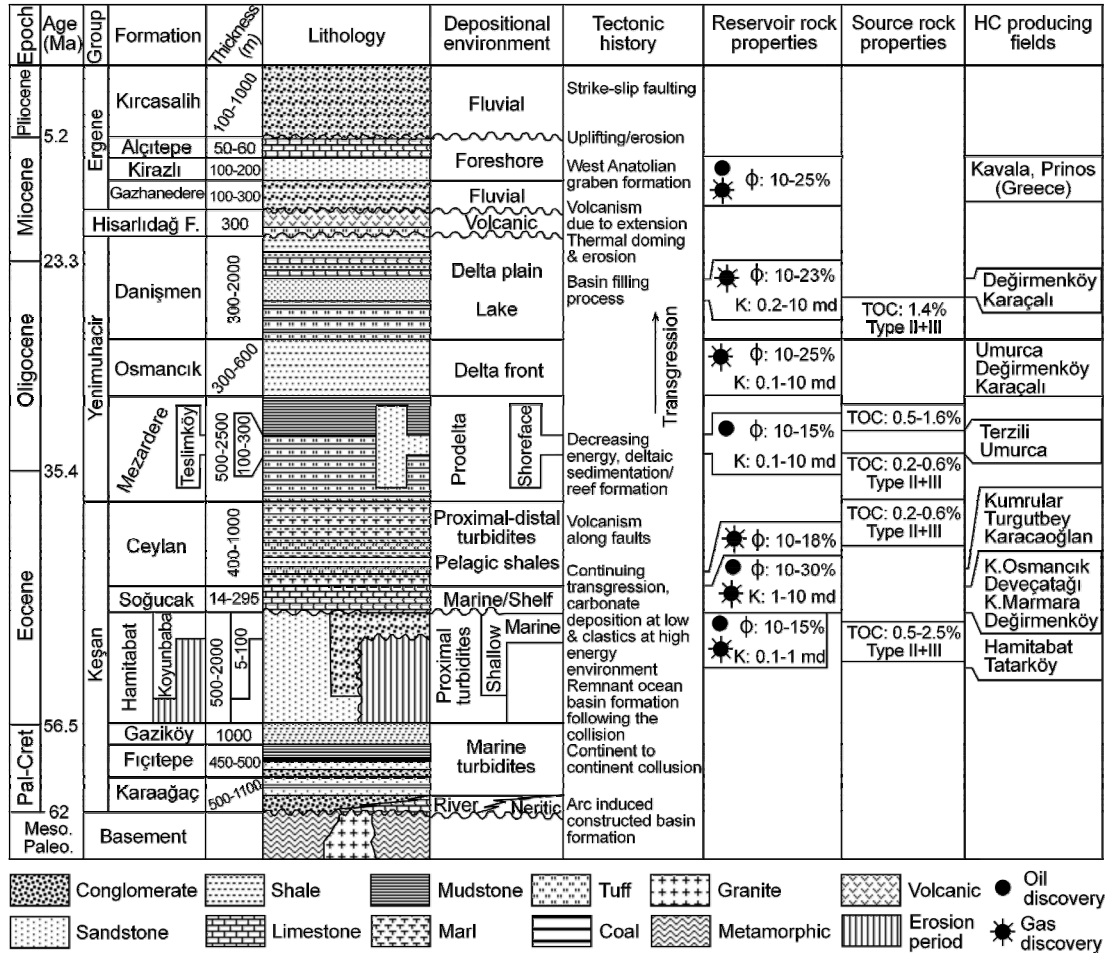


Figure 10. Generalized stratigraphy of the Thrace Basin showing the depositional environment and thickness of formations, petrophysical properties of the reservoirs, type and average total organic carbon (%TOC) of the source rocks, producing fields versus formations and summary of the tectonic history (φ: porosity; K: permeability; HC: hydrocarbon). (Modified from Kasar et al., 1983; Siyako, 2005 and Huvaz et al., in press).

The basement of the Tertiary sequence comprises five different lithostratigraphic units: (1) the Strandja Rodop Massif, composed of Triassic-Jurassic metasedimentary rocks (Aydın, 1974, 1982 and 1988; Üşümezsoy, 1982; Chatalov, 1985a and 1985b; Çağlayan et al., 1988; Çağlayan and

Yurtsever, 1998; Okay et al., 2001); (2) the İstanbul Paleozoic and Kocaeli Triassic sediments bounded by the North Anatolian Fault from south and extending through the western part of the Bosphorus (Şengör and Yılmaz, 1981); (3) the Upper Cretaceous island arc magmatics, which have a transgressive nature with both Strandja metamorphics and İstanbul and Kocaeli sediments (Saner, 1980); (4) the Çetmi Ophiolitic Melange, forming the basement of the southern Tertiary section, extending from Gallipoli Peninsula and Mürefte-Şarköy Region through south (Okay et al., 1990); (5) the Sakarya Continent Units, consisting of post-Triassic deposits, Kazdağ Group metamorphics and Karakaya Complex overlying these metamorphic units tectonically.

Keşan Group overlies the basement and is divided into 7 formations. These are Karaağaç, Fıçitepe, Gaziköy, Hamitabat, Koyunbaba, Soğucak, Ceylan Formations.

The Hamitabat Formation is named from subsurface data because it does not outcrop in the basin. It is widespread at the northern and northwestern and particularly in the central part of the basin. Its thickness changes from 500 to 3000 m. It consists of interbedded gray colored sandstones, siltstones and dark gray colored shales. However, it shows quite a rapid facies variation throughout the basin. Deposition of the Hamitabat clastics are greatly shaped the basement and the northwestern-southeastern trending major normal faults. Some of these major faults have defined the basin-shelf boundary during the Hamitabat deposition. The upper levels of the Hamitabat Formation are represented by marine environment (Gerhard and Alişan, 1986; Ediger and Batı, 1987). However, depositional environment of lower sections is fluvial. Hamitabat sands are gray colored, fine to medium grained, subrounded to subangular to even angular depending on the depositional site, fair to poorly sorted and generally hard and dense. But, locally, they contain up to 11% to 18% porosity. It is the major reservoir rock of the Thrace Basin.

Soğucak Formation is represented by limestones which outcrop on the northern and southern margins of the basin (Holmes, 1961). It consists of shallow marine shelf facies and deeper marine shaly basinal facies. The shelf

facies are consisting of biomicrites and reefoidal organic buildups. The reefal developments are found on the topographically higher elevations in the shelf realm. Some of these organic buildups contain secondary porosity. Carbonates of the Soğucak Formation are the second important hydrocarbon producing reservoir rock of the Thrace Basin.

The Ceylan Formation overlies the Hamitabat Formation and the Soğucak limestones. It is consist of interbedded dark gray to greenish shales, siltstones, marlstones, argillaceous micritic limestones, very fine grained sandstones, tuffs and tuffites and variegated volcanics. Shales of the Ceylan Formation shows good source rock properties. This Formation shows great thickness variations in the basin. The Ceylan Formation shows relatively low thermal conductivity due to its high shale and tuff content. Tuffs of the Ceylan Formation are associated with volcanic activity. Active volcanism, which took place during the Ceylan deposition period, is also indication of a basin that has undergone substantial extensional tectonics and subsidence. The Thrace Basin was located between an arc and its accretionary mélangé from Middle Eocene to Oligocene time which could geographically be defined as a fore-arc position (Letouzey et al., 1977; Şengör and Yılmaz, 1981; Görür and Okay, 1996).

The Yenimuhacir Group overlying Keşan Group comprises Mezardere, Osmancık and Danişmen Formations.

The Mezardere Formation overlies conformably the Ceylan Formation and the Keşan Group. It consists of interbedded greenish gray to green shales, siltstones, marlstones and fine grained sandstones. Sporadic tuffite intercalations are also present. Shales are dominant in this formation and are soapy in character. They have a tendency to flow, rather than break. The formation is sandier at the bottom. It is quite widespread throughout the basin, and outcrops on the southwestern part of the basin. Its thickness ranges from 500 meters on the shelf margins to 2500 meters in the central depocenter. Thickness variation in the Mezardere Formation is not as great as the Ceylan or the Hamitabat formations. Therefore, during Mezardere depositional period, the basin's subsidence slowed down and regressional features are observed in the depositional setting. The formation is mostly

composed of fine grained clastics indicating less tectonic activity and shallow to moderate deep marine depositional environment. Shaley sections of the Mezardere Formation shows fair source rock properties.

The Osmancık Formation overlies the Mezardere Formation conformably and outcrops on the southwestern part of the basin. It is quite widespread throughout the basin. It consists of very fine to medium grained sandstones interbedded with greenish gray shales and siltstones. Towards the upper levels of the formation, thin stringers of coal intercalations are present. The sands are very fine to fine grained, very silty, moderately sorted, subangular to subrounded, calcite cemented. Depositional environment is delta front. Sands are unconsolidated and present high porosity. The formation is sandier towards south and southeastern part of the basin and shale and silt content increases towards north. The Osmancık Formation is the third important reservoir rock for the Thrace Basin.

The Ergene Group of Miocene-Pliocene age forming the upper most section of the Tertiary sequence of the Thrace Basin consists of Gazhanedere, Kirazlı, Alçitepe and Kırçasalılı Formations. This group has no importance from hydrocarbon exploration point of view.

### **2.3. Tectonics**

Significant tectonic events of the western Anatolia occurred in the Eocene between the Menderes-Tauride platform on the south, the Sakarya Continent in the center and Pontid Continent on the north (Şengör and Yılmaz, 1981). At the end of consumption of oceanic crusts and completion of the convergence in the Eocene, the Menderes-Tauride Platform and the Sakarya Continent clamped. This thickening reached to 15 kilometers in the Menderes block on the south. This thickening and resultant anatexis caused granitic intrusions. However, traces of this extensive intrusive events are not observed between the Sakarya Continent and the Pontides. Rather than welding together and united, the two plates started to slide with respect to each other causing intense shear stresses between the plates. This shear was the instigator of the NAFS. The Sakarya Continent's motion was

westerly with respect to the Pontides which started in the Eocene. The basin started to develop in the Early Eocene. While westerly motion of the welded Menderes and Sakarya plates with respect to the Pontide plate continued, an extensional tectonic phase started to develop over the Pontides along the former suture zone with the Sakarya Continent. This extension bounded by an intense normal fault on the north which was accelerated by numerous normal basement faults caused probably by the intense shear stress developed in the suture zone. Thus, development of the Thrace Basin began with an extension over the Pontide Plate during the Eocene following a period of intense compressional tectonics.

The earlier extensional phase caused rapid subsidence of the basin and hence deposition of thick interceded sandstone, conglomerate and shale packages in the Late-Middle to Late Eocene time. These early sediments over 5000 meters thick are mostly turbidites. During the early subsidence and deposition, much of the large basement faults became growth faults causing great thickness variations in the sedimentary column. Basement faults are usually oriented in a northwest-southeast or southwest-northeast direction. However, northwest-southeast oriented normal faults took an active part in the early subsidence and deposition shaping facies characteristics and thickness variations of the sediments. Especially north bounding large normal basement faults separated clastic basin from the shelf area causing a southwesterly tilting. However, most of the southern faulting is associated with the Late Miocene tectonics and the formation of the extension of the NAFS. The southern faults trend in the direction of the NAFS. Much of the pre-Miocene sedimentary cover to the south of the NAFS has been removed. Therefore, sedimentary tectonics of the southern margin of the basin is not decipherable.

Rapid subsidence during Eocene, thick turbidite sedimentation and volcanic intercalations from Eocene to Miocene indicate that early formation of the basin was accompanied by an active extensional type tectonics. The early extension and ensuing thick clastic sedimentation must have caused thinning of the continental crust of the Pontide Plate under the Thrace Basin to compensate additional sedimentary column.



Following the deposition of the Hamitabat Formation during Early Eocene, there is an increase in the tectonic activity in the basin. This revival of the tectonic activity has been represented by uplifts of certain areas, rejuvenation of some of the normal or growth faults and great quantities of acidic tuff flows extruded into the basin. Again, at this time, the major northwest-southeast bounding normal fault was reactivated causing local sinking and active volcanism in this trend. The Ceylan Formation was affected by the volcanism and Ceylan sedimentation became volcanoclastic in the early stages. The lower Ceylan sedimentary section consists of tuffs.

Rest of the depositional period from the Early Oligocene to Early Miocene did not experience an active tectonics. However, Late Miocene time is associated with extensive tectonic regime. Margins of the basin were uplifted and much of the sedimentary column was removed. Some of the previously developed normal fault trends were reactivated causing flexures and flexure slips. Some of the faulting just involved upper horizons of the sedimentary column and did not reach to basement. However, the Miocene tectonics has superimposed a new cycle of tectonic imprint over the previously developed tectonic features causing a complex array of new tectonic trends in the basin. Therefore, it is quite difficult to estimate the age of the faulting and folding in the basin.

Southern and southwestern parts of the basin were subjected to a more intense tectonics with the formation of the right-lateral NAFS in the Late Miocene. Intense faulting and folding took place in the region. This right-lateral strike-slip motion has created additional slippages and deformation in the sedimentary column in the over-all basin. The latest generation of tectonics and basin settlement in the Pliocene and Pleistocene have created small scale deformation and faulting in the upper levels of the sedimentary column and formed the present day Thrace basin topography.

## CHAPTER III

### THERMAL GRADIENT HISTORY OF THE THRACE BASIN

In general, the thermal gradient concept is considered to be an unrealistic description of the temperature variation with depth. The thermal gradient is the average temperature change over a given depth interval and should only be used if no other data is available. Also the assumption that the thermal gradient is constant through time should only be used in special cases. It is argued that a constant thermal gradient with time can be applied to the Thrace Basin and may give meaningful results. The arguments are as follows: the chemical kinetic model has higher sensitivity to temperature than to time, indicating that vitrinite reflectance records maximum temperature; the area is close to its maximum burial at the present day (Figure 9); the area experienced rapid burial until the last 13 to 12 Ma and is not affected by a complex tectonic activity (e.g. reverse faulting, inversion). Also, late stage rapid subsidence is clearly seen starting from 5.5 Ma. The erosion period that takes place from 12 to 5.5 Ma is the only burial interruption recorded in the Thrace Basin. Collectively these arguments states that the expected resolution of thermal history is limited in time and the constant thermal gradient over time of thermal history resolution should be valid.

#### **3.1. Determination of the Thermal Gradient from MSR Curves**

The presented inverse scheme is used to investigate the ability to resolve paleo-thermal gradients from %Ro profiles using Easy%Ro. The best average paleo-thermal gradients for each well are calculated using the particular method. The MSR functions are presented in Appendix C with the MSR data. A 90% confidence interval is constructed on the best answer (mean) for performing sensitivity and uncertainty analysis. Each diagram shows the minimum mismatch between measured vitrinite reflection data and the calculated vitrinite reflectance of the investigated wells.

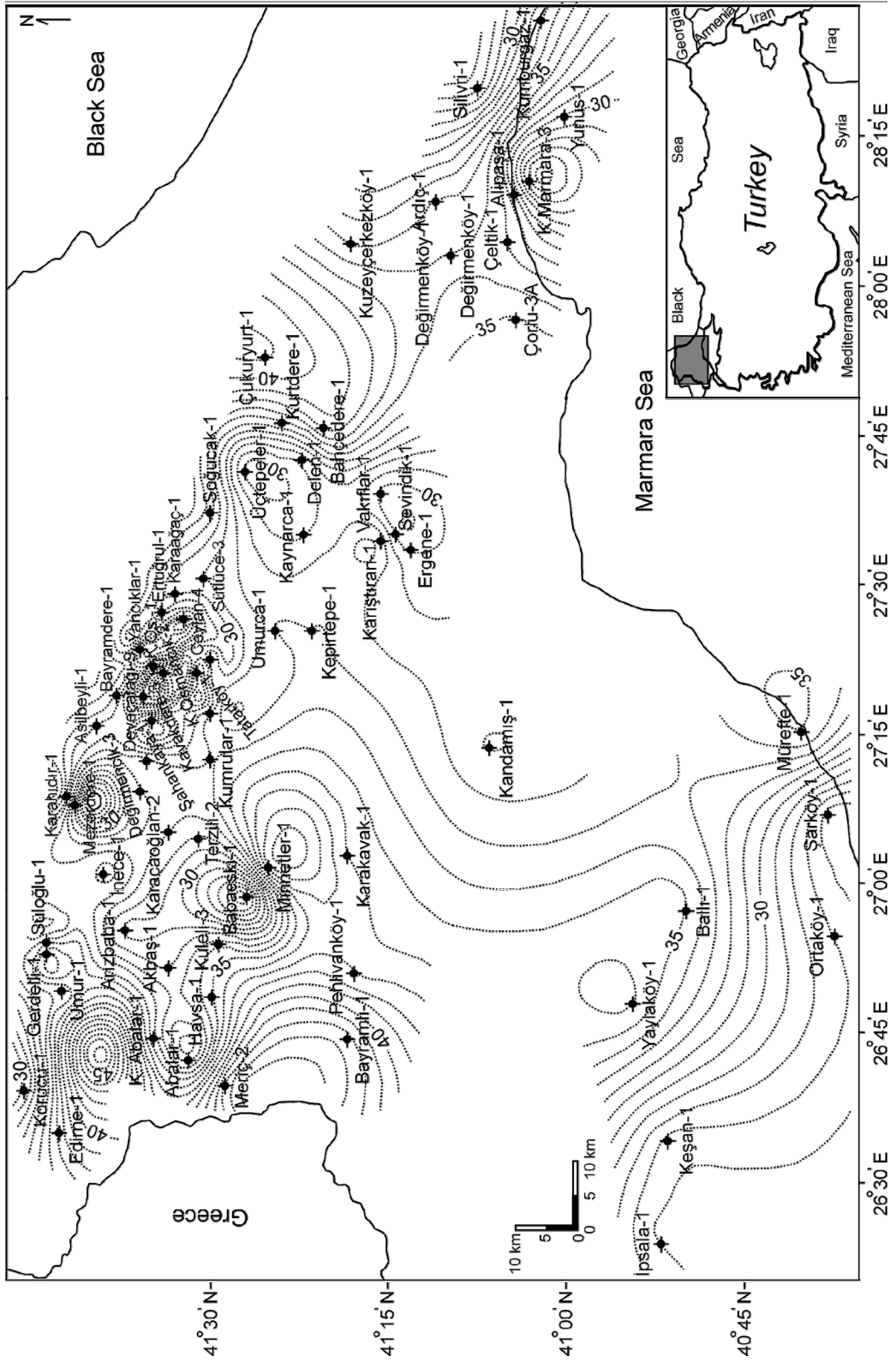
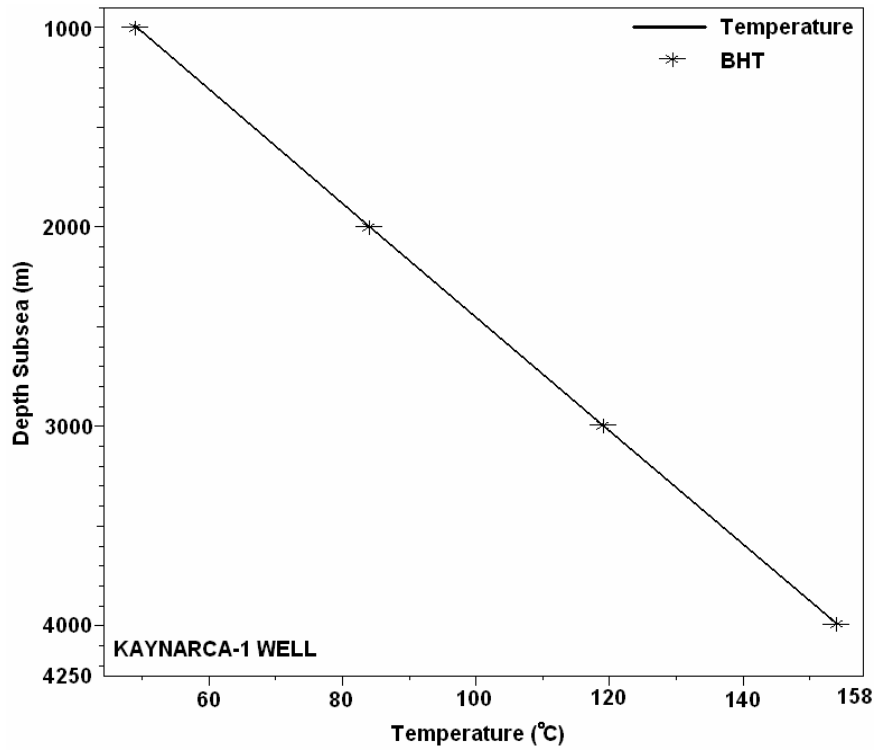


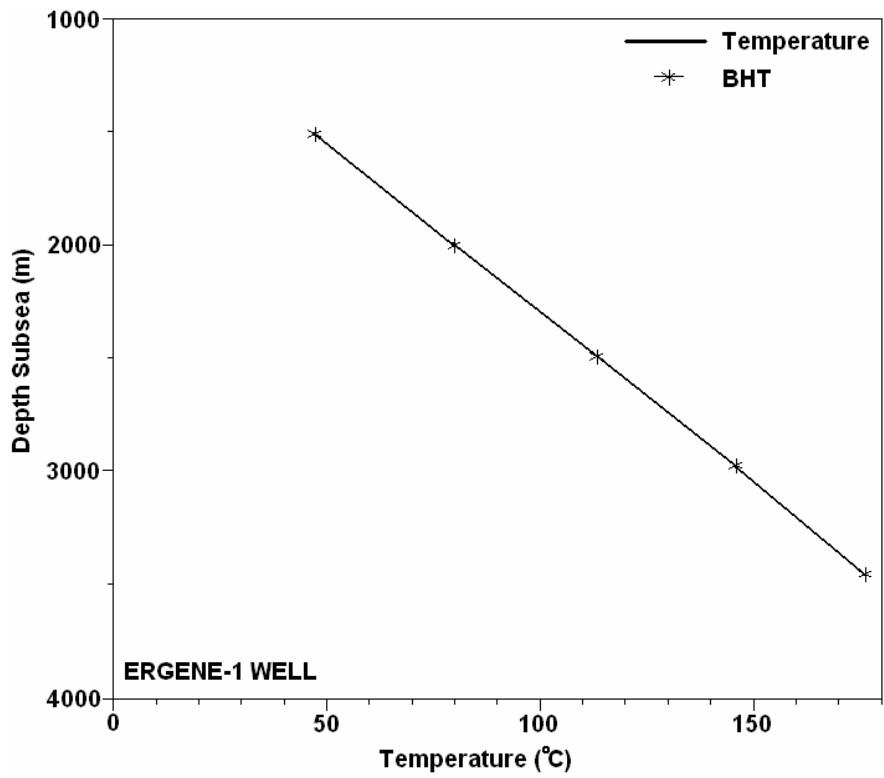
Figure 11. Average paleo-thermal gradients of the Thrace Basin which are obtained from the MSR curves.

The method enables the determination of the best average paleo-thermal gradients for each well location. The thermal gradient value which is associated with the best fit between modeled and calculated maturity trends is predicted as the average paleo-thermal gradient of the particular location. The gathered best thermal gradients are mapped and shown in Figure 11. This thermal gradient map is created by contouring the average paleo-thermal gradient values which have been determined by the applied method. It should be noted that the distances between wells are variable and the uncertainty associated with the obtained thermal gradient values change accordingly. The uncertainty significantly decreases through the central-northern part of the Thrace Basin, where well spacing is relatively smaller.

Average paleo-thermal gradient values are valid under two assumptions. The first assumption we make is that only one thermal gradient trend is valid for one well location. This means that the temperature increases with a constant rate through depth interval. Thus, we do have a constant thermal gradient for each well location. In order to measure the validity of this assumption in Thrace Basin, measured BHT measurements are plotted versus depth for two of the wells (Figure 12). These two wells do also resample the other studied wells in the region where the temperature variation with depth is almost constant which is related to a single thermal gradient associated with the single particular well location. The second assumption we make is that there have not been a strict change in the paleo-thermal gradient structure of the Thrace basin until the present day. The validity of this assumption is also argued to a certain extend, in the first part of Chapter IV by discussing the Sevindik-1 Well and its burial history graph. Constant burial rate does usually create constant thermal gradients versus geologic time. Also, the lack of strong tectonic events such as inversion, indentation tectonics or reverse faulting enable assuming constant thermal gradient through time, particularly in the central parts of the basin where erosional events are almost ineffective.



(a)



(b)

Figure 12. Measured BHT from Kaynarca-1 (a) and Ergene-1 (b) wells and the predicted temperature trend versus depth.

For assessing the validity of this assumption, calculated thermal gradients from the wells using BHT measurements are compared with the best thermal paleo-gradient value gathered from the MSR curves. The fit or similarity between present day thermal gradient and average paleo-thermal gradient show that thermal gradient is not strongly disturbed and/or changed in the geologic history of the basin. When compared, only 6 of the 70 wells show more than 10% variation between predicted and measured thermal gradient values (Appendix D). MSR value between the predicted (modeled) and calculated (measured from BHT) thermal gradients is calculated as 4.9 which indicates a proper agreement between the modeled average paleo-thermal gradients and the measured present day thermal gradients. This shows that the average paleo-thermal gradient observed in the Thrace Basin during the geologic history is similar to the present day thermal gradient.

Besides determining average paleo-thermal gradient, the method enables the application of sensitivity, uncertainty and resolution analysis on the data set and the constructed model. For example, for Abalar-1 well, the best value for the thermal gradient is determined to be 32 °C/km corresponding to the minimum on the misfit function. This point (minimum MSR) represents the best fit of measured to modeled vitrinite reflectance. The lower and the upper limits of the acceptable range of the parameter for this well are determined to be 21.2 and 40.9 °C/km (Appendix C). This is done by constructing a 90% confidence interval on the upper limit of the best value as explained in the methodology chapter in detail. This means that the usage of 21.2 to 40.9 °C/km thermal gradients in a model would honor the 90% of the measured vitrinite reflectance data. This could be evaluated as a high uncertainty range from basin modeling point of view.

Thermal gradient is intimately connected to the uncertainty associated with the scatter in the data where model had limitations in resolving paleo-thermal gradients calculated using the Easy%Ro algorithm. As a result we do calculate a wide uncertainty range.

### **3.2. Statistical Assessment of Sensitivity, Resolution and Uncertainty on Thermal Gradients and MSR Curves**

The range of the uncertainty is related with the resolution. Resolution and uncertainty are inversely related. Resolution, which is a measure of the ability of a model to resolve the paleo-thermal gradients from the vitrinite reflectance data, could be measured from the shape of the misfit (MRS) function. While a high resolution is related with a “V” shaped misfit function, a low resolution show a flat based MSR curve. For example, the misfit functions gathered at Hamitabat-1 and Ergene-1 well locations are associated with high resolution and low uncertainty range. However, Arızbaba-1 and Delen-1 show wider uncertainty range and lower resolution. This analysis also gives clues about the quality of the data set and the scatter associated with the vitrinite reflectance values. The more scattered the data, the less sensitive the model gets and the less resolution is gathered. Thus, by using the method, the data which fall outside the limits of the 90% uncertainty range could be rejected.

It should be noted that the chosen confidence interval is subjective and may vary depending on the individual uncertainty range associated with a given level of confidence.

Besides uncertainty, sensitivity analysis could be performed using the MSR functions. It is observed that all of the misfit functions except Meriç-2 has a steeper right flank compared to the left one. This means that most of the basin models constructed in the Thrace Basin are more sensitive to higher temperatures than the lower ones. In other words, the use of a wrong or an unknown thermal gradient as an input parameter for a model does not have influence on the model result as much as the use of a thermal gradient at higher ends. Thus, if not known or predicted, it is suggested to the basin modelers to work with low thermal gradients for sustaining an average fit between the paleo-heat flux and the pre-assumed thermal history.

As argued above, for vitrinite reflectance, the right flank (higher thermal gradients) of the function shows higher sensitivity to changes in the thermal gradient (steeper than the left flank, the upper limit of curve). The absolute boundaries for vitrinite reflectance changes with depth are from 0 to

infinity. The boundaries for vitrinite reflectance below the best fit are limited between 0 and the best fit value. However, the vitrinite reflectance above the best fit value departs from the best fit and goes to infinity within the increase of the heat. Thus, the modeled maturity profile is expected to vary significantly from the measured especially within the variations higher than the best fit.

### **3.3. Geological Interpretation of the Thermal Gradients in Thrace Basin**

The best paleo-thermal values predicted using the misfit functions are ranked for investigating the relation between thermal gradient and geological processes (Figure 13).

Thrace Basin can be classified as moderate-high heated basin. The thermal gradients observed in the Thrace Region are above the world average. While the Babaeski-1 and İpsala-1 wells are showing the lowest thermal gradient as 26 °C/km, the highest gradient is tested as 43 °C/km at K.Marmara-3 Well. The average thermal gradient gathered from the studied wells is 34.7 °C/km. It is observed that, the central part of the basin is associated with lower thermal gradient compared to the margins of the basin. This is a significant signature of the fossil rift basins or rift basins which are in the post rift stage (Şengör, 1995).

The lateral changes in thermal gradient in the Thrace Basin are investigated and the link between thermal gradient and geological properties is established.

It is observed that most of the heat is concentrated to the margins of the basin. Particularly, northeastern margin of the Thrace Basin, where the sediment starvation is observed, show quite to very high thermal gradient values. Also, high thermal gradients are observed at the Western edge of the basin.



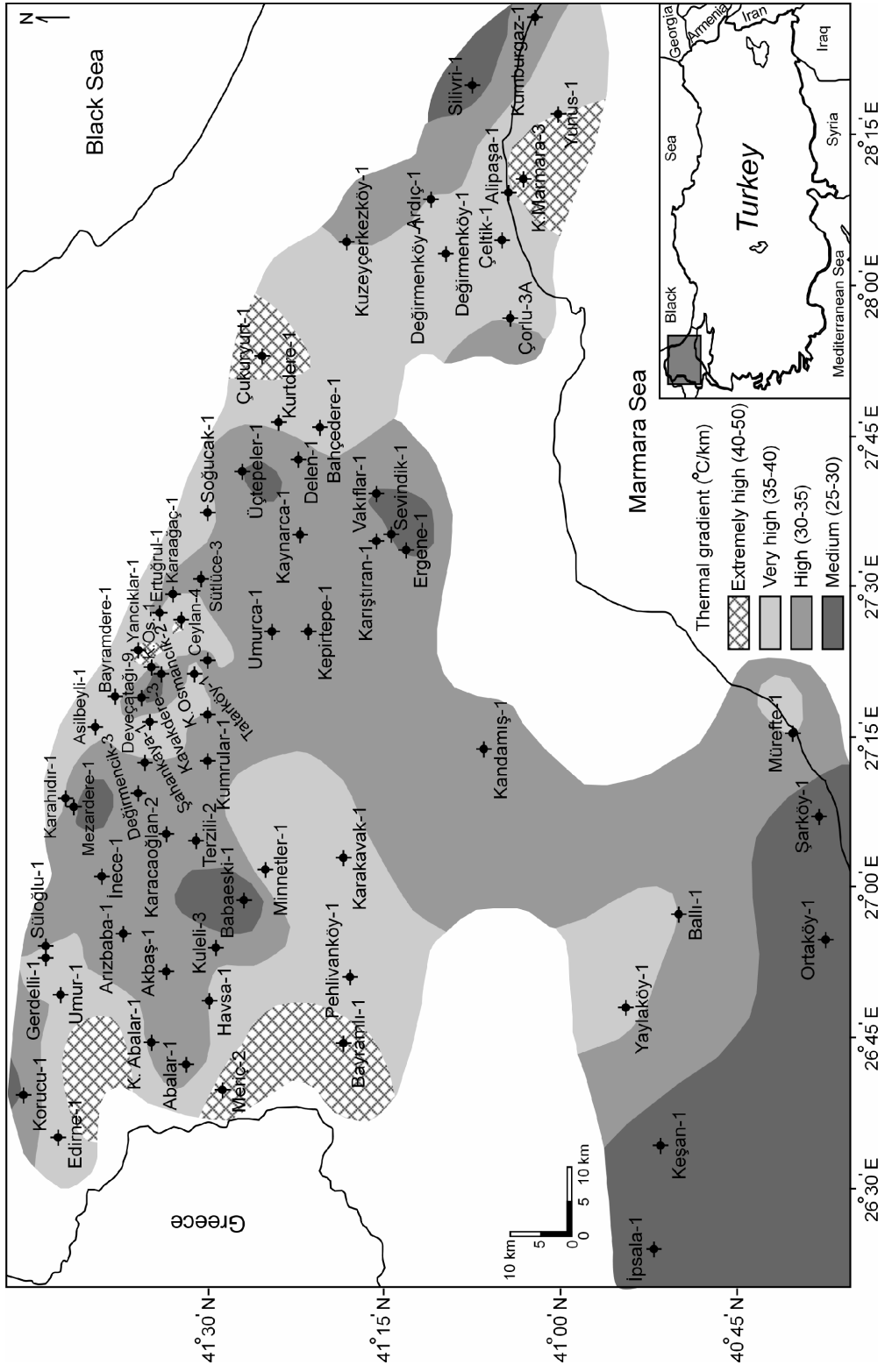


Figure 13. Average paleo-thermal gradients created using the bestfit values which are obtained from the MSR curves. Thermal gradients are ranked using the value windows

The variations in thermal gradients from the depocenter (central part) through the edges are associated with the following geological processes and events:

- 1- Basement edge effect,
- 2- Crustal thickness variations and basement heat flow,
- 3- Lateral thermal conductivity variations,
- 4- Transient heat flow affect,
- 5- Influence of the tectonic features.

### 3.3.1. Basement Edge Affect

The edges of the basins and/or graben margins are usually associated with high heatflux (Figure 14). Heat prefers to be retained in the highly conductive rock by focusing the heat into the graben margin resulting heat anomalies at the edge of the graben (Yu et al., 1995).

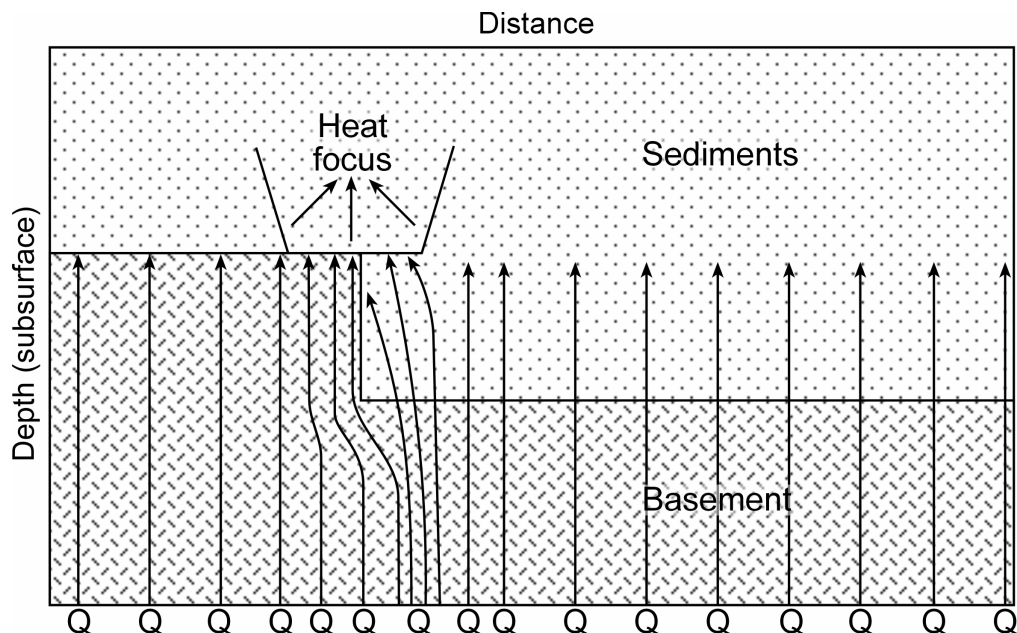


Figure 14. Concentration of heat to the edge of the graben margin due to the heat that is preferred to be retained in the highly conductive basement rock rather than being transferred into the relatively low conductive sediments (Q: Heat flow) (Modified from Yu et. al, 1995).

The basement edge effect is traced on a line between the sedimentary depocenter of the basin and the Strandja Mountains where the sediment are starved abruptly at northern edge of the Basin (Figure 15).

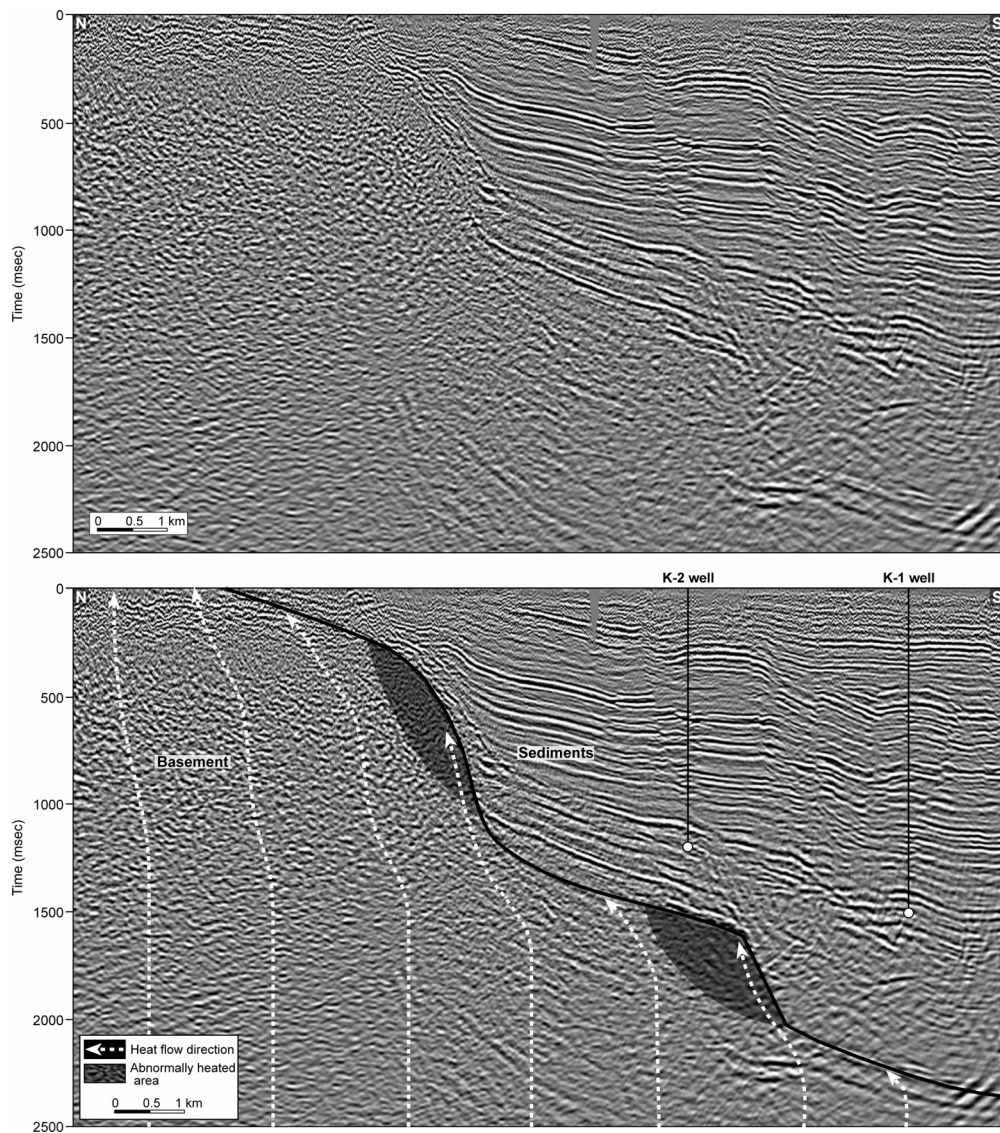


Figure 15. Uninterpreted and interpreted seismic sections from the northern Thrace Basin. Sedimentary pile truncates and pinches out through north where the basement edge is bound by the Strandja Mountains. Heat flow paths are shown by white dash lines and arrows and the abnormally heated areas are painted to transparent dark gray. Heat flow paths, simulating heat transfer directions within the basement, are controlled by the geometry of the basement-sediment contact geometry. Heat prefers to be retained in the basement which has higher thermal conductivity than the sediments. Location of the seismic section and the wells (K-1 and K-2) are shown on Figure 8.

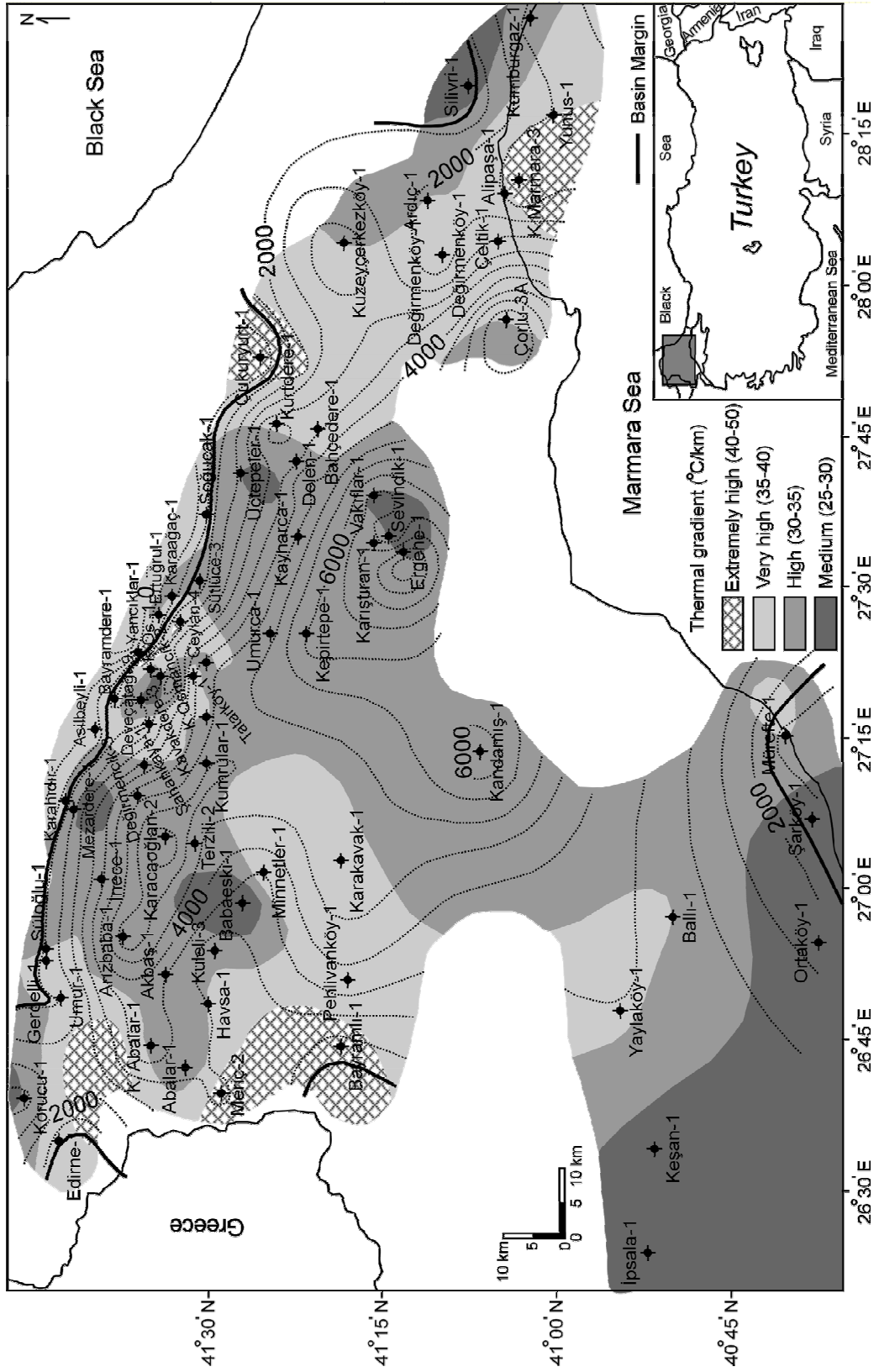


Figure 16. Total sediment thickness map of the Thracian Basin and basin margins overlain by thermal gradient windows.

In order to investigate the influence of basement edge effect on variation of thermal gradients, total sediment thickness map is created using the 70 wells (Figure 16). Only the northern and northwestern margins of the Thrace Basin have a steep margin. Thus, graben or basement edge effect play a major role in controlling lateral variation of thermal gradients only at the northern and northwestern margins of the basin. But has almost no effect at the southern and eastern margins.

### 3.3.2. Crustal Thickness Variations and Basement Heat Flow

As indicated in the section 1.2.2 and is validated using examples from various studies from different basins (Table 1), the major thermal source affecting the sediments in a basin is the radiogenic heat generated within the upper crust. Thus, necessity of determining heatflux made crustal modeling a central theme in basin modeling (Hopper and Buck, 1996).

Almost all of the industrial basin modeling software, particularly 3D modules, would require a crustal model for determining the amount of radiogenic heat produced in the upper crust and entered through sediments from the basement. The thicker the crust, higher the radiogenic heat produced within the upper crust (Figure 17).

According the basement heatflow concept, inner parts of the basin where the sediment load is higher and the crust is thinner, due to the isostasy, is expected to be cooler compared to the areas with a thicker upper crust. Thus, the thermal gradient is expected to increase through the highs such as Strandja Mountains.

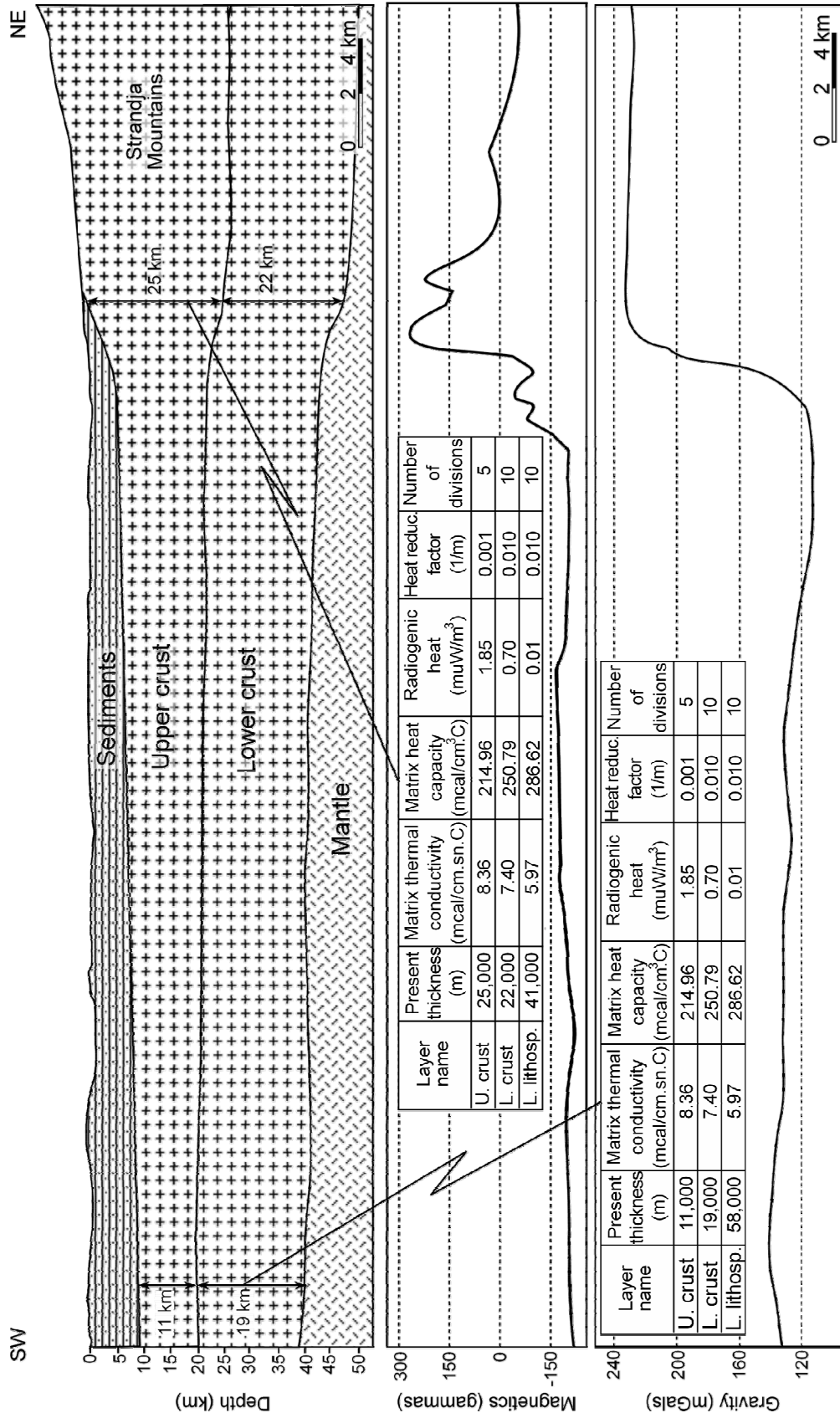


Figure 17. Crustal thickness model created using gravity and magnetic data. Basement heat flow parameters for calculation of heat generated by radiogenic minerals within the upper crust are demonstrated in tables (Personal communication: Yüksel, 2005)

### 3.3.3. Lateral Thermal Conductivity Variations

Thermal conductivity of the sediments is one of the major factors effecting the thermal gradient variation in a basin. Not only the matrix but the liquid conductivity is important by means of heat transformation through the sediments. Different lithologies have different thermal conductivity values according to their composition (Table 3). For instance, thermal conductivity of sandstone is approximately four times greater than shales. Thus, sandstone transmits heat four folds efficiently than shale. In consequence, it is expected to have lower thermal gradient values where a thicker shale deposition is observed due to the heat transfer reduction from the crust through the surface which is a function of low thermal conductivity of the shale.

Table 3. Thermal conductivity of various lithologies and rocks (Brigaud and Vasseur, 1989) (TC: thermal conductivity).

Lithology	TC (mcal/cm sec)	TC (W/m °C)
Limestone	4.7-7.0	1.9-3.0
Dolomite	4.7-13	1.9-5.4
Anhydrite	12.1	5.06
Marl	2.2-6.6	0.9-2.8
Mudstone	3.07-5.5	1.5-2.3
Shale	1.4-7.0	0.6-2.9
Sandstone	4.7-17.7	1.9-7.4
Quartzite	8.9-17.9	3.7-7.5
Chalk	6.9	2.9
Halite	14.1	5.90
Gypsum	2.5	1.05
Basalt	3.6	1.5
Dunite	9.75-13.5	4.0-5.6
Diabase	4.5-5.3	1.9-2.2
Granite	5.3-8.0	2.2-3.4

A thermal conductivity survey interconnected with experimental thermal conductivity measurements performed on the cores taken from various wells in Thrace basin is performed by Geophysical Survey Department of MTA (Table 4). Ceylan formation shows lower thermal conductivity compared to the others. Thus, it is expected to lower the thermal gradient by blocking the heat transfer from crust through the surface.

Table 4. Arithmetic average of various thermal conductivity measurements performed on cores (Appendix E) taken from different wells and formations in the Thrace Basin (Engin, 1999).

Number of	Formation name	Number of	Thermal conductivity
2	Danişmen	65	3.0162
3	Mezardere	54	2.8624
8	Ceylan	73	1.7580
2	Ceylan (tuff)	38	0.9511
13	Hamitabat	55	2.4220
18	Hamitabat (deep)	29	2.8936
Surface	Koyunbaba	7	2.6736

Besides thermal conductivity values, thickness of the formations are important in evaluating the amount of heat transferred through sediments. From this point of view, Ceylan is also expected to have high influence on the thermal regime due to its thickness variation from 400 to 1000 meters and its basin scale lateral continuity (Figure 18).

#### 3.3.4. Transient Heat Flow Affect

A transient heat flow model is one of the most developed algorithms which handle heat transfer in the basin in a significantly realistic way (Schegg et al., 1999). According to the transient heat flow concept, temperature of a sediment layer varies not only by the absorbed amount of heat but also over time (Bethke, 1985). The model is consisting of diffusive and adjective thermal transformation schemes (Jessop, 1990; Lerche, 1990a; Lerche, 1990b). This effect accounts for loss of heat in the sediment column due to the heat capacity of the sediments. Thus, younger sediments tend to be cooler compared to the older ones. The areas of high sediment influx are associated with low thermal gradient due to the transient heat flow affect of the younger, cooler and recently derived immature sediments that have a reduction effect on the thermal gradients.

The sediments deposited at the depocenter of Thrace Basin are cooler and thicker (Figure 16) compared to the marginal thinner sediments. Thus,



central part of the basin, where sediment thickness is greater, shows low thermal gradients due to the transient heat flow affect.

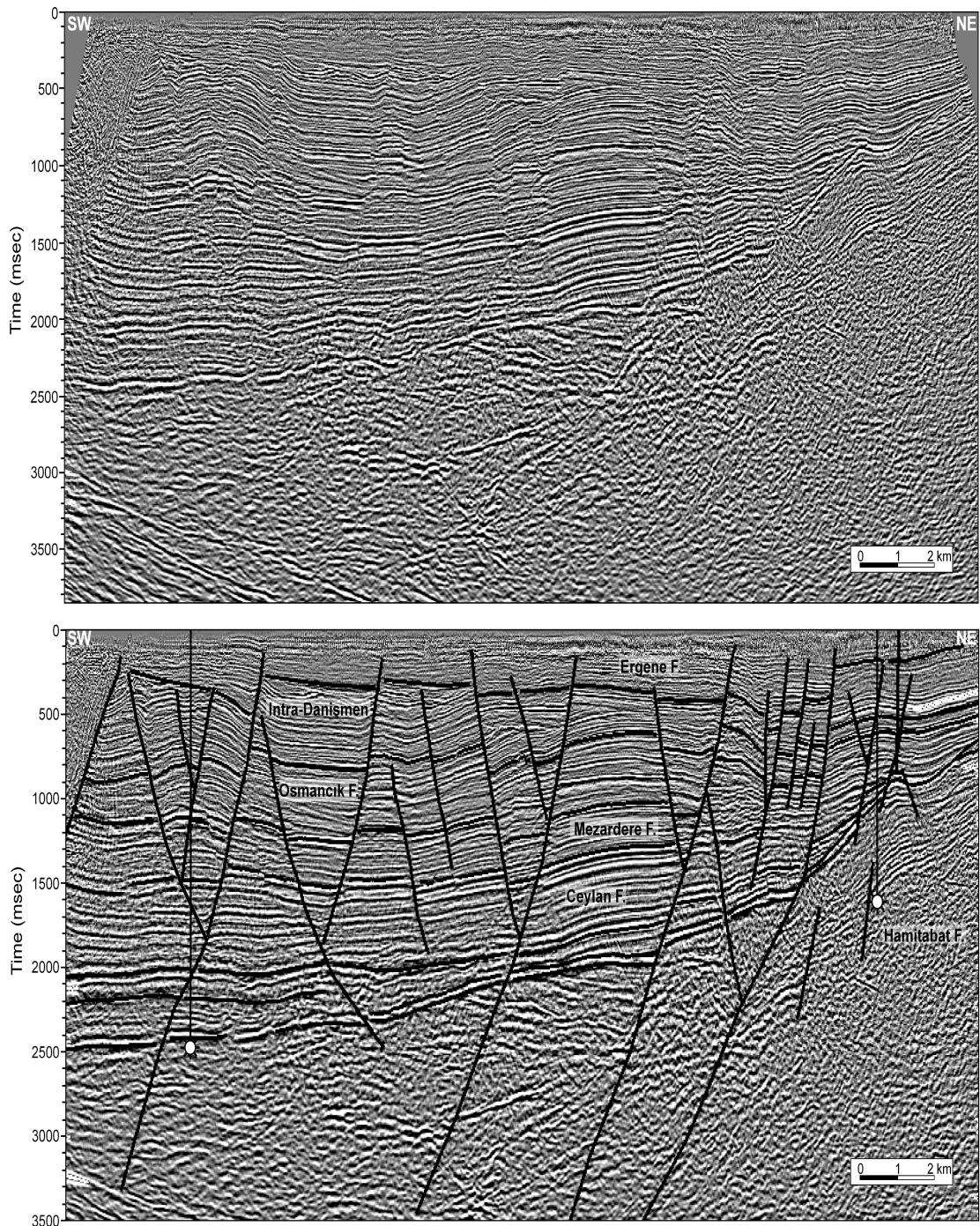


Figure 18. Regional seismic section from SE to NW showing thickness variation of the Ceylan Formation from the depocentre through the margin of the basin. Location of the seismic section is shown on Figure 8 (from Huvaz et al., in press).

### 3.3.5. Influence of the Tectonic Features

Three of the major fault systems of the Thrace Basin: (1) Kirklareli Fault Zone; (2) Lüleburgaz Fault Zone; (3) Babaeski Fault Zone creates a NW-SE aligning structural trend (Figure 19). These fault systems correspond to the Upper-Middle Miocene period and almost all of them are buried, particularly in the central part of the basin, in the present day.

However, a direct relation between the major structural trend and the variation of the thermal gradient could not be established (Figure 19). This may arise from three major reasons: (1) Most of the fault systems which penetrate to the deeper intervals are not working in the present day, thus, they do act as thermal seals rather than a fluid conduit which may transport high temperature fluids through the shallow depths and enable formation of an abnormal thermal gradient system; (2) Structural features do not necessarily play a significant role in controlling the thermal regime compared to the other factors such as lateral thermal conductivity variation and crustal configuration; (3) Due to the steady burial rate, continued since the Early Eocene, corresponding to the almost constant sedimentation rate enabled the creation of a pressure system which is at equilibrium during the geologic time and the present day.

Thus, in the lack of abnormal or subnormal pressure system (excess pressure), fluid movements through the pores are mostly limited which suppresses the efficiency of the available fault systems in plumbing thermal fluids both vertically and laterally in the basin.

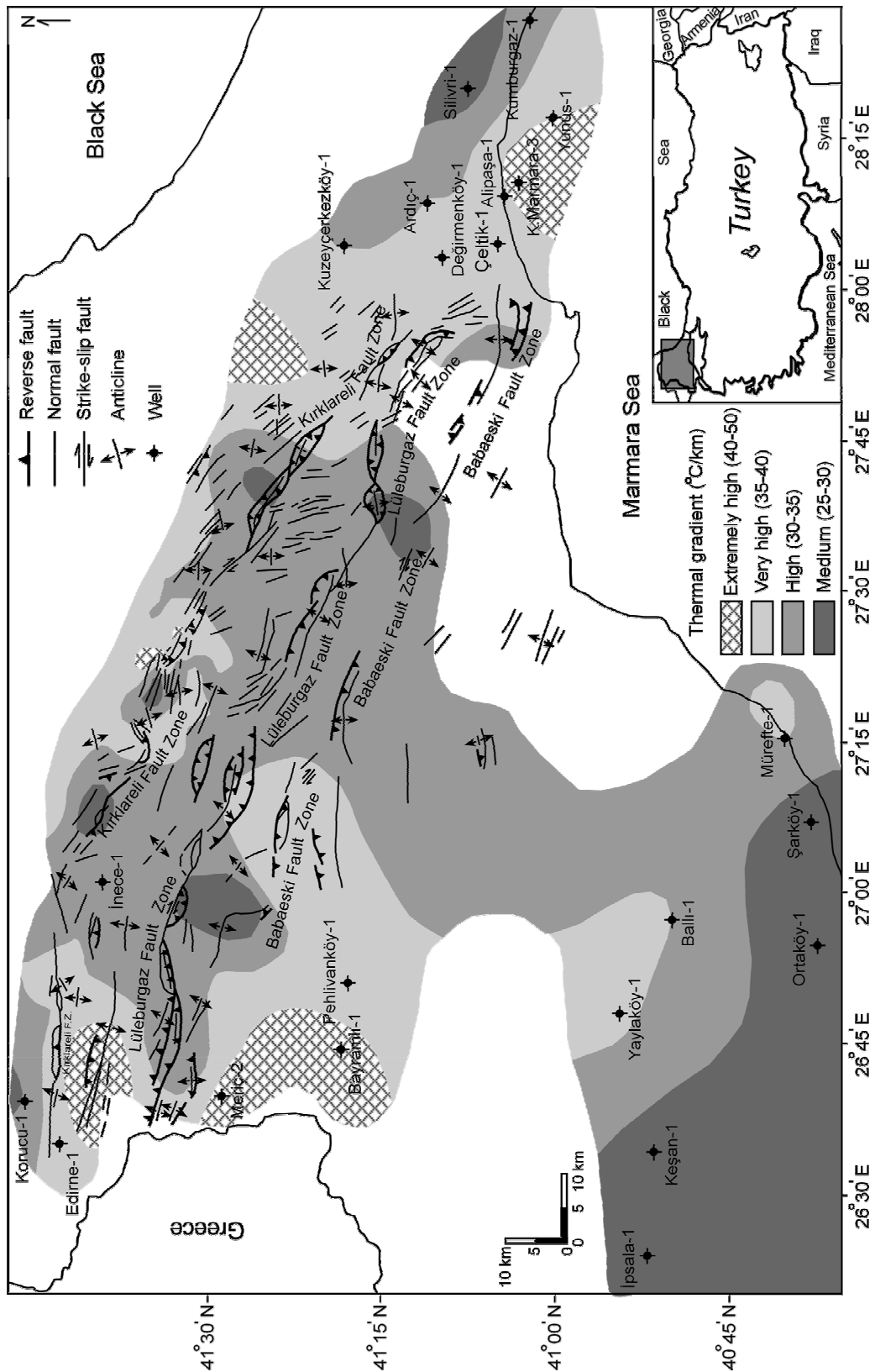


Figure 19 Miocene structures of the Thrace Basin (Modified from Perinçek, 1991).

## CHAPTER IV

### DISCUSSION AND CONCLUSIONS

#### 4.1. Discussion

The maturity level of a source rock is controlled by the thermal history and this should be determined with the highest accuracy possible (Nielsen, 1996). Maturity modeling should be performed using a well established relationship between the thermal history and thermal indicators such as %Ro (Armagnac et al., 1988).

The best thermal gradient value for each well is estimated from the MSR curve by obtaining the lowest MSR which refers to the minimum mismatch between the observed and modeled %Ro values. The best gradient (best fit) determined for each well is compared to the results of the previous thermal gradient studies (Siyako, 1984) in the area (Appendix D). This comparison clearly indicates that the thermal history of the study area can in general be resolved from the calibration data, and that the thermal stress can be assessed using the presented method.

In addition to calculation of the average thermal gradient history, the applied method enables evaluating the validity of model results by assessing uncertainty range of various parameters, obtained by the model (e.g. the thermal gradient). The shape of the MSR curve enables a quick assessment of the quantitative limits of the thermal gradients for each well within a 10% uncertainty range (90% confidence interval), which translates into a range of variation of the modeled parameter between an upper and lower envelope around the best fit. Thus, the limits of variation, in this parameter, which cannot be said to be statistically significant (so-called “resolution limits”) can be determined (Huvaz et al., 2005). The range of uncertainty associated with a given confidence level is related to the shape of the misfit function, which in turn is a result of the underlying model Easy%Ro and scatter in the data.

The shape of the MSR curve indicates the sensitivity of the fit between the modeled and measured values controlled by the variation of the investigated parameter which is directly related to the scatter in the calibration data (Huvaz et al., 2005). If one flank of the misfit function is steeper than the other, this indicates that results are more sensitive to changes in the domain of the steeper flank values of the parameter. However, it should be noted that for the vitrinite reflectance, the right flank of the MSR curve is typically steeper than the left, close to the upper limit of the curve (Huvaz et al., 2005). The upper limit of the gradient is therefore better determined than the lower limit, and departure of the modeled %Ro from the “best fit” is more dramatic for  $TG_{best} + \Delta T$  than  $TG_{best} - \Delta T$ . This also shows that the model is more sensitive against the abnormal thermal gradient (high geothermal gradients) values compared to the lower end, where misfit between measured and calculated %Ro values is much lower.

#### **4.2. Conclusions**

Similarity between the gradient values, obtained using the applied method (average paleo-thermal gradients), and present day measured thermal gradients (from BHT) indicates that, Thrace Basin was undergone a steady thermal gradient history without major thermal fluctuations during Tertiary period. Only 6 of the 70 wells show more than 10% variation between predicted and measured thermal gradient values. This argument is also supported by the burial history data, which demonstrates an almost constant burial rate from 53 Ma to the present day, except two recent erosional periods.

Thermal gradients in the Thrace Basin changes in a wide range from 26 to 43 °C/km which is associated with any or combination of the following factors: 1) basement edge affect; 2) crustal thickness variations and basement heat flow; 3) lateral thermal conductivity variations; 4) transient heat flow affect; and 5) influence of the tectonic features. Structure map of the Hamitabat Formation which also resembles the total sediment thickness of the basement shows that sediment starvation through the edges of the

basin is gradual except the northern margin. Thus, graben or basement edge effect is not a major driving mechanism for the lateral changes of the thermal gradients at western, southern and eastern margins of the Thrace basin. However, it significantly affects thermal gradients at the northern margin, where the basin margin has a steeper geometry.

## REFERENCES

- Akartuna, M., 1953, Çatalca–Karacaköy bölgesinin Jeolojisi, İstanbul University, Faculty of Science Monographies, v. 13, p. 1-88.
- Arıç, C., 1955, Haliç-Küçükçekmece Gölü bölgesinin jeolojisi, PhD Thesis, İstanbul Technical University, Faculty of Mines, 120 p.
- Armagnac, C., Kendall, C., Kuo, C., Lerche, I. and Pantano, J., 1988, Determination of paleoheat flux from vitrinite reflectance data, and from sterane and hopane isomer data: Journal of Geochemical Exploration, v. 30, no. 1, p. 1-28.
- Aydın, M.M., 1974, Etude petrographique et geochemique de la parti centrale du massif d'Istrance (Turquie), PhD Thesis, Nancy University, 100 p.
- Aydın, M.M., 1982, Yıldız Dağları (Istranca) masifinin jeolojisi, Thesis for Associate Professorship, İstanbul Technical University, 106 p.
- Aydın, M.M., 1988, Yıldız Dağları Masifinin Jeolojisi, Selçuk University, Architecture and Engineering Faculty Bulletin, Selçuk Üniv. Müh. ve Mimarlık Fak. Dergisi, v.2, p. 61-74.
- Bethke, C.M., 1985, A numerical model of compaction-driven groundwater flow and heat transfer and its application to the paleohydrology of intracratonic sedimentary basins, Journal of Geophysical Research, v. 90, p. 6817-6828.
- Birch, F., Roy R.F. and Decker, E.R., 1968, in: Studies of Appalachian Geology: Northern and Maritime, Zen, E., White, W.S., Hadley, J.B. and Thompson, J.B. Jr., eds., Interscience, New York, p. 437-451.
- Bostic, J.L., Nuelle, L.M., Smith, D.C., Carter, M.D., Rega, N. and Krohn, K.K., 1989, Calculation of coal resources of the Bronaugh 7 1/ 2' Quadrangle, southwestern Missouri, using the National Coal Resources Data System, U.S. Geological Survey Circular no. 1043, p. 1-4.
- Brigaud, F. and Vasseur, G., 1989. Mineralogy, porosity and fluid control on thermal conductivity of sedimentary rocks, Geophysical Journal, v. 98, p. 525-542.

- Burnham A.K., and Sweney, J.J., 1989, A chemical kinetic model of vitrinite maturation and reflectance: *Geochimica et Cosmochimica Acta*, v. 53, no. 10, p. 2649-2657.
- Bürkan, K.A., 1991, Trakya Havzasının organik jeokimyasal değerlendirmesi, TPAO Company Report, no. 2988, 55 p.
- Castano, J.R. and Sparks, D.M., 1974, Interpretation of vitrinite reflectance measurements in sedimentary rocks and determination of burial history using vitrinite reflectance and authigenic minerals, in: *Carbonaceous materials as indicators of metamorphism*, Dutcher, R.R., Hacquebard, P.A., Schopf, J.M. and Simon, J.A. eds., Geological Society of America Special Paper no. 153, p. 31-52.
- Chatalov, G.A., 1985a, Stratigraphy of the Jurassic system in Strandzha area, Bulgaria, *Geologica Balcanica*, v. 15, no. 4, p. 3-39.
- Chatalov, G.A., 1985b, Stratigraphy Strandzha-type Triassic (Strandzha Mountain, southeast Bulgaria), *Geologica Balcanica*, v. 15, no. 6, p. 3-38.
- Corrigan J. and Bergman, S., 1996, Thermal modeling and interpretation of thermal indicator data: Annual Meeting Abstracts - American Association of Petroleum Geologists and Society of Economic Paleontologists and Mineralogists, v. 5, p. 1-30.
- Coşkun, B., 2000, Influence of the Istranca-Rhodope Massifs and strands of the North Anatolian Fault on oil potential of Thrace Basin, NW Turkey, *Journal of Petroleum Science and Engineering*, v. 27, p. 1-25.
- Çağlayan, A.M., Şengün, M. and Yurtsever, A., 1988, Main fault systems shaping the Istranca Massif, Turkey, METU, *Journal of Pure Applied Science, Serie A Geosciences*, v. 21, p. 145-154.
- Çağlayan, A.M. and Yurtsever, A., 1998, Burgaz-A3, Edirne-B2 ve B3; Burgaz-A4 ve Kırklareli-B4; Kırklareli-B5 ve B6; Kırklareli-C6 paftaları, 1:100 000 ölçekli açınısama nitelikli Türkiye jeoloji haritaları, General Directorate of Mineral Research and Exploration maps, no. 20, 21, 22 and 23.
- Doust, H. and Arıkan, Y., 1974, The geology of the Thrace Basin: *Proceedings of the 7<sup>th</sup> Petroleum Congress of Turkey*, p. 119-136.



- Dow, W., 1977, Kerogen studies and geological interpretations, *Journal of Geochemical Exploration*, v. 7, p. 79-99.
- Druitt, C.E., 1961, Report on the petroleum prospects of Thrace – Turkey, TPAO Company Report, no. 1427, 20 p.
- Ediger, V.Ş., 1982, Kuleli-Babaeski sırtı (kuzey batı Trakya'nın) paleo-ortamsal incelenmesi ve kuzey Trakya Havzasının hidrokarbon potansiyelinin değerlendirilmesinde yeni bir yaklaşım, TPAO Company Report, no. 1995, 194 p.
- Ediger, V.Ş. and Batı, Z., 1987, Detailed stratigraphic, sedimentologic and palynologic investigation of the Hamitabat Formation from the Hamitabat-25 well, TPAO Company Report, no. 1185, 1250 p.
- Ediger, V.Ş., Gurgey, K. and Batı, Z., 1988, Kuzey Trakya Havzasında açılan Hamitabat Formasyonuna ait polimorfların cluster ve PCA analizleri, TPAO Company Report, v. 2515, 250 p.
- Ediger, V.Ş., Batı, Z. and Alişan, C., 2003, Paleopalynology and paleoecology of Calamus-like disulcate pollen grains, *Review of Palaeobotany and Palynology*, v. 62, p. 97-105.
- Engin, M. E., 1999, Trakya Bölgesindeki bazı kuyulara ait değişik formasyonların ısı iletkenlik katsayıları: Research Group Thermal Study Documents, 4 p.
- Gallagher, K., and Sambridge, M., 1992, The resolution of past heat flow in sedimentary basins from non-linear inversion of geochemical data: the smoothest model approach, with synthetic examples: *Geophysical Journal International*, v. 109, no.1, p. 78-95.
- Gerhard, J.J., and Alişan, C., 1986, Palynostratigraphy, paleoecology and visual organic geochemistry, Turgutbey-2, Değirmencik-3 and Pancarköy-1, Thrace Basin Turkey, TPAO Company Report, no. 983, 80 p.
- Gopel C., Manhès, G. and Allegre, C.J., 1985, Concordant 3,676 Myr. U-Pb formation age for the Kodaikanal iron meteorite, *Nature*, v. 317, p. 341-344.

- Gökçen, N., 1971, Güneydoğu Trakya'nın Paleojen stratigrafisinde Ostracod'lar açısından yeni görüşler, Proceedings of the First Petroleum Congress of Turkey, p. 81-85.
- Gökçen, N., 1973, Pınarhisar Formasyonu'nun yaşı ve ortam şartlarında görülen yanal değişimler (Kuzey, Kuzeydoğu Trakya), Proceedings of the 50<sup>th</sup> Earth Sciences Congress, p. 128-142.
- Görür, N. and Okay, A., 1996, A fore-arc origin for the Thrace Basin, NW Turkey, Geologische Rundschau (International Journal of Earth Sciences), v. 85, p. 662-668.
- Gürgey, K., 1999, Geochemical characteristics and thermal maturity of oils from the Thrace Basin (western Turkey) and western Turkmenistan, Journal of Petroleum Geology, v. 22, no. 2, p. 167-189.
- Haack, U., 1983, Regional metamorphism in the Damara orogen, Earth Planetary Science Letters, v. 62, p. 360-373.
- Harput, O.B., İlleez, H.I. and Göker, T., 1991, Trakya Havzası, Karacaoğlan-2,3A; Delen-1; K. Çerkezköy-1; Habiller-2; Çorlu-2/A ve Kexan-1 kuyuları olgunlaşma ve kaynak kaya değerlendirmesi, TPAO Company Report, no. 2865, 62 p.
- He, Z. and Lerche, I., 1992, Determination of paleoheat-flux using multiple thermal indicator tomography, Mathematical Geology, v. 24, no. 7, p. 825-845.
- Holmes, A.W. Jr., 1961, A stratigraphic review of Thrace, American Overseas Petroleum Ltd. Company Report, 78 p.
- Hopper, R. J. and Buck, W.R., 1996, The effect of lower crustal flow on continental extension and passive margin formation, Journal of Geophysical Research, v. 101, no. B9, p. 20175-20194.
- Houseknecht, D.W., Bensley, D.F., Hathon, L.A. and Kastens, P.H., 1993, Rotational reflectance properties of Arkoma basin dispersed vitrinite, insights for understanding reflectance population in high thermal maturity regions: Organic Geochemistry, v. 20, p. 187-196.
- Huvaz, O., 2003, An inverse method for determining various basin parameters using the basin modeling tools, thermal regime of the Thrace

- Basin: 14<sup>th</sup> International Petroleum and Natural Gas Congress and exhibition of Turkey, p. 150-157.
- Huvaz O., Thomsen, R.O. and Noeth, S., 2000, Investigation of the Resolution Limits of Easy%Ro by Inversion, Proceedings of the 2000 America Association of Petroleum Geologists Annual Convention, New Orleans, Louisiana, USA, p. 46-51.
- Huvaz, O., Thomsen R.O. and Noeth, S., 2005, A method for analyzing thermal gradient history using the statistical assessment of uncertainties in maturity models, Journal of Petroleum Geology, v.28, no. 2, p.3-14.
- Huvaz, O., Sarikaya, H. and Nohut, O.M., in press, Nature of a regional dogleg pattern in maturity profiles of the Thrace Basin, Northwestern Turkey: A newly discovered unconformity or a thermal anomaly?, American Association of Petroleum Geologists Bulletin.
- İlleez, H.I., 1984, Trakya Bölgesi petrolerinin ve kondensatların organik jeokimyasal değerlendirilmesi, TPAO Company Report, no. 1971, 28 p.
- İlleez, H.I., 1985, A study of timing of hydrocarbon generation in the Northern Thrace Basin, METU, PhD Thesis, 140 p.
- İztan, Y.H., 1994, İğneada-1 kuyusunda gözlenen hidrokarbon kirlenmesinin jeokimyasal değerlendirilmesi, TPAO Company Report, no. 3417, 29 p.
- Jessop, A.M., 1990, Thermal geophysics, Developments in solid earth geophysics, New York, Elsevier, v. 17, 306 p.
- Karahanoğlu, N., Erler, A. and İlleez, H.İ., 1995, Mathematical approach to hydrocarbon generation history and source rock potential in the Thrace Basin, Turkey, Marine and Petroleum Geology, v. 12, n. 6, p. 587-596.
- Kasar, S. and Eren, A.A., 1986, Kırklareli–Saray–Kıyıköy bölgesinin jelojisi, TPAO Company Report, no. 2208, 45 p.
- Kasar, S., Bürkan, K.A., Siyako, M. and Demir, O., 1983, Geology and hydrocarbon potential of the Tekirdağ–Şarköy–Keşan-Enez area, TPAO Company Report, no. 1771, 80 p.
- Kemper, E., 1961, The Kırklareli limestone (Upper Eocene) of the northern basin rim, General Directorate of Petroleum Affairs Company Report, 37 p.

- Keskin, C., 1971, Pınarhisar alanının jeolojisi, Turkish Geological Society Bulletin, v. 14, p. 31-84.
- Keskin, C., 1974, The stratigraphy of the northern Ergene basin-Thrace, Proceedings of the 2<sup>nd</sup> Petroleum Congress of Turkey, p. 137-163.
- Kilby, W.E., 1988, Recognition of vitrinite with non-uniaxial negative reflectance characteristics: International Journal of Coal Geology, v. 9, no. 3, p. 267-285.
- Larter, S., 1989, Chemical models of vitrinite reflectance evolution: Geologische Rundschau, v. 78, no. 1, p. 349-359.
- Lerche, I., 1988, Inversion of multiple thermal indicators; quantitative methods of determining paleoheat flux and geological parameters; II, Theoretical development for chemical, physical, and geological parameters, Mathematical Geology, v. 20, no. 2, p. 73-96.
- Lerche, I., 1990a, Basin analysis: Quantitative methods, Academic Press Inc. New York-London-Tokyo, v. 1, 562 p.
- Lerche, I., 1990b, Basin analysis: Quantitative methods, Academic Press Inc. New York-London-Tokyo, v. 2, 570 p.
- Lerche, I., Yarzab, R. E. and Kendall, C., 1984, Determination of paleoheat flux from vitrinite reflectance data, American Association of Petroleum Geologists Bulletin, v. 68, no. 11, p. 1704-1717.
- Letouzey J., Biju-Duval, B., Dorkel A., Gonnard, R., Kristchev, K., Montadert, L. and Sungurlu, O., 1977, The Black Sea: a marginal basin-geophysical and geological data, in: Structural history of the Mediterranean basins, Biju-Duval B., Montadert, L. eds., Editions Technip, Paris, p. 363-376.
- Lopatin, N., 1971, Temperature and geologic time as factors in coalification, Izvestiya Akademii Nauk SSSR Seriya Geologicheskaya, v. 3, p. 95-106.
- McKenzie, D., 1978, Some remarks on the development of sedimentary basins, Earth and Planetary Science Letters, v.40, p. 25-32.
- Mukhopadhyay, P.K., 1994, Vitrinite reflectance as maturity parameter, petrographic and molecular characterization and its applications to basin modeling, in: Vitrinite reflectance as a maturity parameter: applications

- and limitations, Mukhopadhyay, P.K. and Dow, W.G. eds., American Chemical Society Symposium Series 570, p. 1-24.
- Nicolaysen, L.O., Hart, R.J. and Gale, N.H., 1981, The redford radioelement profile extended to supracrustal strata at Carletonville with implications for continental heat flow, *Journal of Geophysical Research*, v. 86, p. 10653–10661.
- Nielsen, S. B., 1993, Uncertainties in resolving tectonic subsidence and palaeo heat flow in sedimentary basins, *Terra Abstracts*, v. 5, p. 1-21.
- Nielsen, S. B., 1996, Sensitivity analysis in thermal and maturity modeling, *Marine and Petroleum Geology*, v. 13, no. 4, p. 415-425.
- Noeth, S., Thomsen, R.O. and Littke, R., 2002, A method for assessing statistical Significance and uncertainties for calibration of 1-D thermal basin maturation models, *American Association of Petroleum Geologists Bulletin*, v. 86, no. 3, p. 417-431.
- N.V. Turkse Shell, 1969, AR/NTS/837,838 ve 839 hak sıra nolu arama sahalarına ait terk raporu, TPAO Company Report, no. 1408, 5 p.
- N.V. Turkse Shell, 1972, I nolu Marmara petrol bölgesinde N.V. Turkse Shell'in AR/NTS/832-836, 997-998 hak sıra nolu arama sahalarına ait terk raporu, TPAO Company Report, no. 769, 2 p.
- N.V. Turkse Shell, 1986, Tightgas study Thrace Basin, Turkey, TPAO Company Report, no. 2211, 120 p.
- N.V. Turkse Shell, 1988, Well proposal Kaynarca-2 Thrace Western Turkey, TPAO Company Report, no. 2402, 7 p.
- N.V. Turkse Shell, 1989, Geology and reservoir quality of the cored Hamitabat Formation (4313-4542) in well Kaynarca-2, Thrace Basin, Turkey, TPAO Company Report, no. 711, 65 p.
- Okay, A.I., Siyako, M. and Bürkan, K.A., 1990, Biga Yarımadası'nın jeolojisi ve tektonik evrimi, *Turkish Association of Petroleum Geologists Bulletin*, v. 2, p. 83-121.
- Okay, A.I., Satır, M., Tüysüz, O., Akyüz, S. and Chen, F., 2001, The tectonics of the Stradja Massif: Late-Variscan and Mid-Mesozoic deformation and metamorphism in the northern Aegean, *Geologische Rundschau*, v. 90, p. 217-233.

- Pamir, H.N. and Baykal, F., 1947, Istranca Masifi'nin jeolojik yapısı, Turkish Geological Society Bulletin v. 1, p. 7-74.
- Perinçek, D., 1991, Possible strand of the North Anatolian Fault in the Thrace Basin, Turkey-an interpretation, American Association of Petroleum Geologists Bulletin, v. 75, no. 2, p. 241-257.
- Rao, R.U.M. and Jessop, A.M., 1975, A Comparison of the Thermal Characters of Shields, Canadian International Earth Sciences, v.12, p. 347-360.
- Rao, R.U.M., Rao, G.V. and Narain, H., 1976, Radioactive heat generation and heat flow, in the Indian shield. Earth and Planetary Science Letters, v. 30, p. 57-64.
- Saltık, O., 1975, I. Bölge Malkara-Tekirdağ-Işıklardağı sahalarının jeolojisi ve petrol olanakları, TPAO Company Report, 918 p.
- Saner, S., 1980, Explanation of the formation of neighboring basins of Eastern Pontides by plate tectonics, NW Turkey, General Directorate of Petroleum Affairs Journal, v. 93/94, p. 1-20.
- Sass, J. H., Blackwell, D.D., Chapman, D.S., Costain, J.K., Decker, E.R., Lachenbruch, A.H., Lawver, L.A., Marshall, B.V. and Munroe, R.J., 1981, Heat flow from the crust of the United States, in: Physical Properties of Rocks and Minerals, Touloukian, Y.S., Judd, W.R. and Roy, R.F. eds., New York, p. 503-548.
- Schegg, R., Cornford, C. and Leu, W., 1999, Migration and accumulation of hydrocarbons in the Swiss Molasse Basin: implications of a 2D basin modeling study, Marine and Petroleum Geology, v.16, p. 511-531.
- Sclater, J.G., Jaupart, C. and Galson, D., 1980, The heat flow through oceanic and continental crust and the heat loss of the earth, Reviews of Geophysics and Space Physics, v. 18, no. 1, p. 269-311.
- Siyako, M., 1984, Temperature and thermal gradient of the Thrace Basin, TPAO Company Report, 30 p.
- Siyako, M., 2005, Trakya ve yakın çevresinin tersiyer stratigrafisi, TPAO Company Report, no. 4608, 104 p.
- Siyako, M. and Kasar, S., 1985, Edirne-Lalapaşa-Kırklareli bölgesinin jeolojisi, TPAO Company Report, no. 2062, 78 p.

- Sonel, N., 1981, Trakya Havzası kuzeyinin sedimantolojik modelinin saptanması, detay stratigrafisinin çıkartılması ve petrol olanaklarının araştırılması, TPAO Company Report, no. 1600, 73 p.
- Stach, E., 1968, Basic principles of coal petrology; macerals, microlithotypes and some effects of coalification, in: Coal and coal bearing strata, Murchison W.D. eds., University of Newcastle Upon Tyne, p. 3-17.
- Sweeney, J.J. and Burnham, A.K., 1990, Evaluation of a simple model of vitrinite reflectance based on chemical kinetics, American Association of Petroleum Geologists Bulletin, v. 74, no. 10, p. 1559-1570.
- Şengör, A.M.C., 1979, The north Anatolian transorm fault:its age, offset and tectonic significance, Journal of Geological Society of London, v. 136, p. 269-282.
- Şengör, A.M.C., 1995, Sedimentation and Tectonics of Fossil Rifts, in: Tectonics of sedimentary basins, Busby, C.J. and Ingersoll, R.V., eds., Blackwell Science, Cambridge, p. 53-118.
- Şengör, A.M.C. and Yılmaz, Y., 1981, Tethyan evolution of Turkey:a plate tectonic approach, Tectonophysics, v. 75, p. 181-241.
- Taylor S.R., 1982, Lunar and terrestrial crusts: a contrast in origin and evolution, Physics of the Earth and Planetary Interiors, v. 29, p. 233-241.
- Teichmüller, M. and Durand, B., 1983, Fluorescence microscopical rank studies on liptinites and vitrinites in peat and coals, and comparison with results of the rock-eval pyrolysis, International Journal of Coal Geology, v. 2, no. 3, p. 197-230.
- Thomsen R.O., 1998, Aspects of applied basin modeling: sensitivity analysis and scientific risk, Geological Society Special Publications, v. 141, p. 209-221.
- Tissot, B. and Espitalie, J., 1975, Thermal evolution of organic materials in sediments; application of a mathematical simulation; petroleum potential of sedimentary basins and reconstructing the thermal history of sediments, Revue de l'Institut Francais du Petrole et Annales des Combustibles Liquides, v. 30, no. 5, p. 743-777.

- Tissot, B. and Welte, D.H., 1985, Petroleum formation and occurrence; a new approach to oil and gas exploration, *Journal of Sedimentary Petrology*, v. 55, no. 6, p. 942-943.
- Turgut, S., 1997, Depositional Sequences and Hydrocarbon Potential of the Tertiary Sediments of the Eastern Thrace Basin, Based on Sequence Stratigraphic Concepts, PhD Thesis, Middle East Technical University, 366 p.
- Turgut S., Siyako, M. and Dilki, A., 1983, Trakya Hazvasının jeolojisi ve hidrokarbon olanakları, *Proceedings of the 4<sup>th</sup> Geological Congress of Turkey*, p. 35-46.
- Turgut, S., Kasar, S., Siyako, M., Bürkan, K.A., İvak, M., Yılmaz, İ., Aksoy, Z., Atalık, E., Olcay, K., Çubukçu, A., Erten, T., Ertürk, O., Soylu, C. and Erenler, M., 1987, The geological evaluation of the Thrace Basin, Northeast Turkey, TPAO Company Report, no. 2338, 88 p.
- Turgut, S., Turkarslan, M. and Perincek, D., 1991, Ecolution of the Thrace sedimentary basin and its hydrocarbon prospectivity, in: *Generation, accumulation and production of Europe's hydrocarbons*, Spencer, A.M., Special Publication of the European Association of Petroleum Geoscientists, no. 1, p. 415-437.
- Uğur, F.A., 1990, Karacaoğlan-1 kuyusu organic jeokimya değerlendirmesi, TPAO Company Report, no. 2822, 19 p.
- Uğur, F.A., 2002, Trakya baseni petrol sistemi modellemesi, TPAO Company Report, no. 4448, 387 p.
- Umut, M., Kurt, Z., İmik, M., Özcan, İ., Sakıkaya, H. and Saraç, G. 1983, Tekirdağ, Silivri, Pınarhisar alanının jeolojisi, General Directorate of Petroleum Affairs Company Report, no. 7349, p. 1-59.
- Üşümezsoy, Ş., 1982, Istanca masifinin petrojenetik evrimi, PhD Thesis, İstanbul University, Earthsciences Faculty, 94 p.
- Van, G.P., 1989, Transmittance color index (TCI) of amorphous organic matter; new thermal maturity indicator for hydrocarbon source rocks, correlation with mean vitrinite reflectance and thermal alteration index (TAI), *American Association of Petroleum Geologists Bulletin*, v. 73, no. 9, p. 1177.



- Waples, D.W., 1980, Time and temperature in petroleum formation: application of Lopatin's method to petroleum exploration, American Association of Petroleum Geologists Bulletin, v. 64, p. 916-926.
- Yalçın O. and Altan, G., 1997, History of Petroleum and Oil wells drilled in Turkey, General Directorate of Petroleum Affairs Company Report, 178 p.
- Yaltırak, C. and Alpar, B., 2002, Kinematics and evolution of the Northern Branch of the North Anatolian Fault (Ganos Fault) between the Sea of Marmara and the Gulf of Saros, Marine Geology, v. 190, p. 351-366.
- Yu, Z., Thomsen R. O. and Lerche, I., 1995, Crystalline basement focusing of heat versus fluid flow/compaction effects: a case study of the I-1 well in the Danish North Sea, Petroleum Geoscience, v. 1, p. 31-35.
- Yükler, M.A., 1988a, Habiller-2 kuyusu kantitatif basen analizi raporu, TPAO Company Report, no. 2460, 24 p.
- Yükler, M.A., 1988b, Alipaşa-1 kuyusu kantitatif basen analizi raporu, TPAO Company Report, no. 2461, 26 p.
- Yükler, M.A., 1988c, Şarköy-1 kuyusu kantitatif basen analizi raporu, TPAO Company Report, no. 2462, 22 p.
- Yükler, M.A., Engin, M.A., Şemşir, D., Kakülâh, Z., Erdoğan, L.T., Aksu, R., Çokuğraş, A.R. and Uğur, F.A., 1989, Kantitatif basen analizi, Trakya bölgesi çalışması, TPAO Company Report, no. 2601, 347 p.

# APPENDIX A

## GENERAL FLOW CHART OF THE MODIFIED EASY%Ro CODE

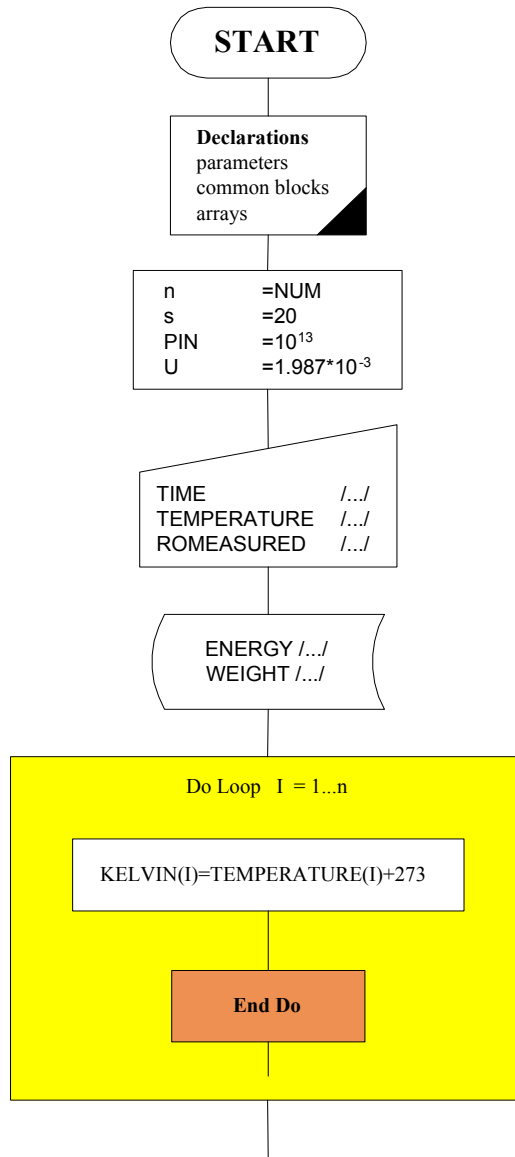


Figure A.1.

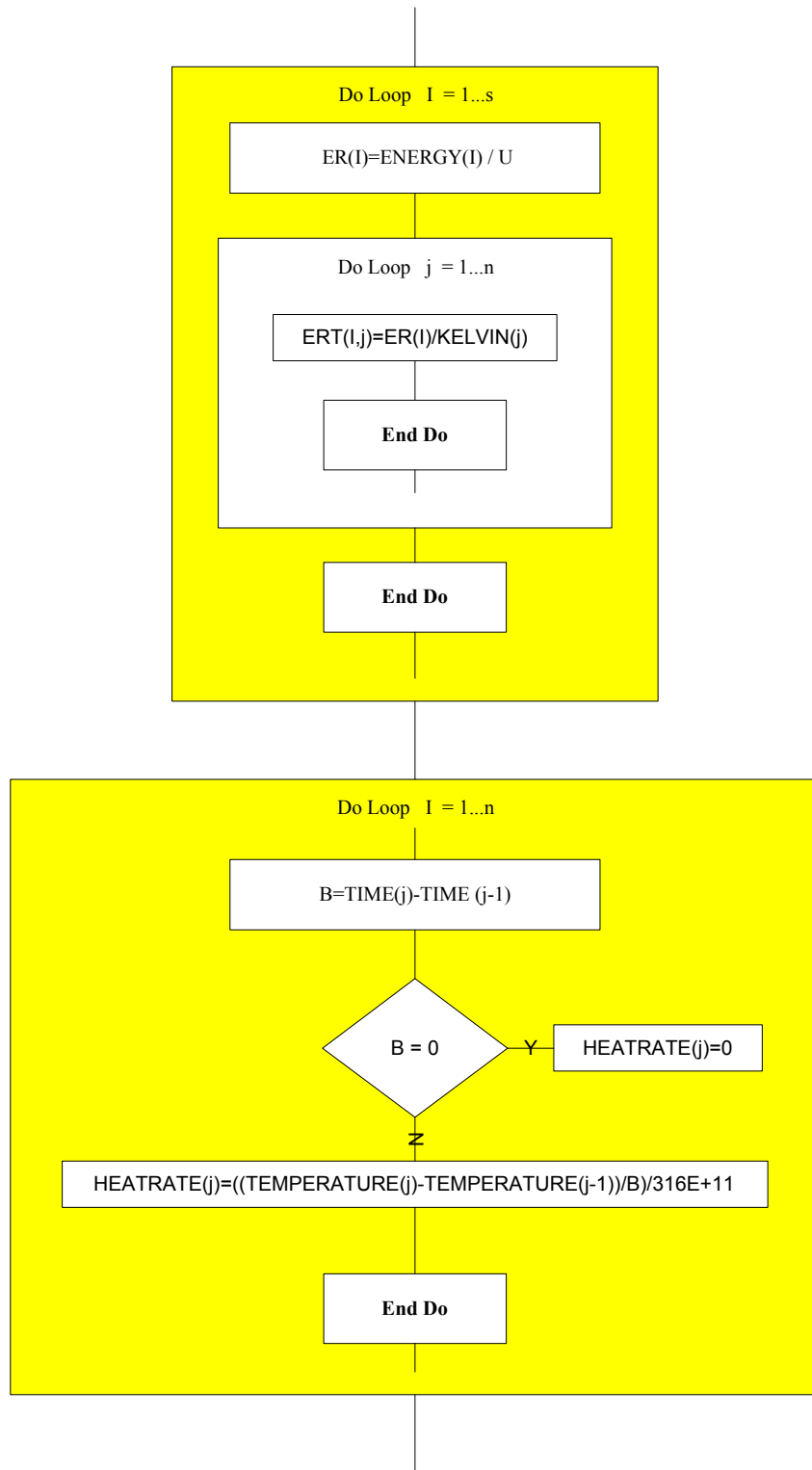


Figure A.1 cont'd.

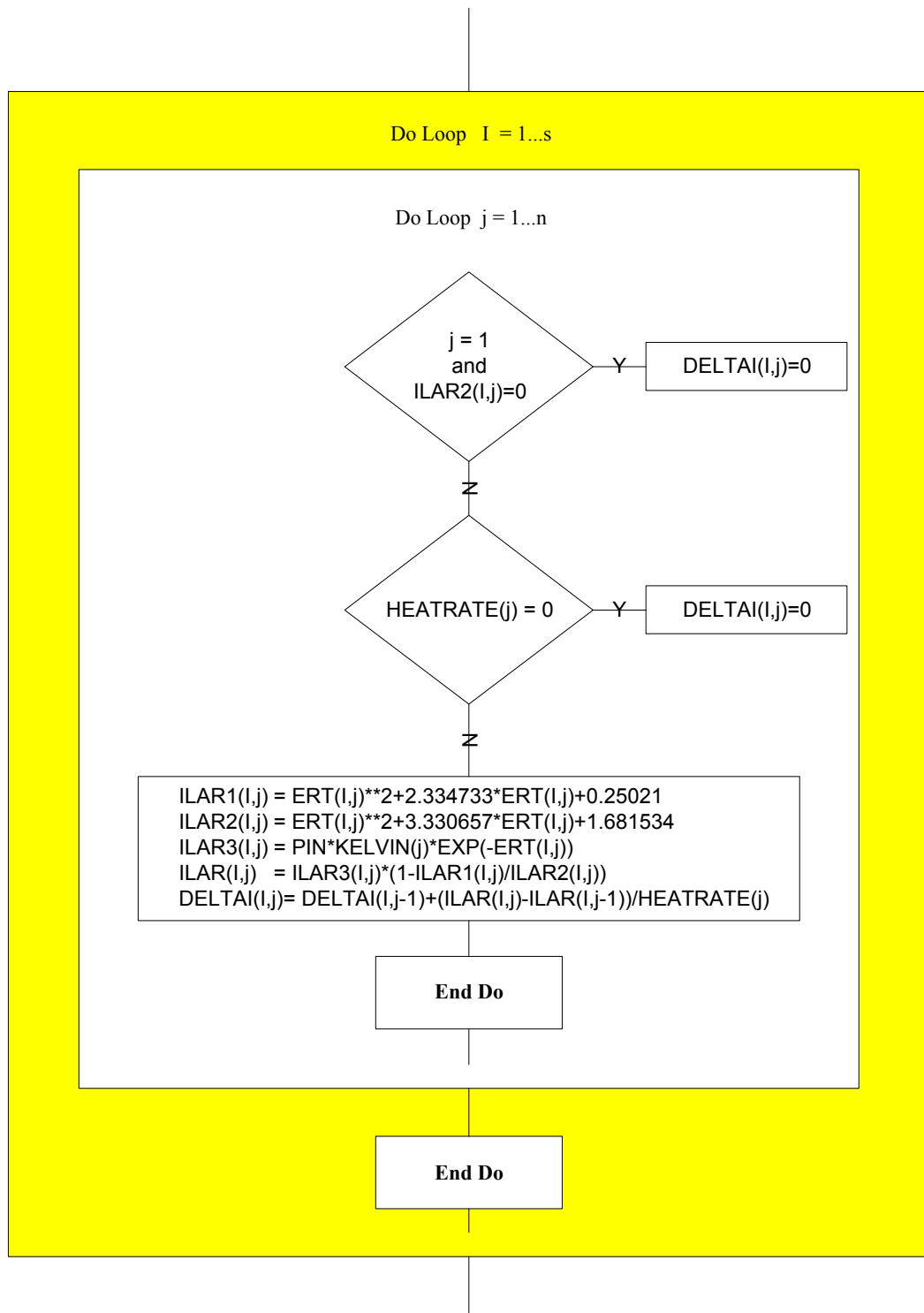


Figure A.1 cont'd.

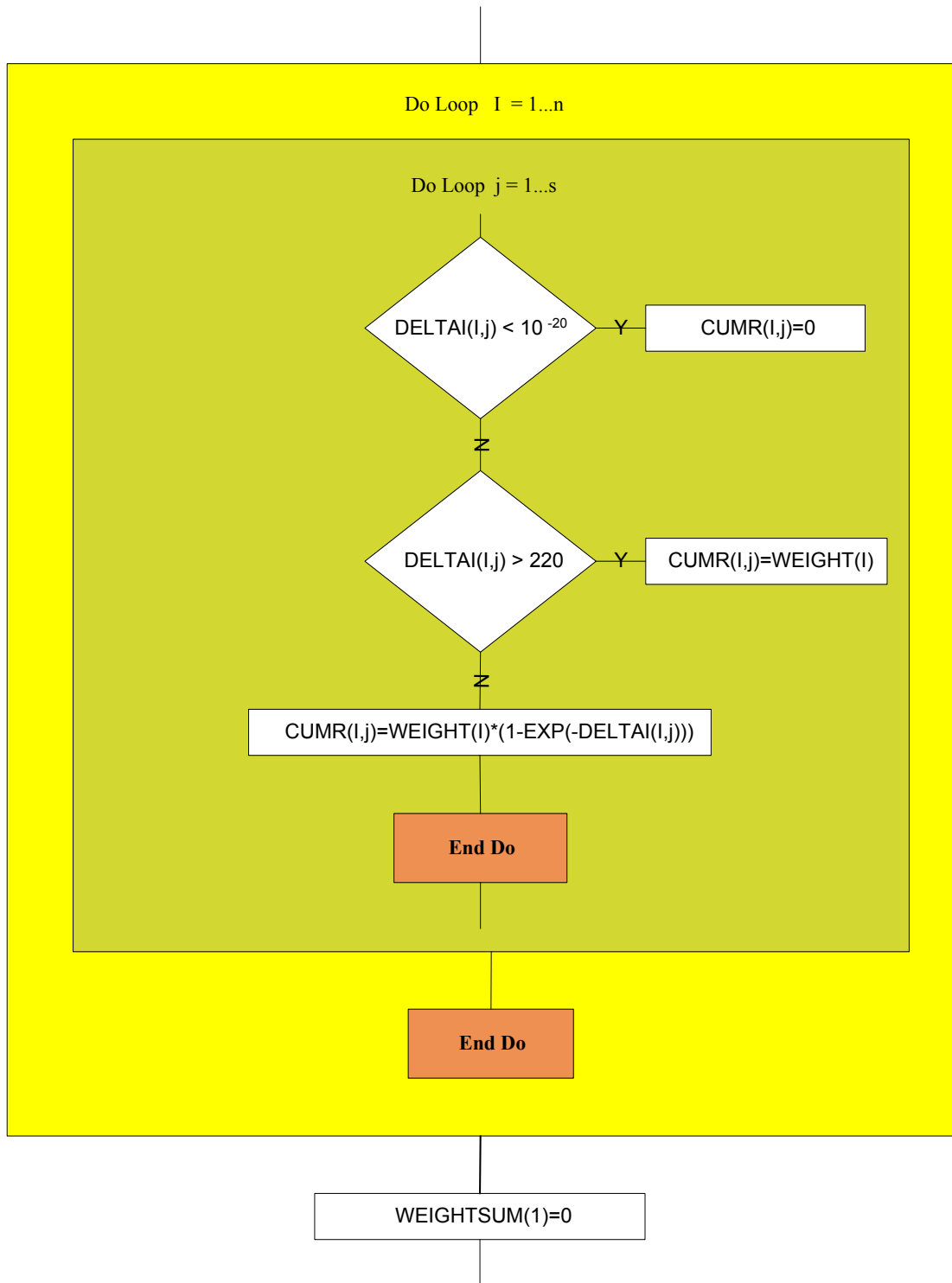


Figure A.1 cont'd.

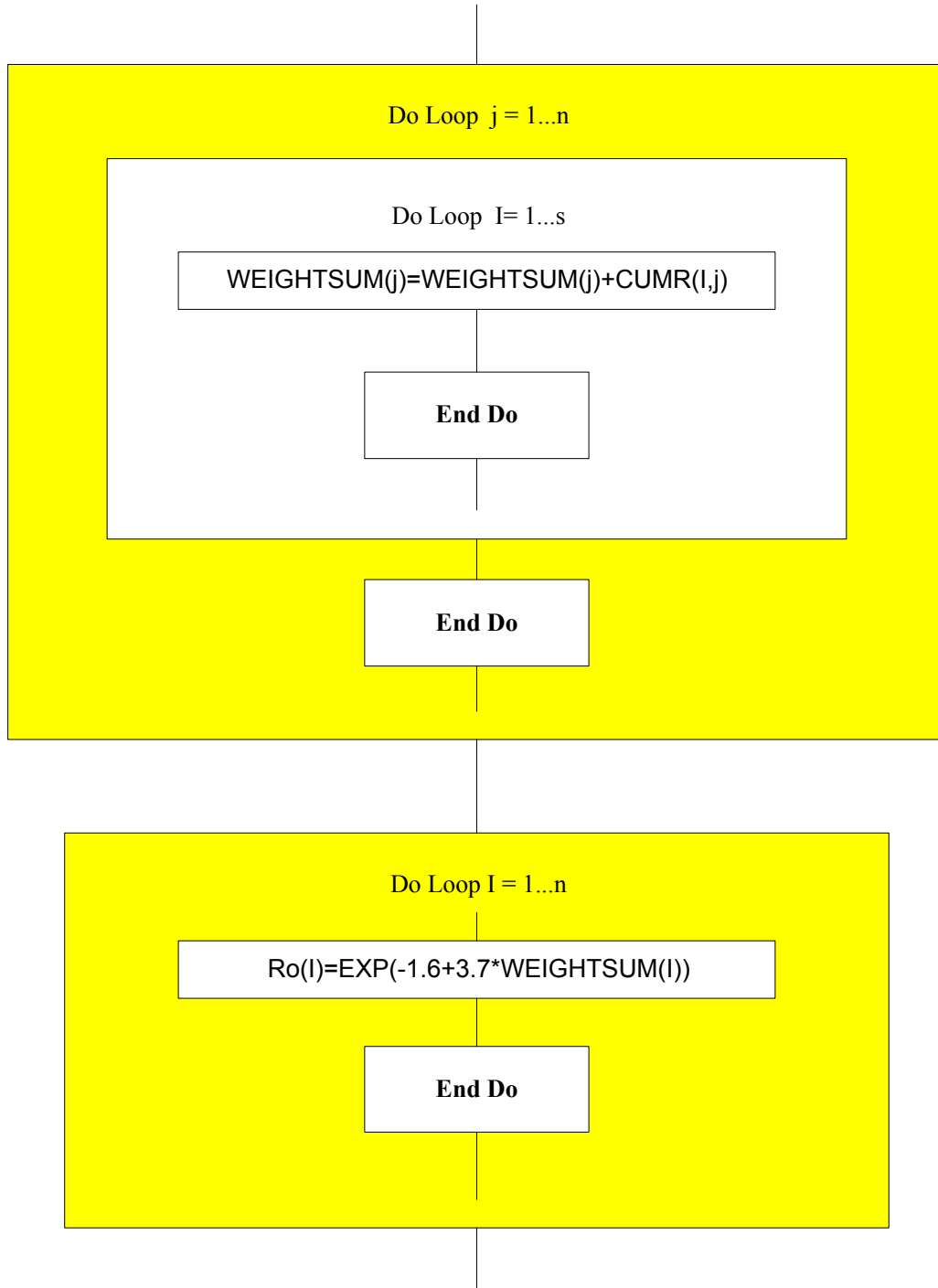


Figure A.1 cont'd.

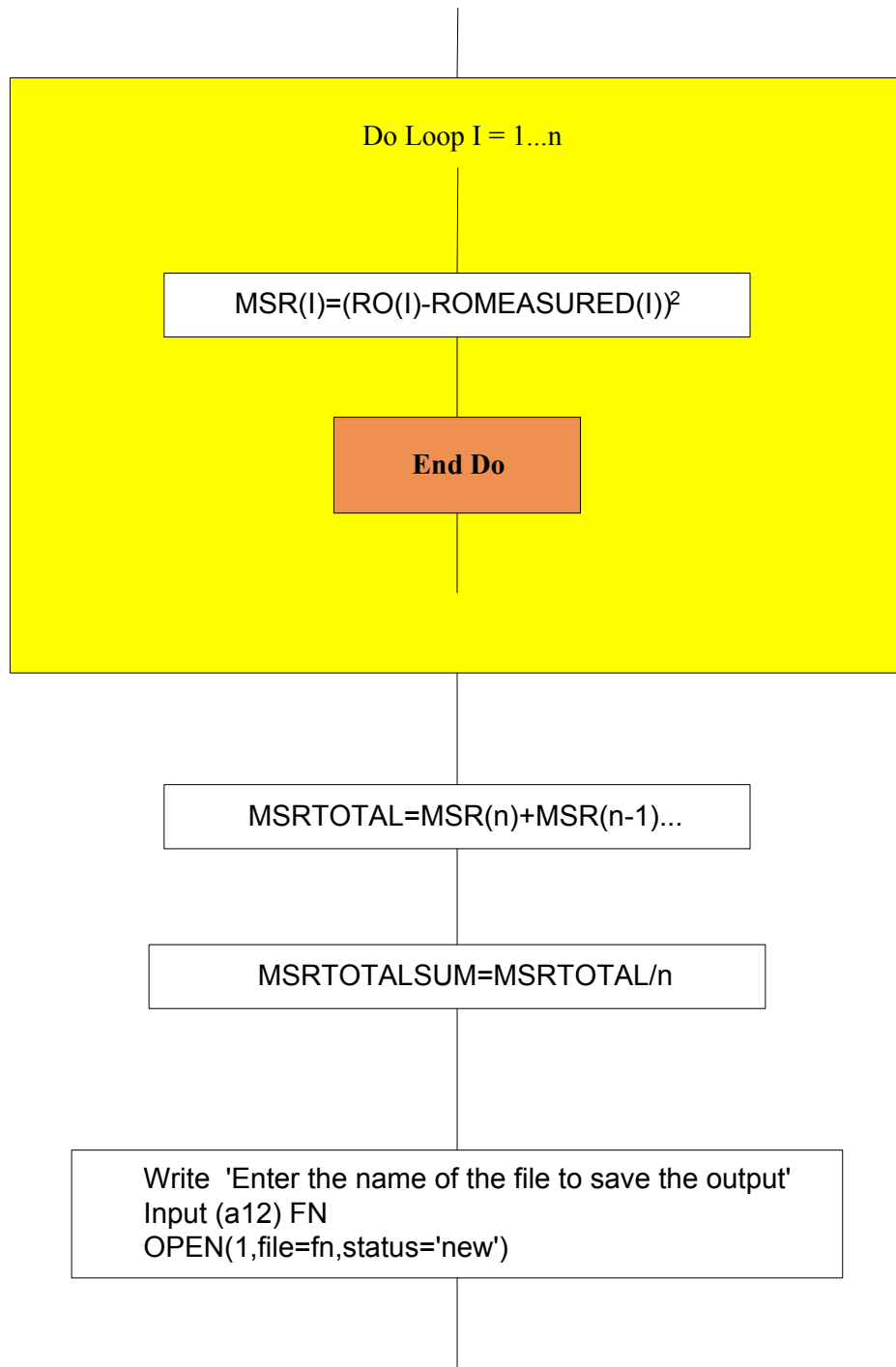


Figure A.1 cont'd.

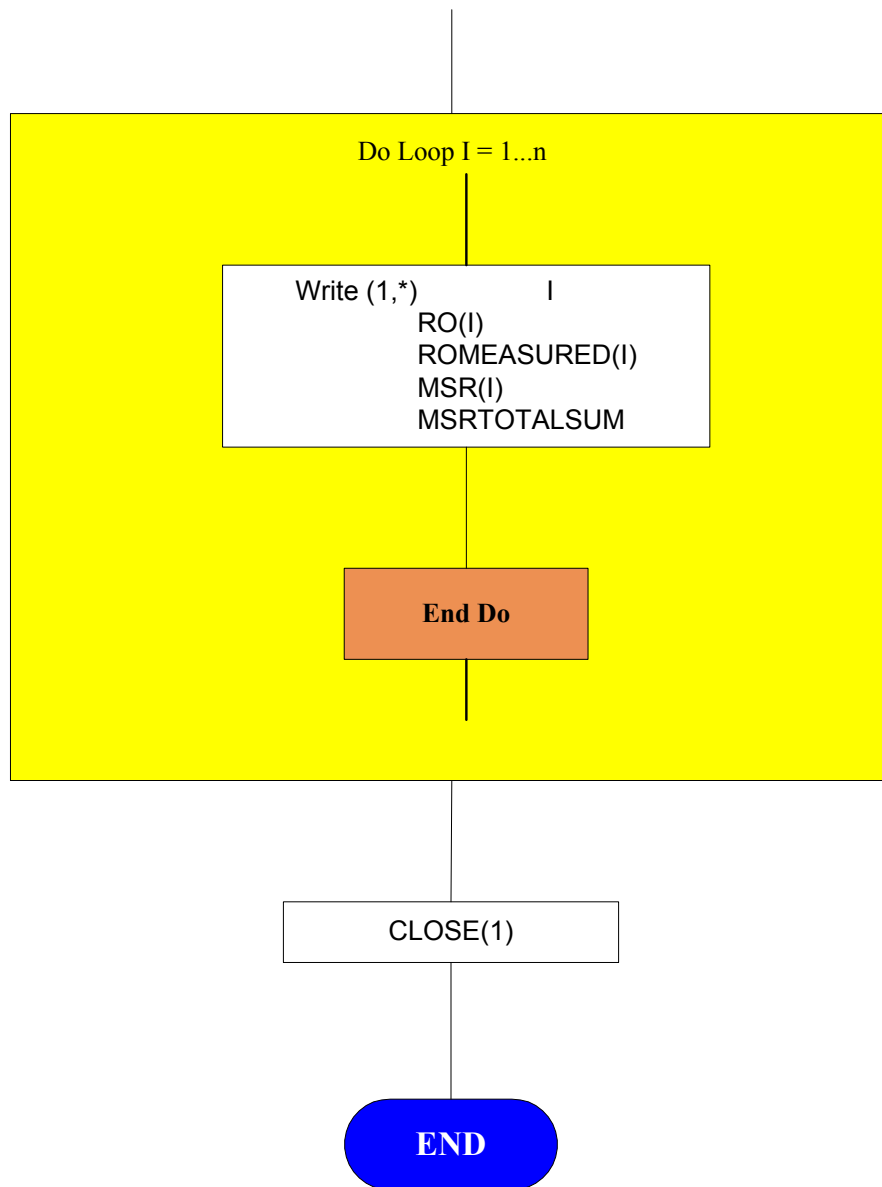


Figure A.1 cont'd.



## APPENDIX B

### LIST OF THE 70 STUDIED WELLS

List of the 70 studied wells, operator companies, their coordinates, ground level (GL), bottom hole formation (BHF) and results. (TPO: Turkish Petroleum Corporation, CAO: California Asiatic Oil Company, NTS: N. V. Turkse Shell, TOP: Texaco Overseas Petroleum Company, TTI: Tennessee Turkey Inc., MTA: Institute of Technical Mine Exploration; BHT: The last formation that the well penetrated through; N/A: Not applicable) (Yalçın and Altan, 1997).

Table B.1.

Well Name	Oil Company	Location		GL	TD	BHF	Result
		Latitude	Longitude				
Abalar-1	TPO	41 31 59.0	26 42 19.0	132	3043	Basement	Dry
Akbaş-1	TPO	41 33 40.5	26 52 09.2	131	4119	Basement	Dry
Alipaşa-1	TPO	41 04 40.0	28 09 59.5	28	1853	Basement	Dry
Ardıç-1	TPO	41 11 26.9	28 09 29.7	206	1647	Hamitabat	Gas
Arızbaba-1	TPO	41 37 38.2	26 55 43.5	98	4335	Hamitabat	Oil+Gas
Asilbeyli-1	CAO+TPO	41 40 11.0	27 16 42.0	211	835	Basement	Oil show
Babaeski-1	TPO	41 27 21.4	26 58 50.0	83	3241	Koyunbaba	Dry
Bahçedere-1	TPO	41 20 29.3	27 46 28.0	149	3582	Basement	Gas show
Ballı-1	TPO	40 50 08.5	26 57 18.4	120	2738	Basement	Dry
Bayramdere-1	TPO	41 37 57.0	27 19 47.0	193	1472	Basement	Dry
Bayramlı-1	NTS	41 18 43.5	26 44 54.0	20	2335	Basement	Dry
Çeltik-1	TPO	41 04 47.0	28 04 46.0	75	2848	Basement	Dry
Ceylan-4	TPO	41 32 37.7	27 27 03.2	161	1209	Basement	Oil show
Çorlu-3A	TPO	41 04 45.0	27 57 01.0	86	5043	Ceylan	Dry
Çukuryurt-1	TPO	41 25 29.0	27 53 30.7	146	904	Hamitabat	Dry
Değirmencik-3	TPO	41 36 25.6	27 10 04.3	154	3800	Hamitabat	Gas show
Değirmenköy-1	TPO	41 16 51.6	28 06 62.5	148	2475	Basement	Gas
Delen-1	TPO	41 22 19.6	27 43 31.5	116	3997	Basement	Gas
Deveçatağı-9	TPO	41 38 18.5	27 19 39.7	163	1487	Basement	Oil
Edirne-1	TPO	41 42 47.5	26 35 15.5	466	1046	Basement	Dry
Ergene-1	TPO	41 22 11.8	27 56 25.5	113	2967	Osmancık	Oil+Gas
Ertuğrul-1	TPO	41 34 15.3	27 28 05.0	194	898	Basement	Dry
Gerdelli-1	TTI	41 72 45.5	26 98 77.5	160	1704	Basement	Dry
Hamitabat-1	TPO	41 30 11.0	27 17 41.0	132	3541	Hamitabat	Gas
Havsa-1	TPO	41 30 21.0	26 49 00.0	66	3015	Basement	Dry
İnce-1	TPO	41 39 30.0	27 01 30.0	119	3401	Yeniköy	Gas show
İpsala-1	TPO	40 52 18.6	26 24 29.8	57	2375	Keşan	Water

Table B.1 cont'd.

Kandamış-1	NTS	41 07 11.0	27 13 58.0	94	3669	Danişmen	Gas show
Karaagac-1	TPO	41 33 24.3	27 29 26.0	185	1022	Basement	Dry
Karacaoğlan-2	TPO	41 33 42.4	27 05 29.5	94	4067	Ceylan	Gas
Karahıdır-1	TPO	41 42 34.5	27 09 32.3	206	1050	Basement	Dry
Karakavak-1	NTS	41 18 55.8	27 03 05.2	90	4243	Gaziköy	Dry
Karıştıran-1	TPO	45 68 56.5	27 58 35.5	115	2295	Mezardere	Gas show
Kavakdere-3	TPO	41 35 20.3	27 16 57.5	172	2118	Hamitabat	Oil
Kaynarca-1	TPO	41 22 44.5	27 35 54.4	109	4828	Hamitabat	Gas
Kepirtepe-1	TPO	41 21 49.3	27 26 22.2	84	3950	Ceylan	Gas
Keşan-1	TPO	40 52 01.0	26 34 30.0	48	3551	Basement	Dry
Korucu-1	TTI	41 45 43.0	26 39 07.0	124	912	Basement	Dry
Kuleli-3	TPO	41 28 28.0	26 54 13.0	51	2749	Basement	Dry
Kumburgaz-1	TPO	41 01 54.0	28 27 35.0	2	1202	Hamitabat	Dry
Kumrular-1	TPO	41 30 35.4	27 12 38.7	134	3288	Hamitabat	Gas
Kurtdere-1	TPO	41 40 80.5	27 78 48.3	115	1398	Basement	Dry
K. Abalar-1	TPO	41 35 21.5	26 44 35.1	100	3458	Koyunbaba	Dry
K. Çerkezkoy-1	TPO	41 18 17.6	28 05 07.3	162	2128	Koyunbaba	Water
K. Marmara-3	TPO	41 05 23.6	28 19 15.0	39	1845	Soğucak	Gas
K. Osmancık-1	TPO	41 34 58.0	27 21 41.0	168	1232	Basement	Oil
Meriç-2	TPO	41 28 53.7	26 40 06.3	132	3267	Basement	Dry
Mezardere-1	CAO+TOP	41 41 40.0	27 08 34.0	183	1745	Hamitabat	Dry
Minnetler-1A	TPO	41 25 22.8	27 02 08.5	48	3492	Basement	Gas
Mürefte-1	MTA	40 40 25.0	27 15 24.0	43	156	Sandstone	Gas show
Ortaköy-1	TPO	40 37 37.0	26 54 53.0	8	1893	Basement	Dry
Osmancık-2	TPO	41 34 14.0	27 21 44.0	180	2414	Basement	Oil show
Pehlivan köy-1	TPO	41 18 21.2	26 51 11.5	71	2970	Basement	Gas show
Şahankaya-1	TPO	41 35 46.3	27 13 10.3	163	3400	N/A	Dry
Şarköy-1	TPO	40 38 07.5	27 06 57.0	127	1849	Basement	Dry
Sevindik-1	TPO	41 24 87.3	27 59 56.6	117	2400	Osmancık	Gas
Silivri-1	TPO	41 07 15.4	28 20 26.4	176	2489	N/A	Dry
Soğucak-1	TPO	41 30 14.5	27 38 23.0	183	1286	Basement	Dry
Süluoğlu-1	TPO	41 43 54.2	26 54 24.0	145	1573	Basement	Dry
Sütluce-3	TPO	41 31 01.5	27 31 46.5	189	1352	Basement	Dry
Tatarköy-1	TPO	41 31 30.7	27 22 09.0	134	3214	Hamitabat	Oil
Terzili-2	TPO	41 31 40.7	27 05 17.4	96	4573	Hamitabat	Dry
Turgutbey-1	TPO	41 30 25.4	27 23 12.2	139	3403	Hamitabat	Gas show
Üctepeler-1	TPO	41 27 12.8	27 42 24.6	144	2210	Basement	Dry
Umur-1	TPO	41 43 00.9	26 49 38.0	157	1680	Basement	Dry
Umurca-1	TPO	41 25 04.0	27 26 19.0	87	4388	Hamitabat	Gas
Vakıflar-1	CAO+TOP	41 15 54.0	27 39 48.0	121	3757	Osmancık	Gas show
Yancıklar-1	TPO	41 60 81.6	27 40 13.8	162	1035	Basement	Dry
Yaylaköy-1	TPO	48 37 10.0	45 29 37.0	164	994	Sogucak	Dry
Yunus-1	TPO	41 06 66.6	28 26 88.8	-58	2274	Soğucak	Water

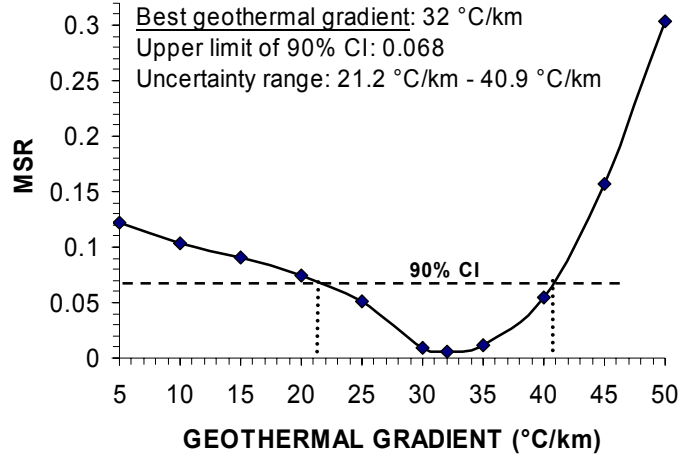
## APPENDIX C

### MSR DATA AND GRAPHS

Calculated MSR values versus the assigned thermal gradients and the MSR curves for each well location (CI: confidence interval).

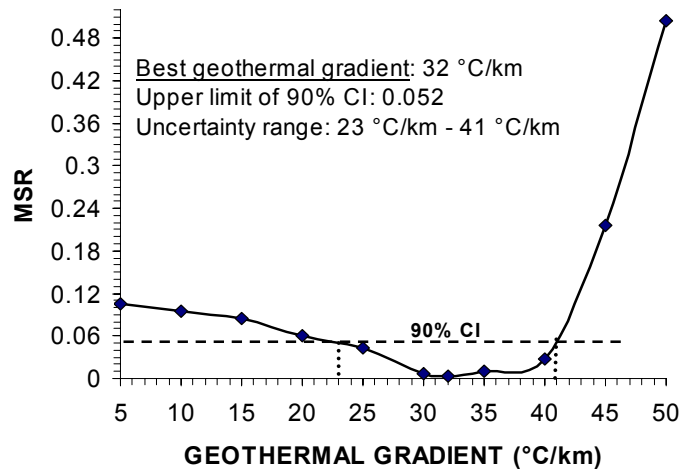
**Abalar-1**

TG (°C/km)	MSR
5	0.12159
10	0.10355
15	0.09025
20	0.07472
25	0.05151
30	0.00957
<b>32</b>	<b>0.00524</b>
35	0.01189
40	0.05445
45	0.15678
50	0.30335



**Akbaş-1**

TG (°C/km)	MSR
5	0.10478
10	0.09524
15	0.08504
20	0.06025
25	0.04289
30	0.00754
<b>32</b>	<b>0.00365</b>
35	0.00988
40	0.02740
45	0.21535
50	0.50502



**Alipaşa-1**

TG (°C/km)	MSR
5	0.11788
10	0.10633
15	0.09441
20	0.07456
25	0.05503
35	0.03406
<b>39</b>	<b>0.00228</b>
40	0.00345
45	0.15354
50	0.30785

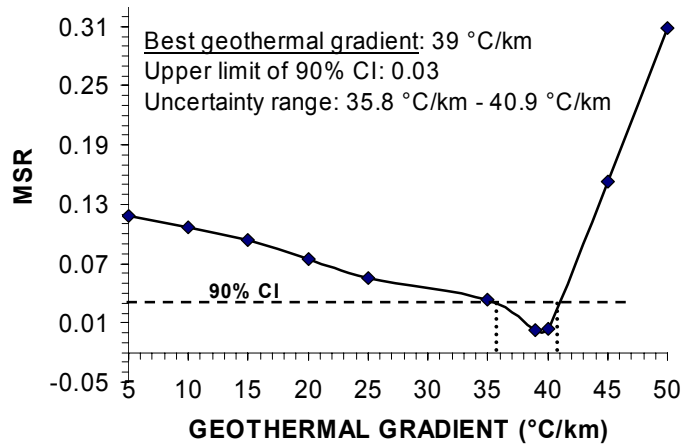
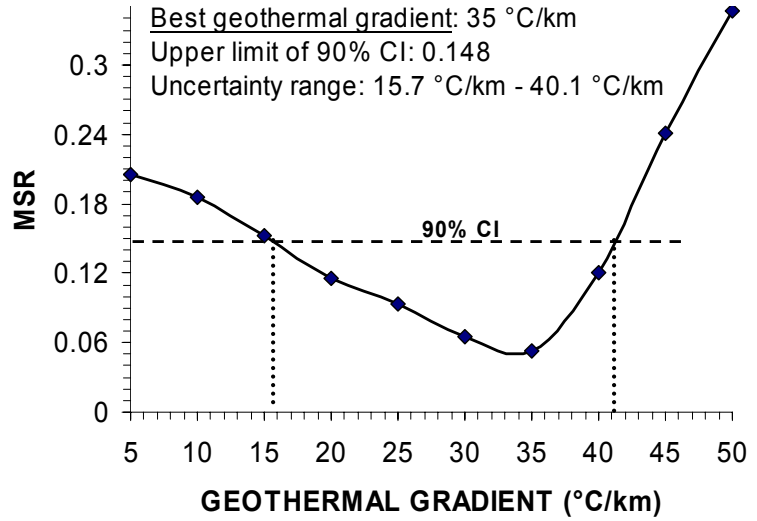


Figure C.1.

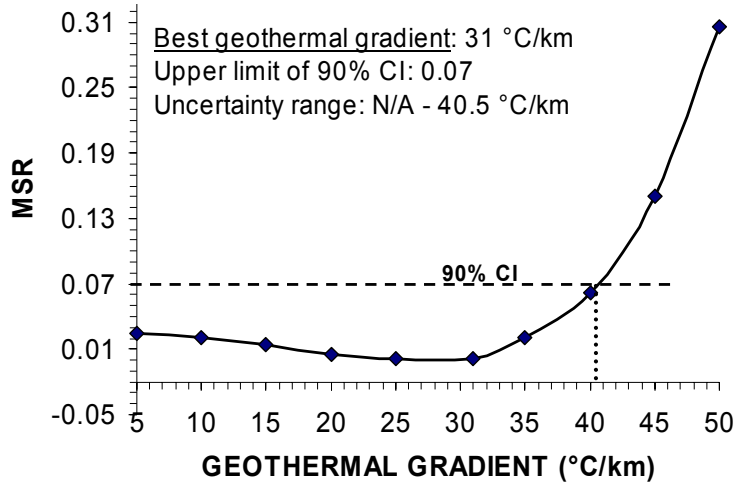
**Arıç-1**

TG (°C/km)	MSR
5	0.20583
10	0.18510
15	0.15258
20	0.11504
25	0.09365
30	0.06555
<b>35</b>	<b>0.05249</b>
40	0.11998
45	0.24143
50	0.34664



**Arızbaba-1**

TG (°C/km)	MSR
5	0.02493
10	0.02067
15	0.01461
20	0.00554
25	0.00094
<b>31</b>	<b>0.00092</b>
35	0.02028
40	0.06236
45	0.15062
50	0.30541
5	0.02493



**Asilbeyli-1**

TG (°C/km)	MSR
5	0.13425
10	0.11365
15	0.11022
20	0.09778
25	0.05225
30	0.01554
35	0.00911
<b>36</b>	<b>0.00428</b>
40	0.03443
45	0.16882
50	0.25289

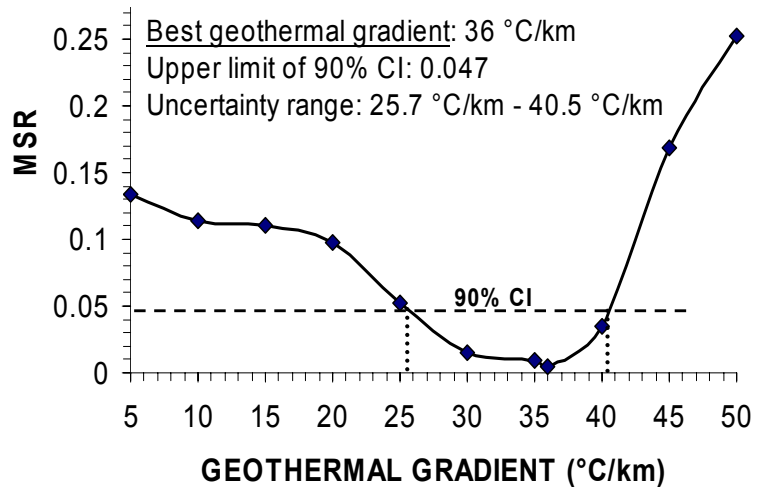
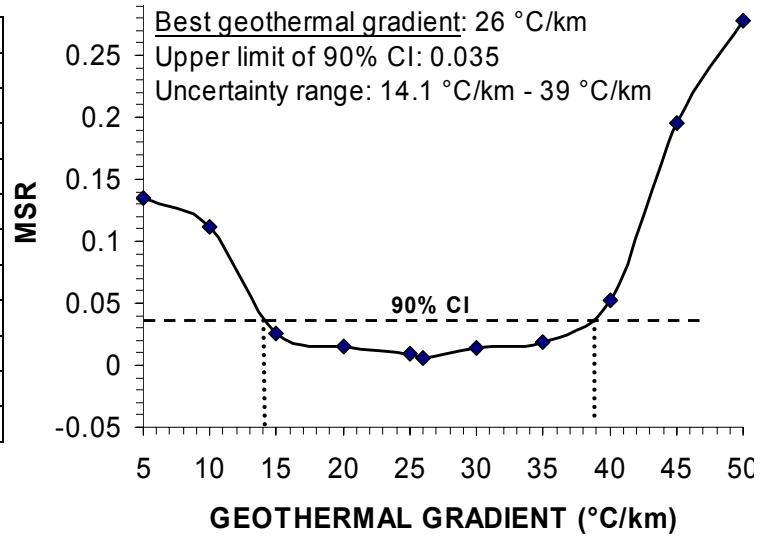


Figure C.1 cont'd.

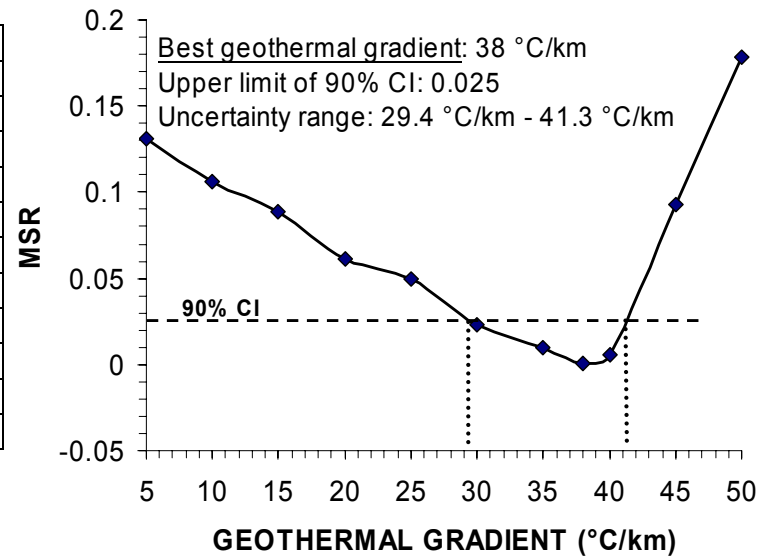
**Babaeski-1**

TG (°C/km)	MSR
5	0.13524
10	0.11214
15	0.02515
20	0.01567
25	0.00976
<b>26</b>	<b>0.00527</b>
30	0.01369
35	0.01877
40	0.05243
45	0.19487
50	0.27755



**Bahçedere-1**

TG (°C/km)	MSR
5	0.13124
10	0.10588
15	0.08854
20	0.06142
25	0.04986
30	0.02302
35	0.0101
<b>38</b>	<b>0.00057</b>
40	0.00551
45	0.09257
50	0.17852



**Ballı-1**

TG (°C/km)	MSR
5	0.13124
10	0.10588
15	0.08854
20	0.06142
25	0.04986
30	0.02302
35	0.0101
<b>38</b>	<b>0.00057</b>
40	0.00551
45	0.09257
50	0.17852

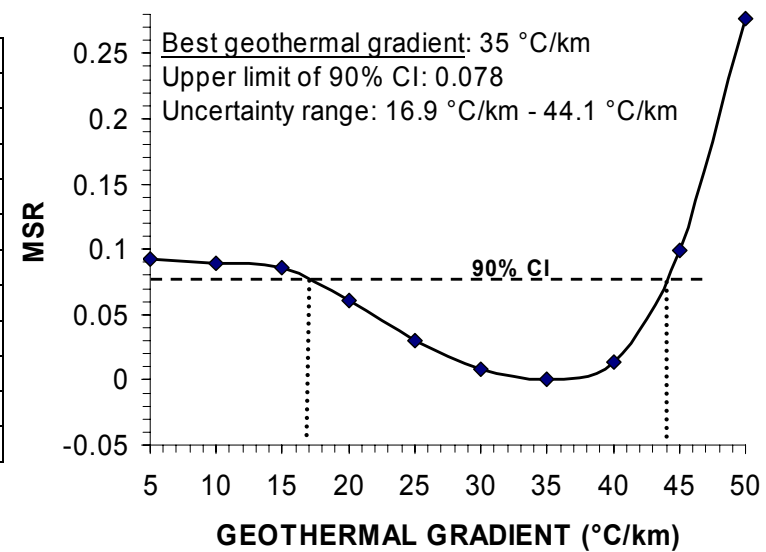
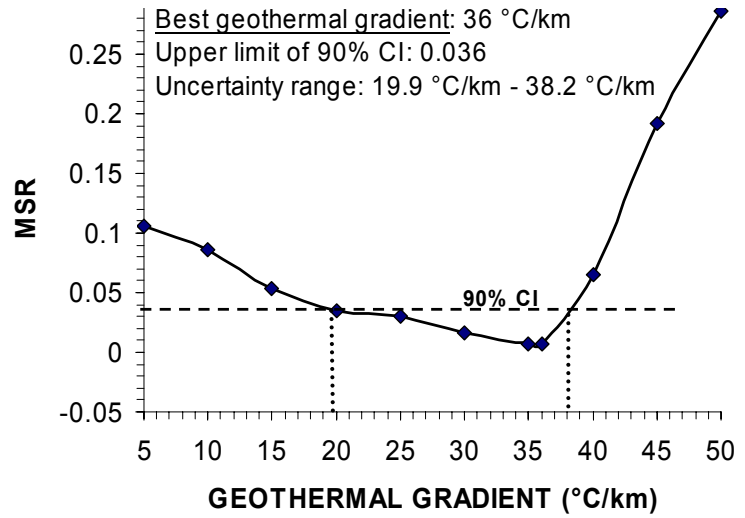


Figure C.1 cont'd.

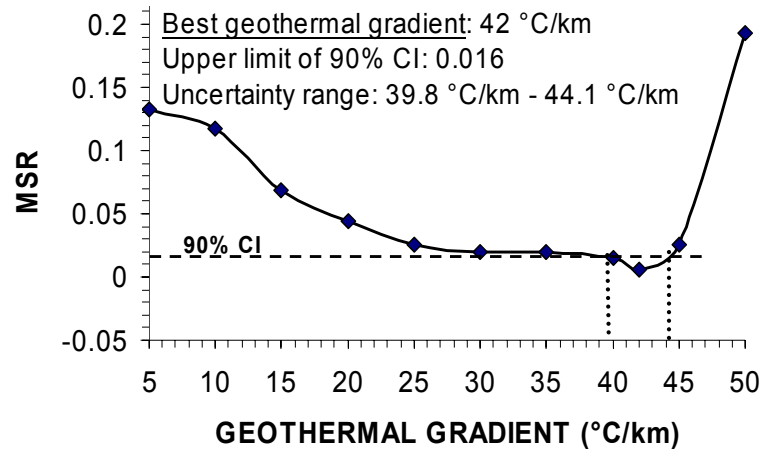
**Bayramdere-1**

TG (°C/km)	MSR
5	0.13231
10	0.11752
15	0.06828
20	0.04372
25	0.02575
30	0.01987
35	0.01952
40	0.0155
<b>42</b>	<b>0.00542</b>
45	0.02584
50	0.19322



**Bayırlılı-1**

TG (°C/km)	MSR
5	0.13231
10	0.11752
15	0.06828
20	0.04372
25	0.02575
30	0.01987
35	0.01952
40	0.0155
<b>42</b>	<b>0.00542</b>
45	0.02584
50	0.19322



**Çeltik-1**

TG (°C/km)	MSR
5	0.17212
10	0.09369
15	0.04574
20	0.02967
25	0.02755
30	0.02225
35	0.01888
<b>37</b>	<b>0.01221</b>
40	0.0554
45	0.12364
50	0.20429

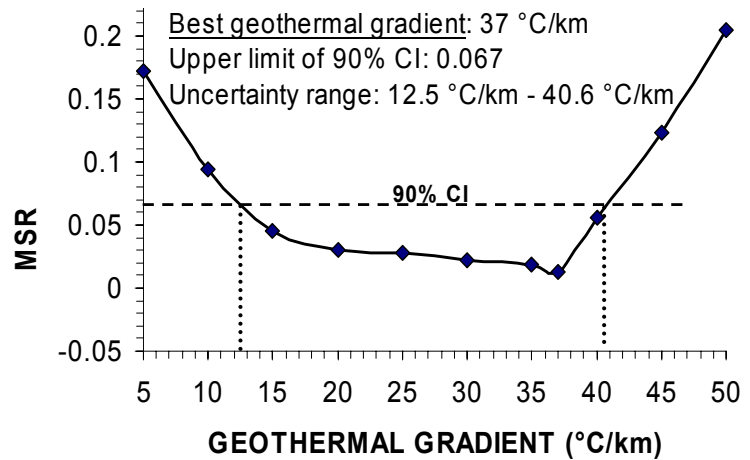
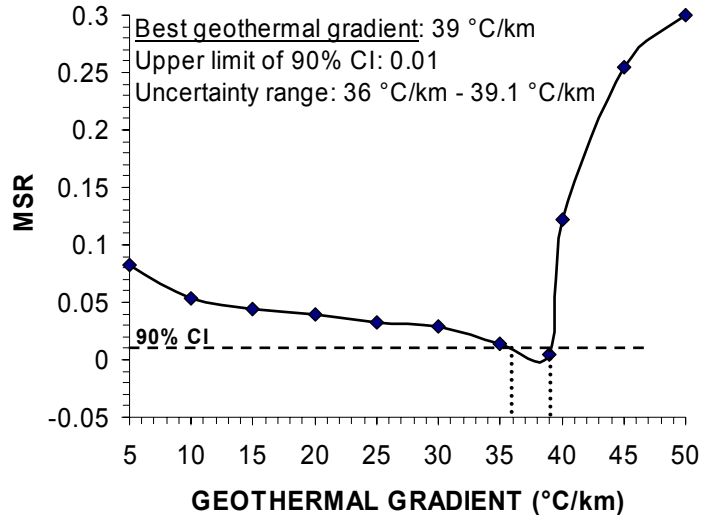


Figure C.1 cont'd.

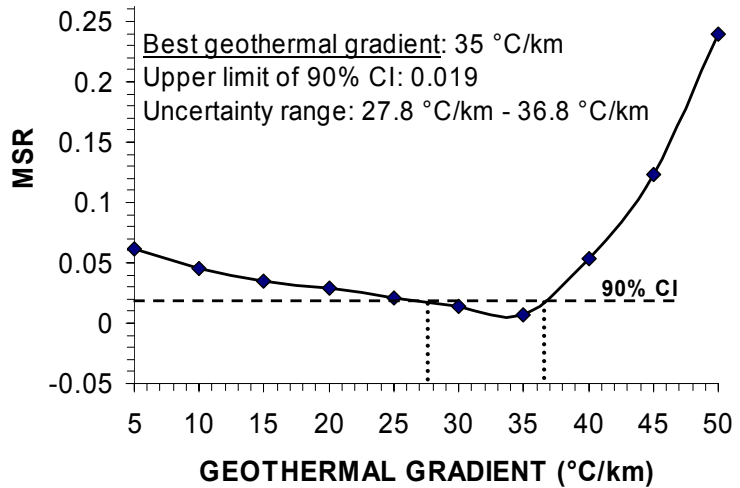
**Ceylan-4**

TG (°C/km)	MSR
5	0.08257
10	0.05324
15	0.04457
20	0.03961
25	0.03247
30	0.02958
35	0.01347
<b>39</b>	<b>0.00508</b>
40	0.1225
45	0.25479
50	0.30028



**Çorlu-3A**

TG (°C/km)	MSR
5	0.06201
10	0.04509
15	0.03405
20	0.02852
25	0.02123
30	0.01405
<b>35</b>	<b>0.00652</b>
40	0.05376
45	0.1233
50	0.23912
5	0.06201



**Çukuryurt-1**

TG (°C/km)	MSR
5	0.14524
10	0.14214
15	0.13517
20	0.12397
25	0.10149
30	0.02321
40	0.01181
<b>41</b>	<b>0.00911</b>
45	0.0858
50	0.24304

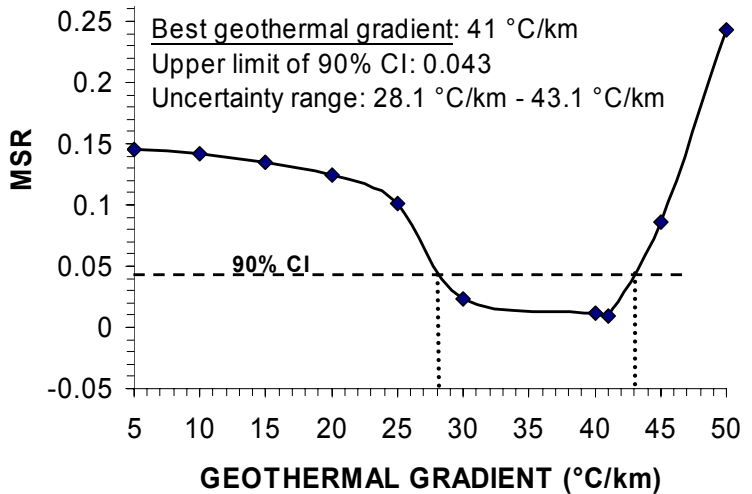
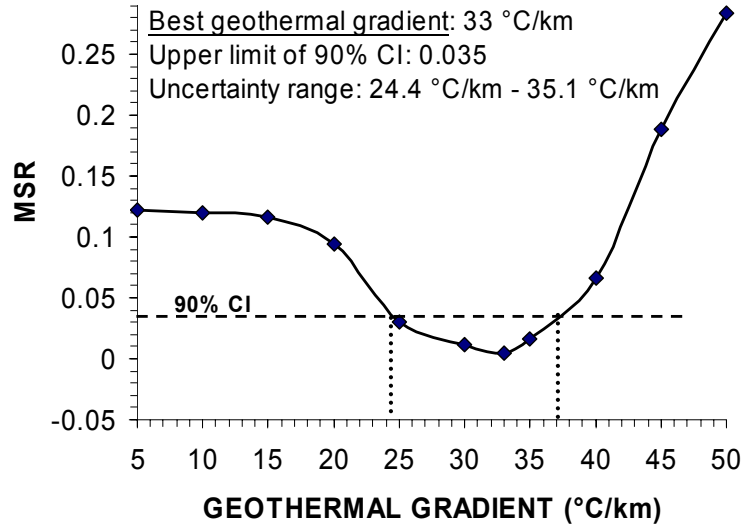


Figure C.1 cont'd.

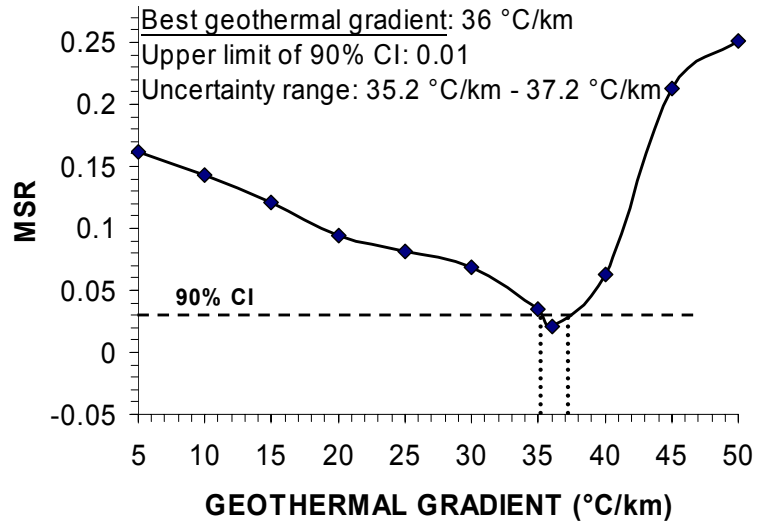
**Değirmencik-3**

TG (°C/km)	MSR
5	0.12156
10	0.11954
15	0.11574
20	0.09364
25	0.03012
30	0.01105
<b>33</b>	<b>0.00421</b>
35	0.01652
40	0.06570
45	0.18850
50	0.2836



**Değirmenköy-1**

TG (°C/km)	MSR
5	0.16202
10	0.14247
15	0.12133
20	0.09408
25	0.08106
30	0.06852
35	0.03460
<b>36</b>	<b>0.02144</b>
40	0.06271
45	0.21232
50	0.25073



**Delen-1**

TG (°C/km)	MSR
5	0.02812
10	0.00764
15	0.00583
20	0.00552
25	0.00446
30	0.00216
<b>33</b>	<b>0.00086</b>
35	0.00096
40	0.01563
45	0.06582
50	0.20660

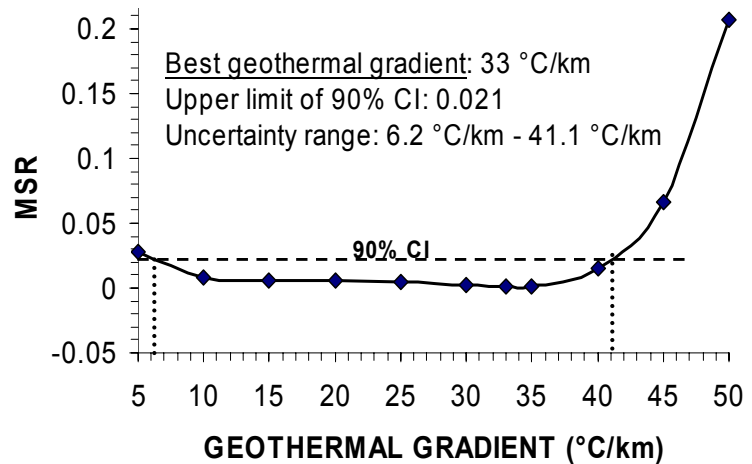
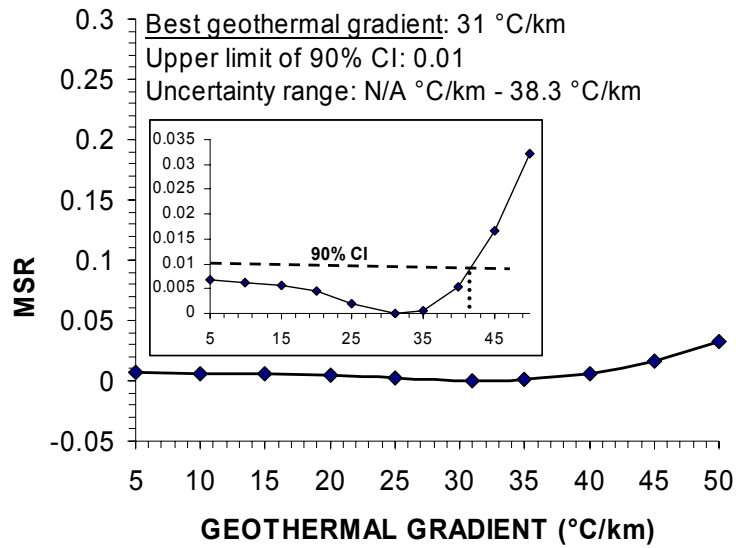


Figure C.1 cont'd.



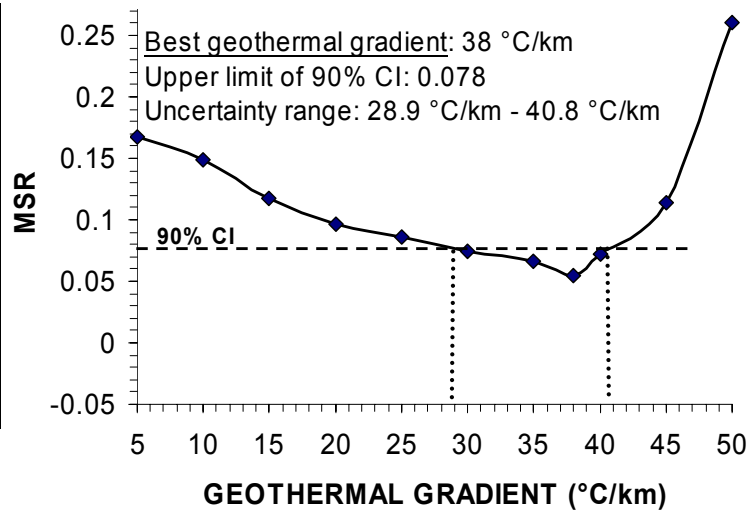
**Deveçatağı-9**

TG (°C/km)	MSR
5	0.00686
10	0.00614
15	0.00572
20	0.00438
25	0.00188
<b>31</b>	<b>0.00002</b>
35	0.00068
40	0.00546
45	0.01662
50	0.03204



**Edirne-1**

TG (°C/km)	MSR
5	0.16733
10	0.14853
15	0.11690
20	0.09602
25	0.08575
30	0.07412
35	0.06625
<b>38</b>	<b>0.05520</b>
40	0.07201
45	0.11361
50	0.26042



**Ergene-1**

TG (°C/km)	MSR
5	0.15402
10	0.12075
15	0.10801
20	0.07562
25	0.06457
<b>30</b>	<b>0.04321</b>
35	0.09210
40	0.14251
45	0.18022
50	0.23884

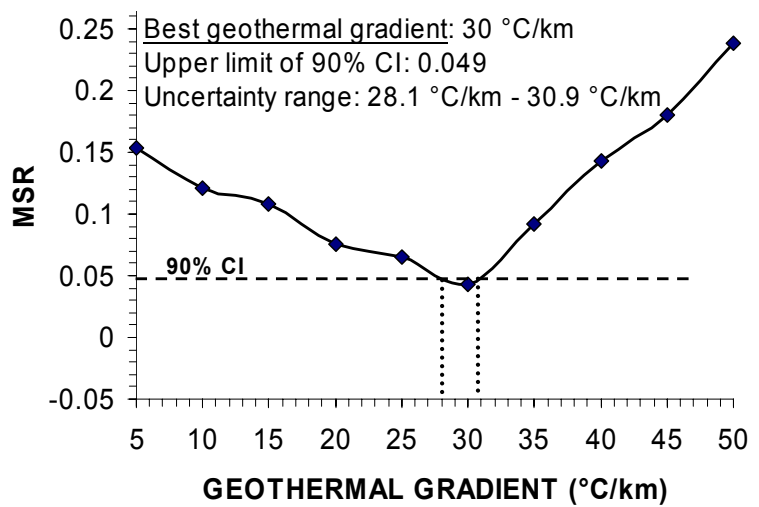
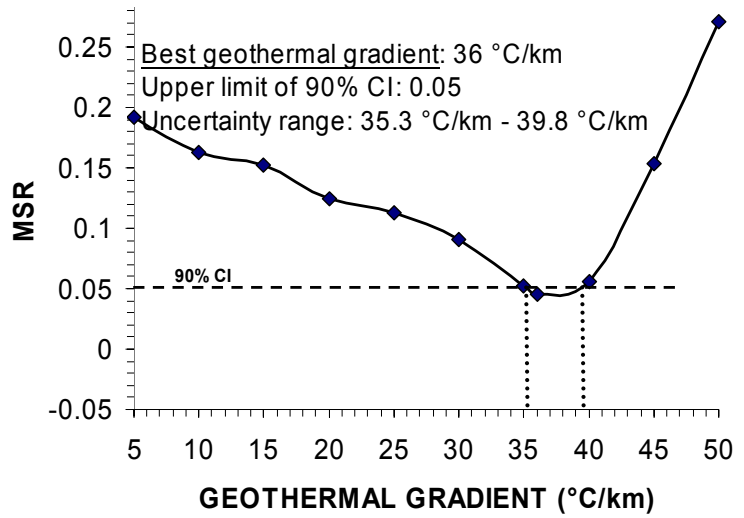


Figure C.1 cont'd.

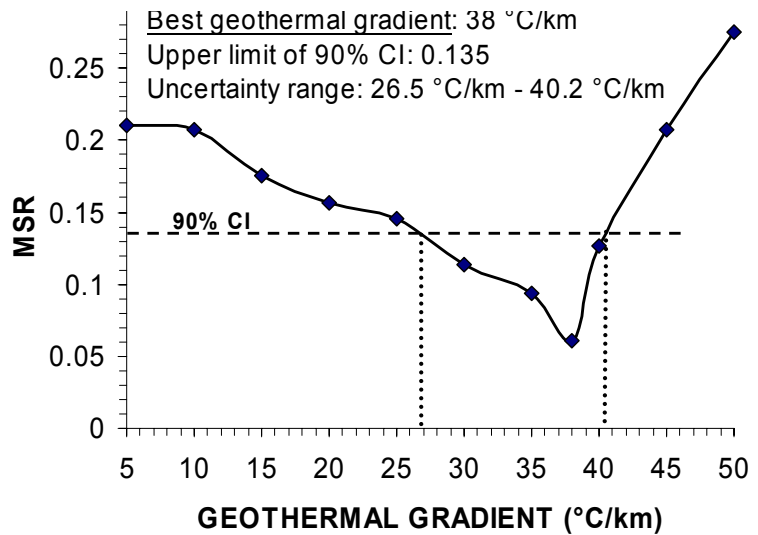
**Ertuğrul-1**

TG (°C/km)	MSR
5	0.19202
10	0.16254
15	0.15211
20	0.12425
25	0.11241
30	0.09012
35	0.05212
<b>36</b>	<b>0.04522</b>
40	0.05555
45	0.15371
50	0.27112



**Gerdelli-1**

TG (°C/km)	MSR
5	0.21012
10	0.20777
15	0.17536
20	0.15665
25	0.14524
30	0.11341
35	0.09354
<b>38</b>	<b>0.06102</b>
40	0.12699
45	0.20702
50	0.27548



**Hamitabat-1**

TG (°C/km)	MSR
5	0.22925
10	0.22652
15	0.21002
20	0.20857
25	0.19621
30	0.16357
<b>34</b>	<b>0.05221</b>
35	0.08567
40	0.12321
45	0.20258
50	0.29333

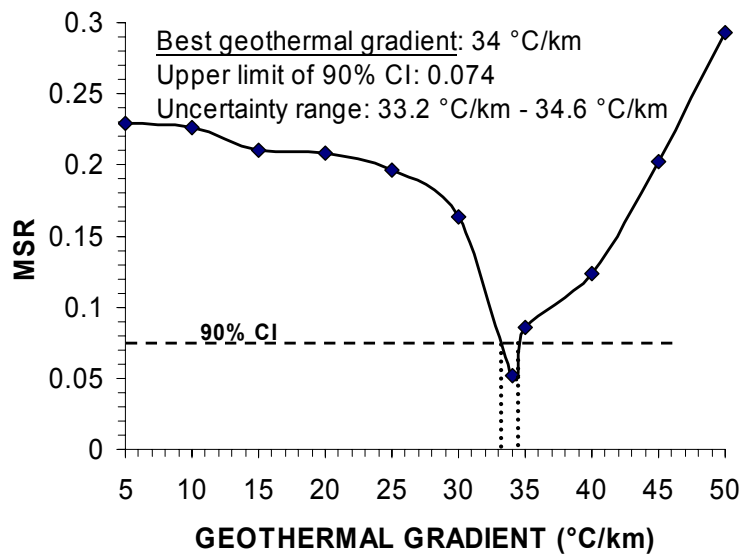
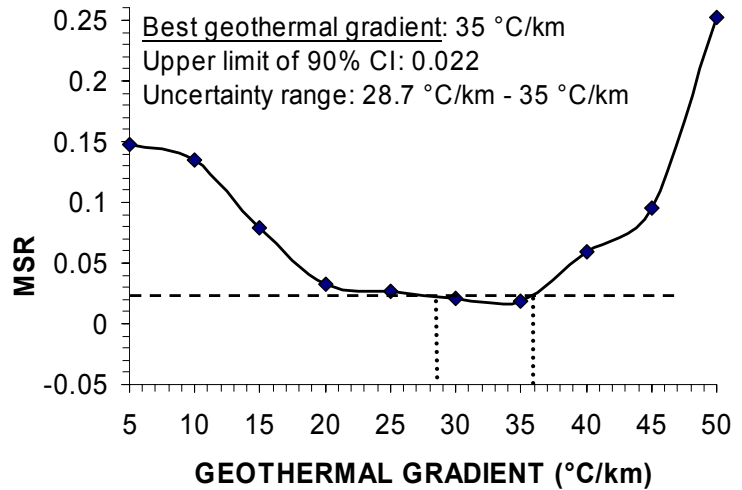


Figure C.1 cont'd.

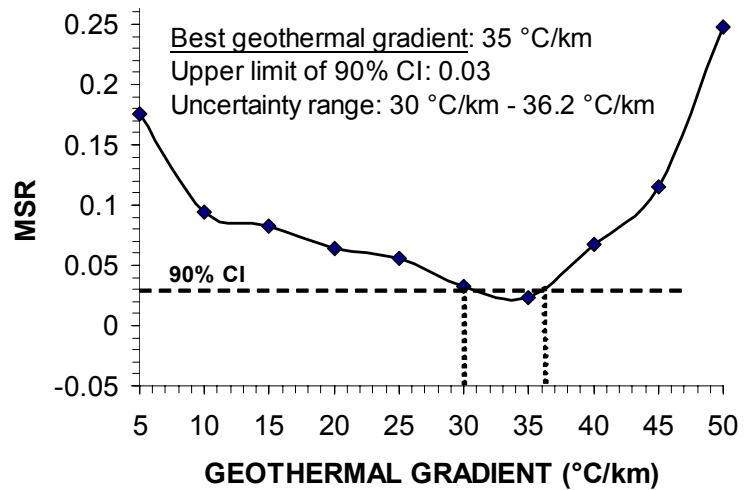
**Havsa-1**

TG (°C/km)	MSR
5	0.14810
10	0.13431
15	0.07877
20	0.03311
25	0.02624
30	0.02102
<b>35</b>	<b>0.01858</b>
40	0.0594
45	0.09521
50	0.25220



**İnece-1**

TG (°C/km)	MSR
5	0.17524
10	0.09410
15	0.08254
20	0.06354
25	0.05557
30	0.03234
<b>35</b>	<b>0.02278</b>
40	0.06690
45	0.11520
50	0.24777



**İpsala-1**

TG (°C/km)	MSR
5	0.13855
10	0.11921
15	0.10324
20	0.09444
25	0.0101
<b>26</b>	<b>0.00858</b>
30	0.01120
35	0.02877
40	0.03205
45	0.12888

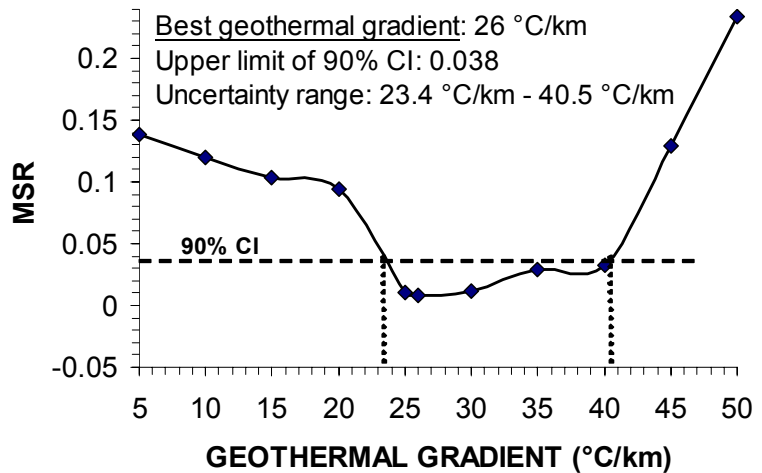
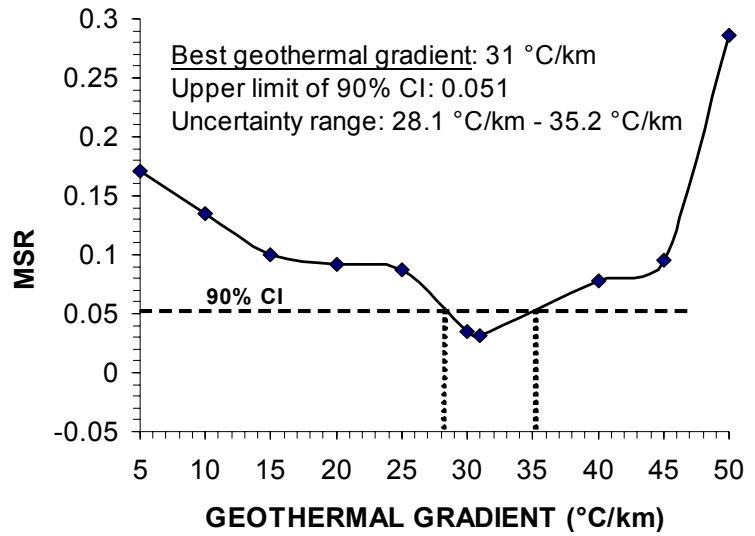


Figure C.1 cont'd.

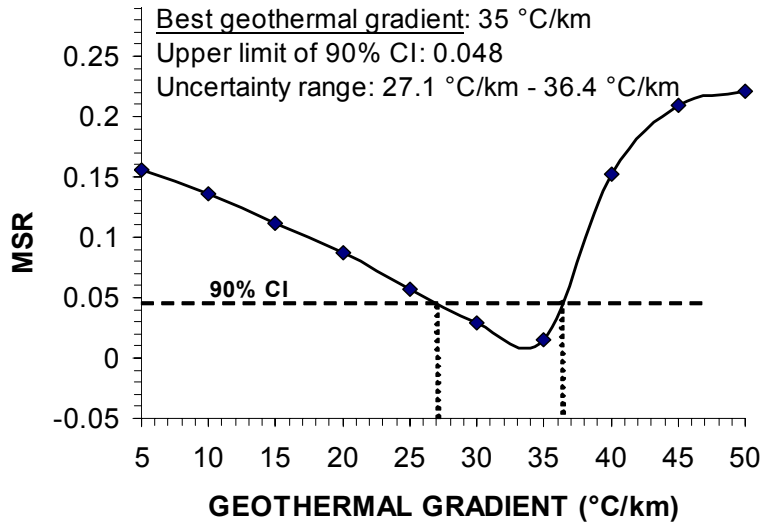
**Kandırmış-1**

TG (°C/km)	MSR
5	0.1712
10	0.13527
15	0.10014
20	0.09202
25	0.08777
30	0.03524
<b>31</b>	<b>0.03167</b>
40	0.07742
45	0.09554
50	0.28586



**Karaağaç-1**

TG (°C/km)	MSR
5	0.1553
10	0.13587
15	0.1115
20	0.08707
25	0.05698
30	0.02852
<b>35</b>	<b>0.01524</b>
40	0.15254
45	0.20875
50	0.22123



**Karacaoğlan-2**

TG (°C/km)	MSR
5	0.12456
10	0.12001
15	0.10495
20	0.09687
25	0.07075
30	0.0526
<b>33</b>	<b>0.03012</b>
35	0.05147
40	0.09975
45	0.1627

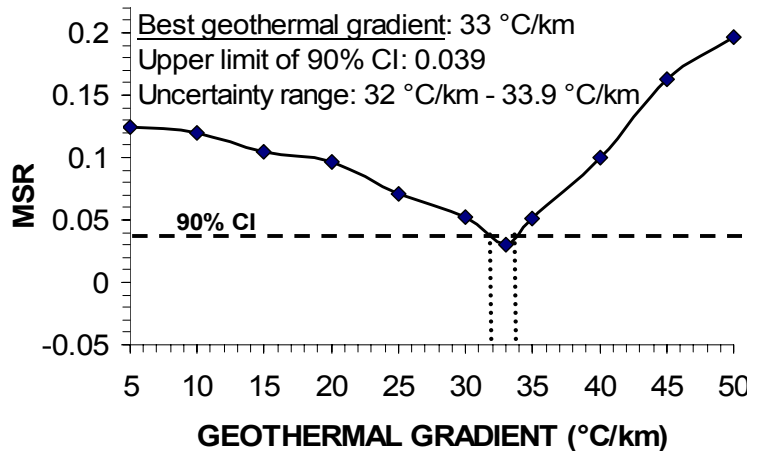
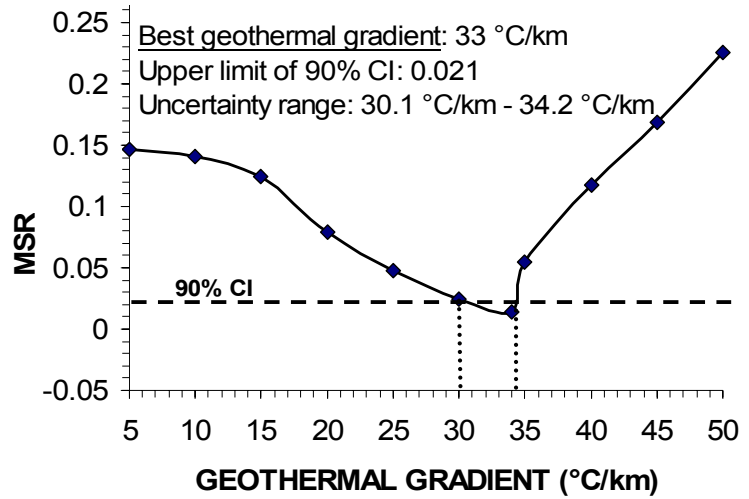


Figure C.1 cont'd.

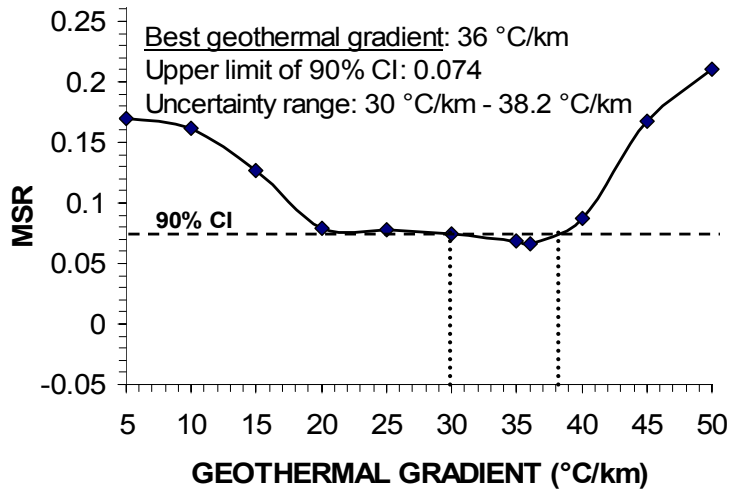
**Karahıdır-1**

TG (°C/km)	MSR
5	0.14678
10	0.14097
15	0.12472
20	0.07899
25	0.0478
30	0.02456
<b>33</b>	<b>0.01345</b>
35	0.05434
40	0.11778
45	0.16888



**Karakavak-1**

TG (°C/km)	MSR
5	0.1697
10	0.16123
15	0.12678
20	0.07934
25	0.07789
30	0.07433
35	0.06803
<b>36</b>	<b>0.06654</b>
40	0.08666
45	0.1671



**Karıştıran-1**

TG (°C/km)	MSR
5	0.02658
10	0.00166
15	0.00166
20	0.00166
25	0.00155
30	0.00126
<b>32</b>	<b>0.00061</b>
35	0.0007
40	0.00941
45	0.02125

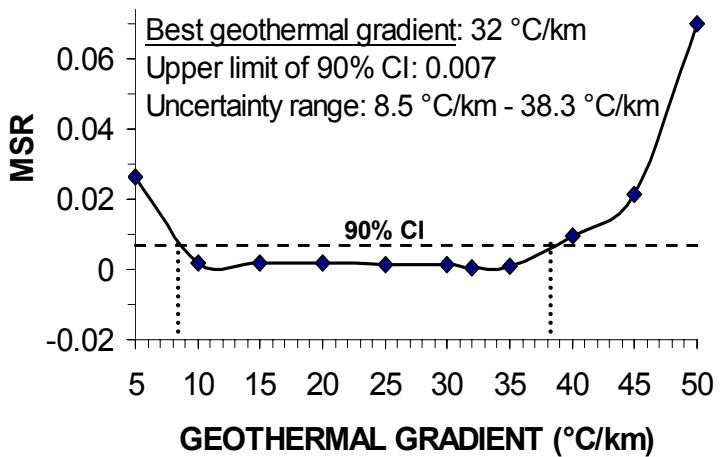
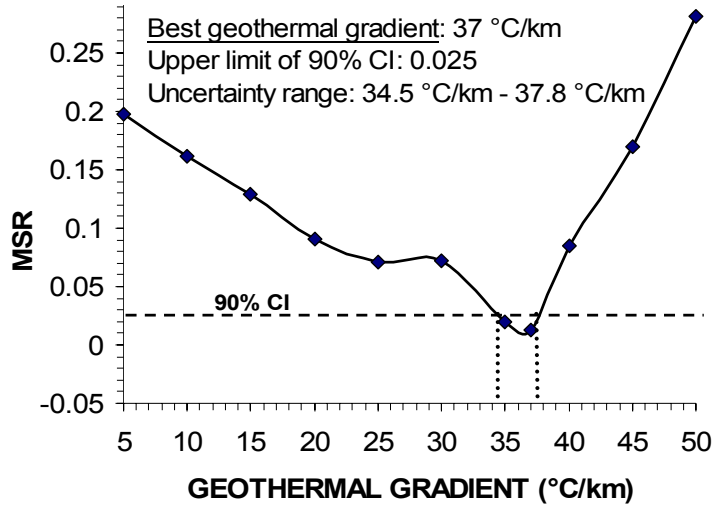


Figure C.1 cont'd.

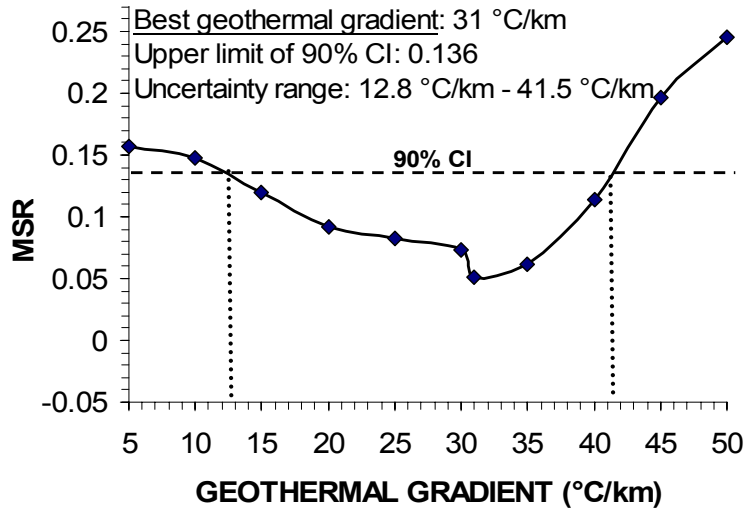
**Kavakdere-3**

TG (°C/km)	MSR
5	0.19788
10	0.16188
15	0.12926
20	0.09021
25	0.0712
30	0.07236
35	0.01997
<b>37</b>	<b>0.01275</b>
40	0.08498
45	0.16988



**Kaynarca-1**

TG (°C/km)	MSR
5	0.15688
10	0.14785
15	0.12001
20	0.09198
25	0.0822
30	0.07346
<b>31</b>	<b>0.05098</b>
35	0.06111
40	0.11433
45	0.19674



**Kepirtepe-1**

TG (°C/km)	MSR
5	0.00793
10	0.0077
15	0.00746
20	0.0073
25	0.00632
30	0.00334
<b>33</b>	<b>0.00063</b>
35	0.00065
40	0.00695
45	0.03952

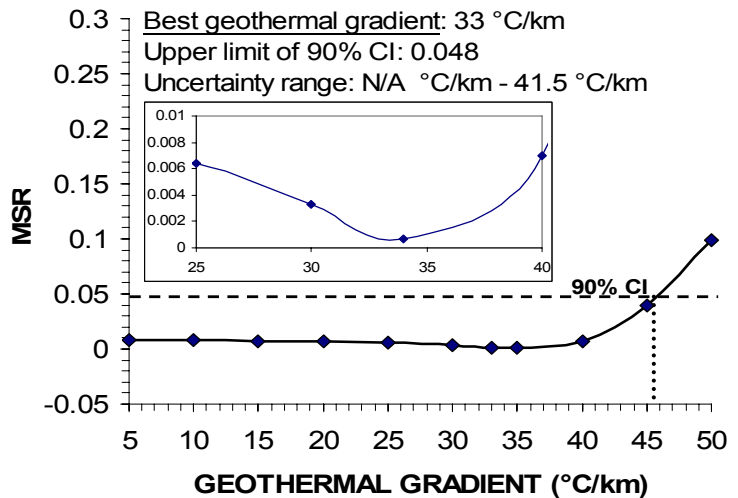
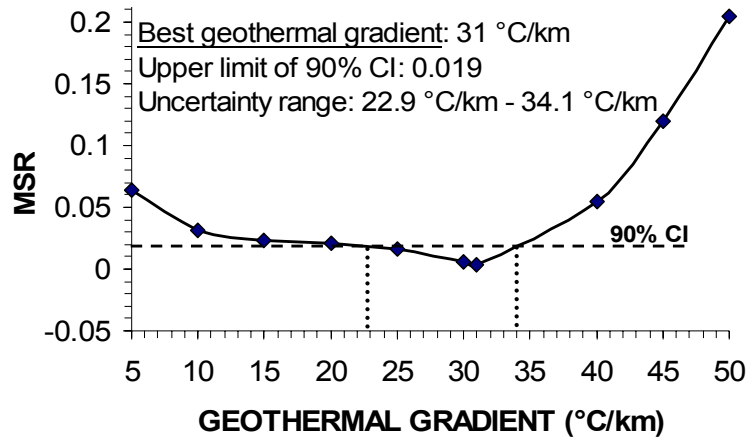


Figure C.1 cont'd.

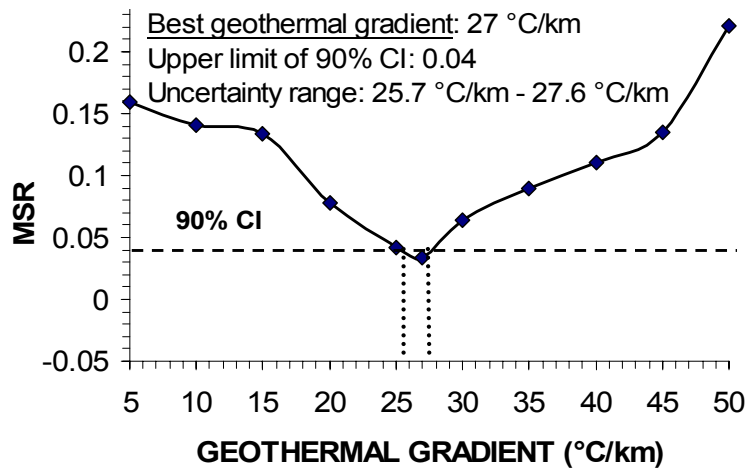
**Keşan-1**

TG (°C/km)	MSR
5	0.06442
10	0.03097
15	0.0234
20	0.02075
25	0.01654
30	0.00543
<b>31</b>	<b>0.00355</b>
40	0.05459
45	0.12007
50	0.20422



**Korucu-1**

TG (°C/km)	MSR
5	0.15876
10	0.14014
15	0.13357
20	0.07746
25	0.04166
<b>27</b>	<b>0.0334</b>
30	0.06345
35	0.09003
40	0.1105
45	0.13543



**Kuleli-3**

TG (°C/km)	MSR
5	0.14666
10	0.12547
15	0.10006
20	0.07630
25	0.06520
30	0.05765
<b>33</b>	<b>0.04194</b>
35	0.07748
40	0.18673
45	0.20670

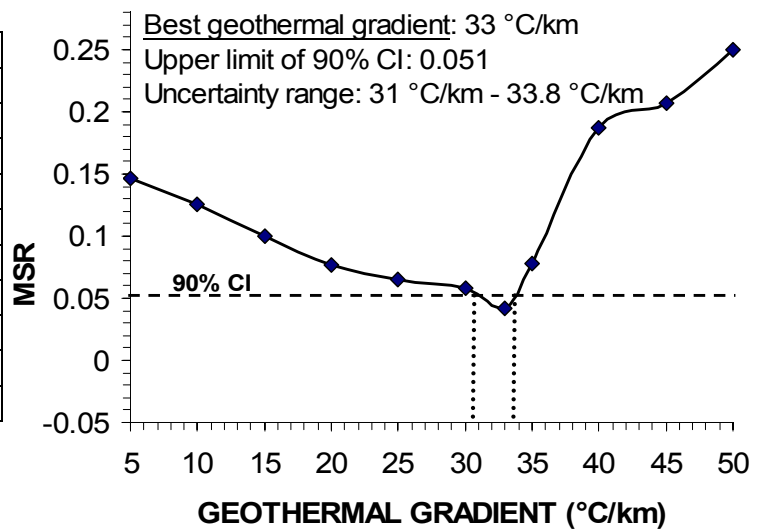
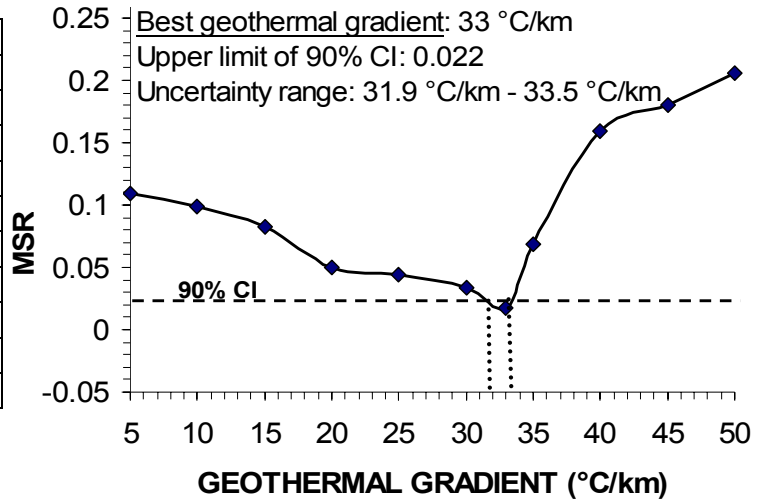


Figure C.1 cont'd.

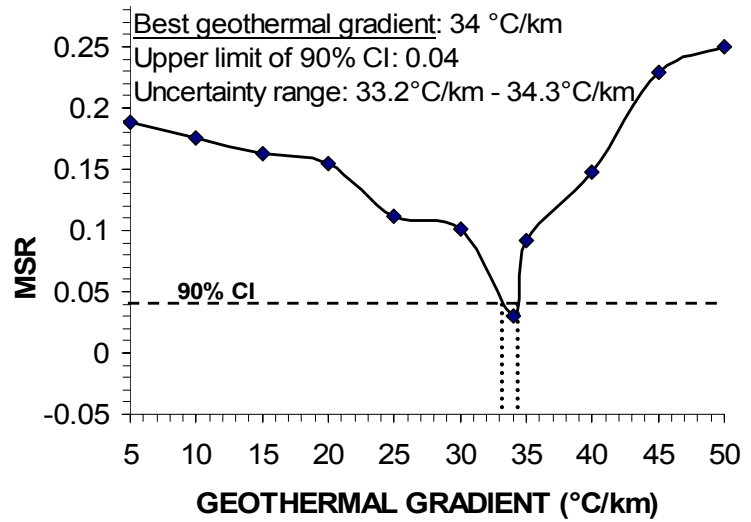
**Kumburgaz-1**

TG (°C/km)	MSR
5	0.10935
10	0.09916
15	0.08284
20	0.05006
25	0.04432
30	0.03345
<b>33</b>	<b>0.01779</b>
35	0.06905
40	0.15900
45	0.18000



**Kumrular-1**

TG (°C/km)	MSR
5	0.18876
10	0.17573
15	0.16307
20	0.15445
25	0.11199
30	0.10085
<b>34</b>	<b>0.03054</b>
35	0.09199
40	0.14755
45	0.22911



**Kurtdere-1**

TG (°C/km)	MSR
5	0.20211
10	0.10368
15	0.08569
20	0.03965
25	0.02754
30	0.01926
35	0.01889
<b>36</b>	<b>0.01022</b>
40	0.06580
45	0.13367
50	0.28431

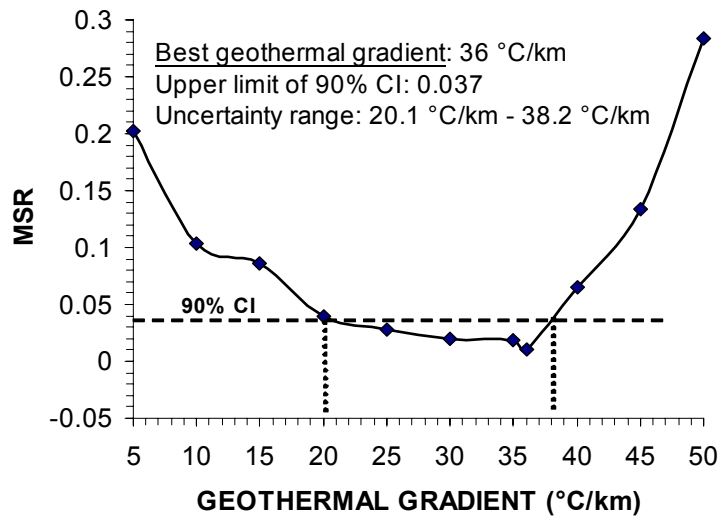
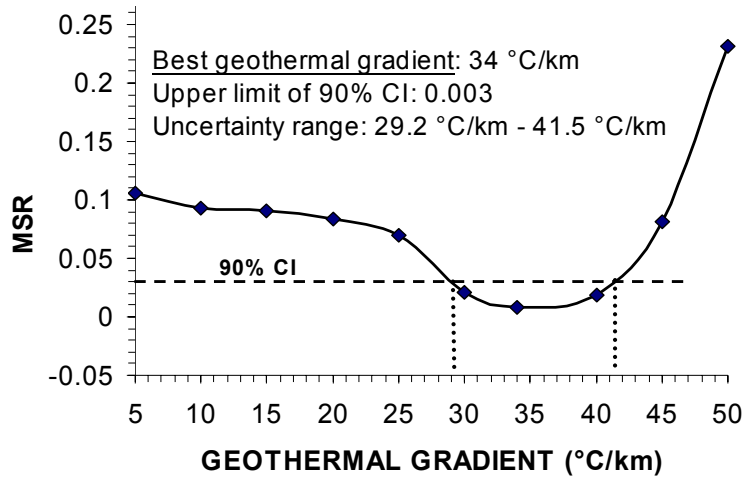


Figure C.1 cont'd.



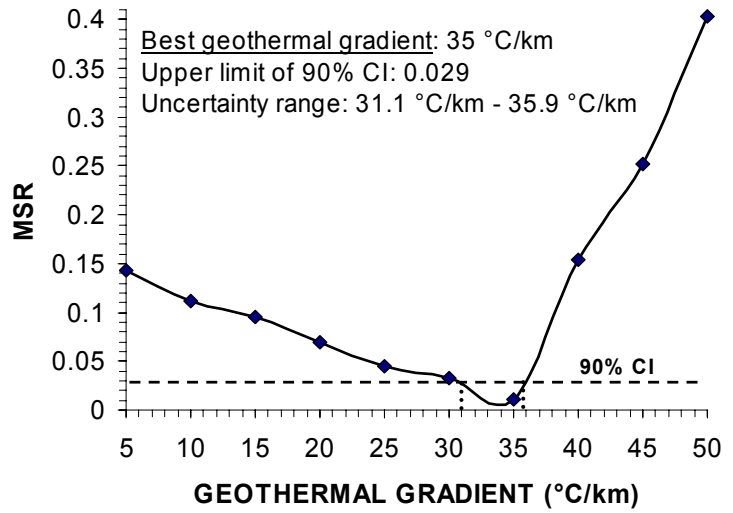
**K. Abalar-1**

TG (°C/km)	MSR
5	0.10524
10	0.092550
15	0.090220
20	0.083854
25	0.070040
30	0.021500
<b>34</b>	<b>0.008220</b>
40	0.01830
45	0.08100
50	0.23112



**K. Çerkezköy-1**

TG (°C/km)	MSR
5	0.14251
10	0.11234
15	0.09520
20	0.07010
25	0.04527
30	0.03230
<b>35</b>	<b>0.01087</b>
40	0.15330
45	0.25137
50	0.40377



**K. Marmara-3**

TG (°C/km)	MSR
5	0.13110
10	0.11252
15	0.10255
20	0.09010
25	0.07222
30	0.06452
35	0.05331
40	0.04197
<b>43</b>	<b>0.03223</b>
45	0.11910
50	0.29440

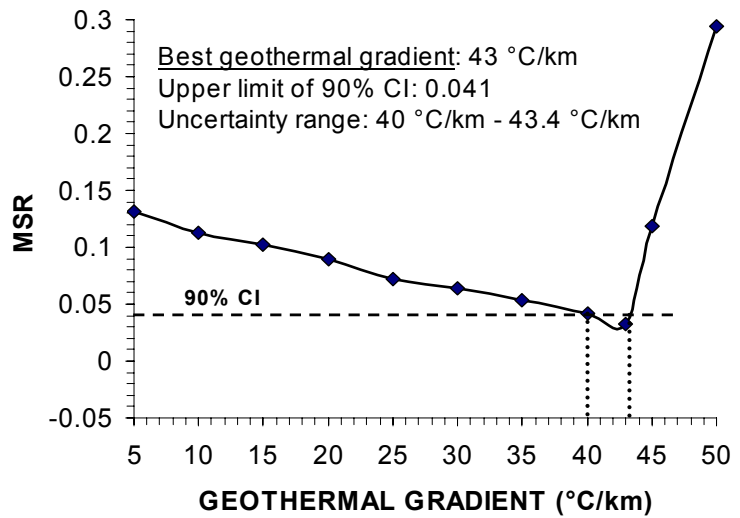
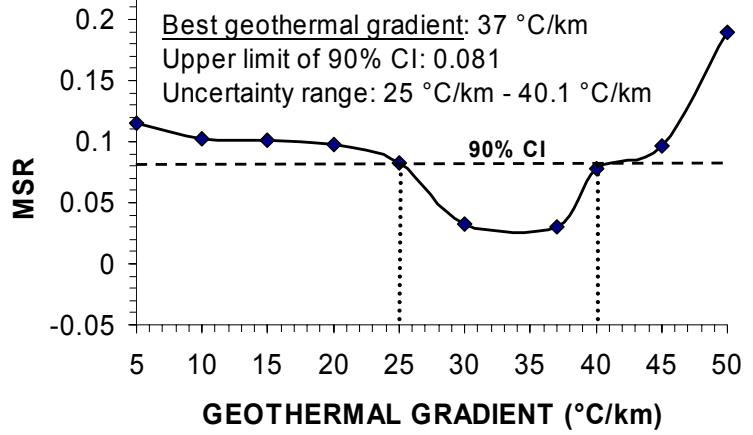


Figure C.1 cont'd.

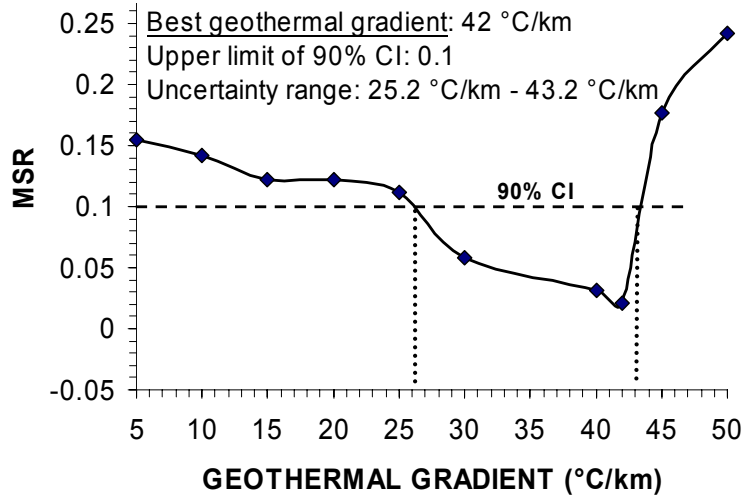
**K. Osmancık-1**

TG (°C/km)	MSR
5	0.11527
10	0.10211
15	0.10169
20	0.09752
25	0.08211
30	0.03221
<b>37</b>	<b>0.03010</b>
40	0.07777
45	0.09600
50	0.19000



**Meriç-2**

TG (°C/km)	MSR
5	0.15425
10	0.14221
15	0.12220
20	0.12201
25	0.11110
30	0.05842
40	0.03110
<b>42</b>	<b>0.02101</b>
45	0.17652
50	0.24228



**Mezardere-1**

TG (°C/km)	MSR
5	0.22552
10	0.14500
15	0.12204
20	0.10257
25	0.09001
<b>30</b>	<b>0.03857</b>
35	0.08324
40	0.11771
45	0.19387
50	0.27111

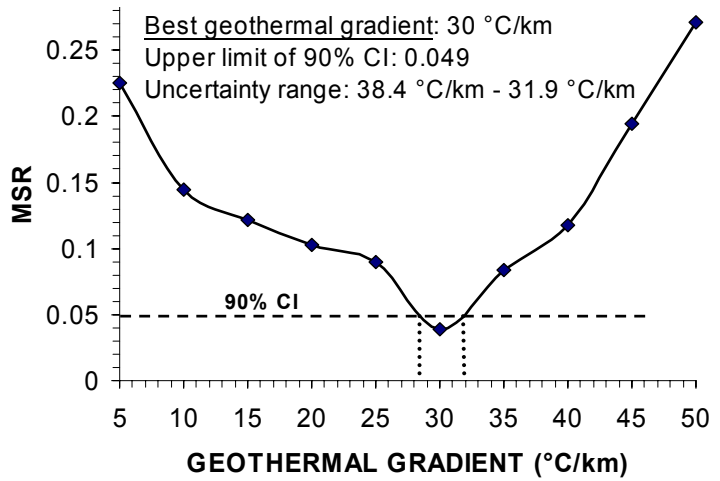
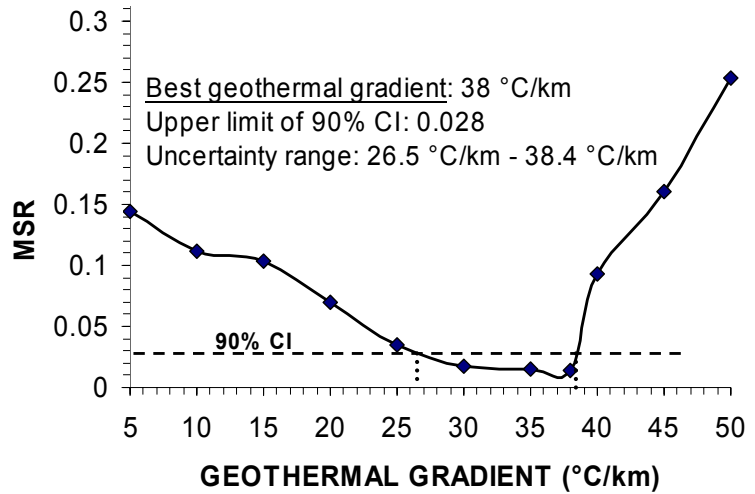


Figure C.1 cont'd.

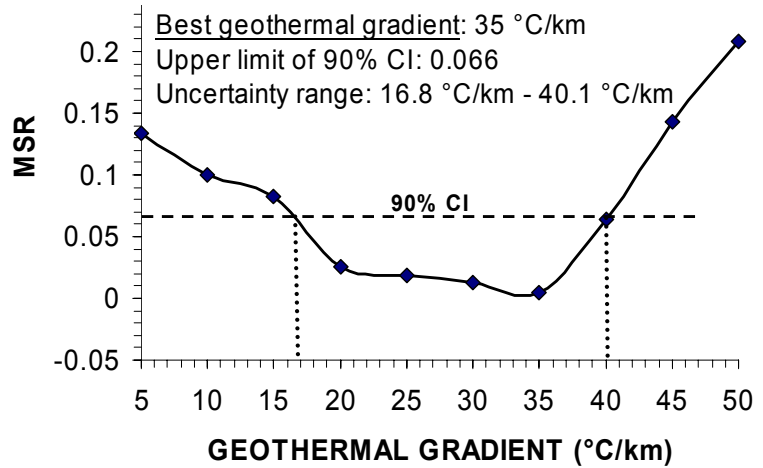
**Minnetler-1A**

TG (°C/km)	MSR
5	0.14420
10	0.11220
15	0.10324
20	0.07004
25	0.03455
30	0.01687
35	0.01527
<b>38</b>	<b>0.01410</b>
40	0.09250
45	0.16007
50	0.25321



**Mürefte-1**

TG (°C/km)	MSR
5	0.13422
10	0.10020
15	0.08311
20	0.02587
25	0.01847
30	0.01234
<b>35</b>	<b>0.00488</b>
40	0.06363
45	0.14311
50	0.20785



**Ortaköy-1**

TG (°C/km)	MSR
5	0.21352
10	0.21214
15	0.20855
20	0.19520
25	0.14304
<b>27</b>	<b>0.04744</b>
30	0.05520
35	0.07224
40	0.13934
45	0.22222
50	0.27886

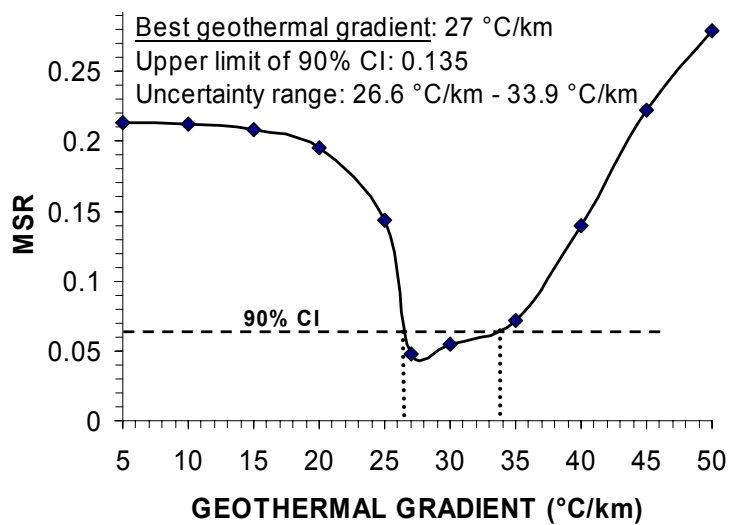
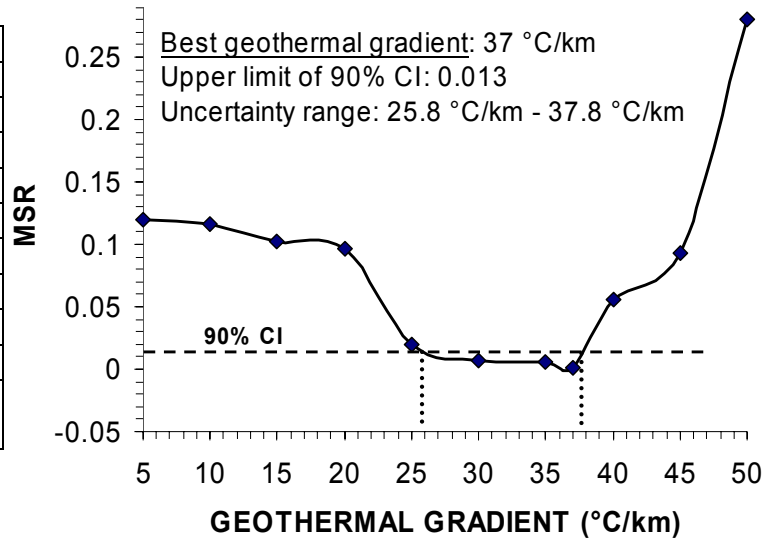


Figure C.1 cont'd.

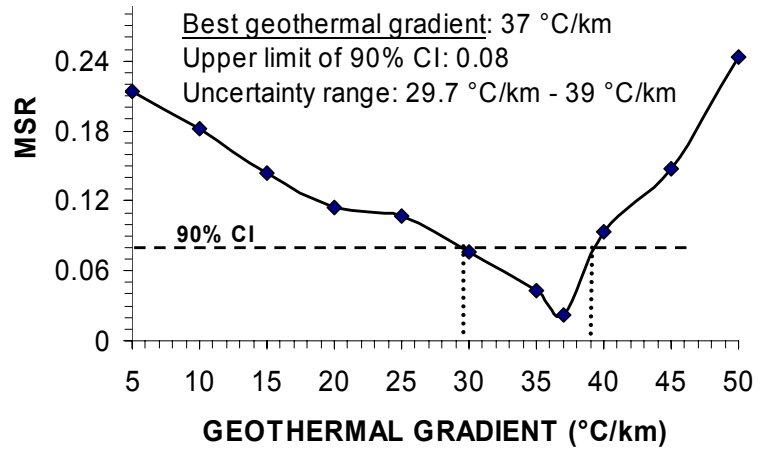
**Osmancık-2**

TG (°C/km)	MSR
5	0.11922
10	0.11578
15	0.10220
20	0.09687
25	0.01988
30	0.00702
35	0.00555
<b>37</b>	<b>0.00124</b>
40	0.05553
45	0.09276
50	0.28002



**Pehlivan köy-1**

TG (°C/km)	MSR
5	0.21381
10	0.18237
15	0.14334
20	0.11409
25	0.10674
30	0.07622
35	0.04347
<b>37</b>	<b>0.02240</b>
40	0.09323
45	0.14753
50	0.24337



**Şahankaya-1**

TG (°C/km)	MSR
5	0.09175
10	0.04500
15	0.02557
20	0.01642
25	0.01008
30	0.01334
<b>34</b>	<b>0.01521</b>
35	0.01012
40	0.01324
45	0.10557
50	0.29650

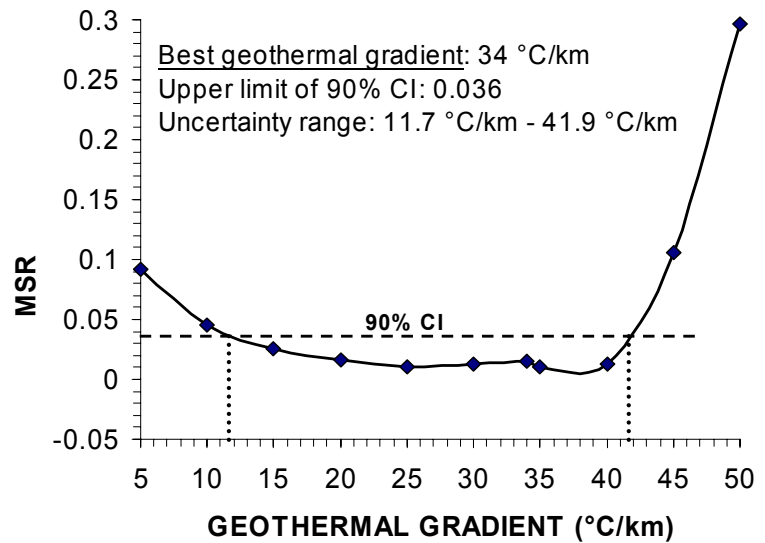
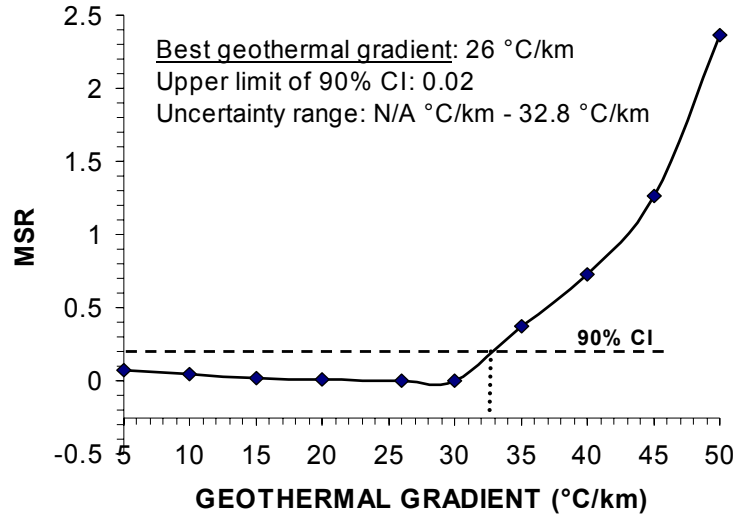


Figure C.1 cont'd.

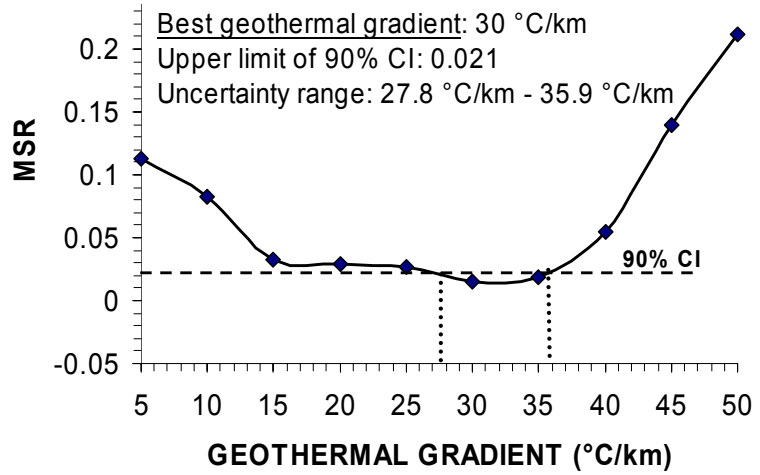
**Şarköy-1**

TG (°C/km)	MSR
5	0.07231
10	0.04582
15	0.01745
20	0.00855
<b>26</b>	<b>0.00235</b>
30	0.00017
35	0.37025
40	0.72416
45	1.26628
50	2.36787



**Sevindik-1**

TG (°C/km)	MSR
5	0.11257
10	0.08224
15	0.03247
20	0.02853
25	0.02650
<b>30</b>	<b>0.01552</b>
35	0.01857
40	0.05522
45	0.14003
50	0.21212



**Silivri-1**

TG (°C/km)	MSR
5	0.14585
10	0.12555
15	0.05223
20	0.03320
25	0.01920
<b>28</b>	<b>0.01352</b>
30	0.01935
35	0.02885
40	0.08331
45	0.19388
50	0.22369

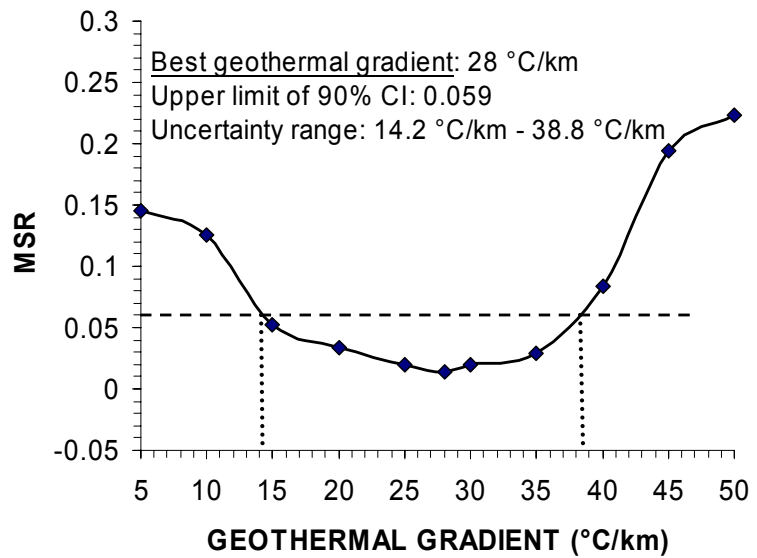
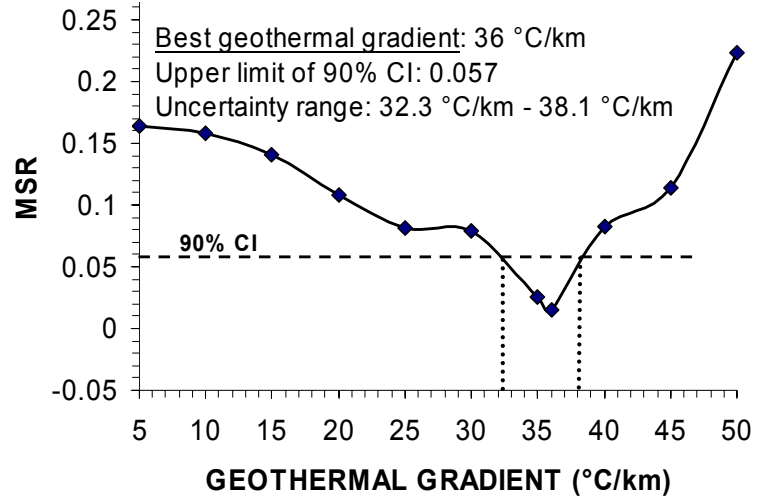


Figure C.1 cont'd.

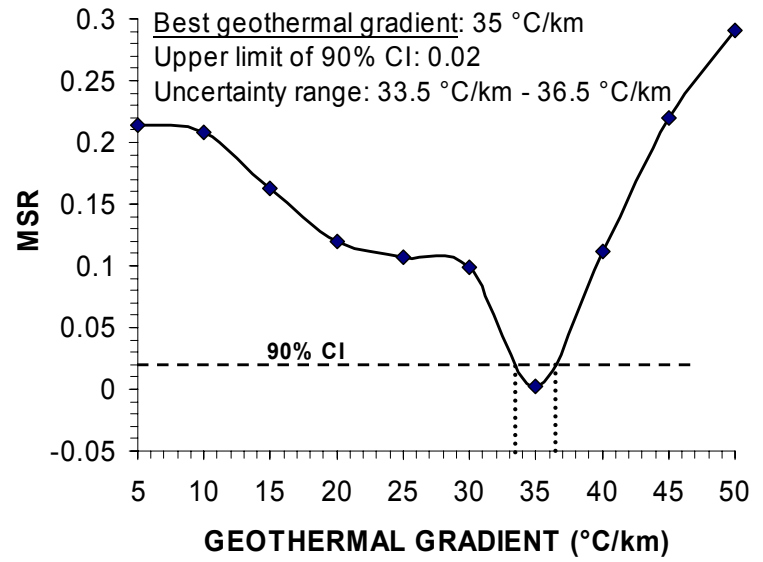
**Soğucak-1**

TG (°C/km)	MSR
5	0.16345
10	0.15854
15	0.14113
20	0.10852
25	0.08150
30	0.07894
35	0.02584
<b>36</b>	<b>0.01555</b>
40	0.08254
45	0.11444
50	0.22321



**Süloğlu-1**

TG (°C/km)	MSR
5	0.21363
10	0.20787
15	0.16334
20	0.11985
25	0.10654
30	0.09894
<b>35</b>	<b>0.00228</b>
40	0.11214
45	0.21956
50	0.29057



**Sütlüce-1**

TG (°C/km)	MSR
5	0.13537
10	0.11621
15	0.09851
20	0.08334
25	0.03112
30	0.01773
<b>34</b>	<b>0.01530</b>
40	0.09014
45	0.16666
50	0.20707

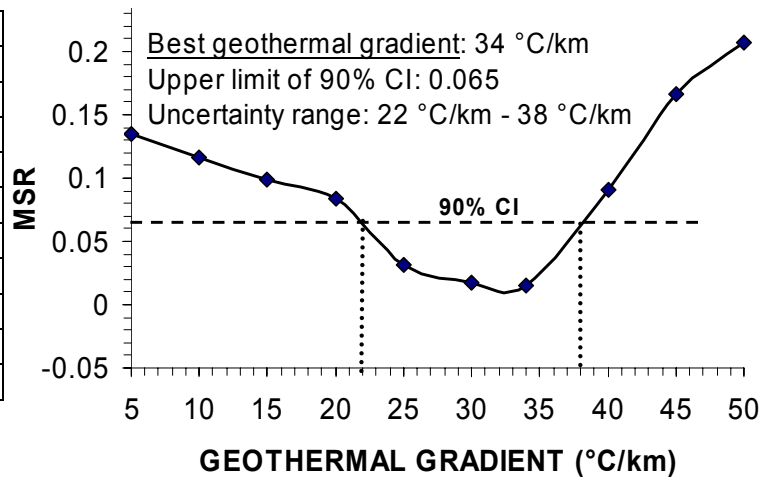
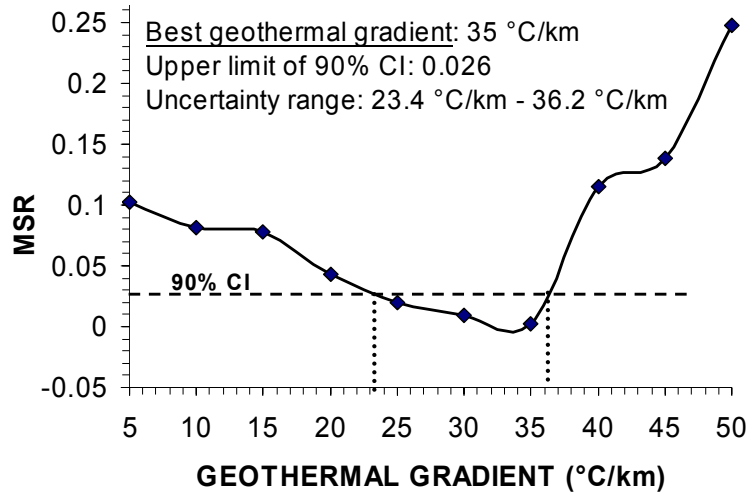


Figure C.1 cont'd.

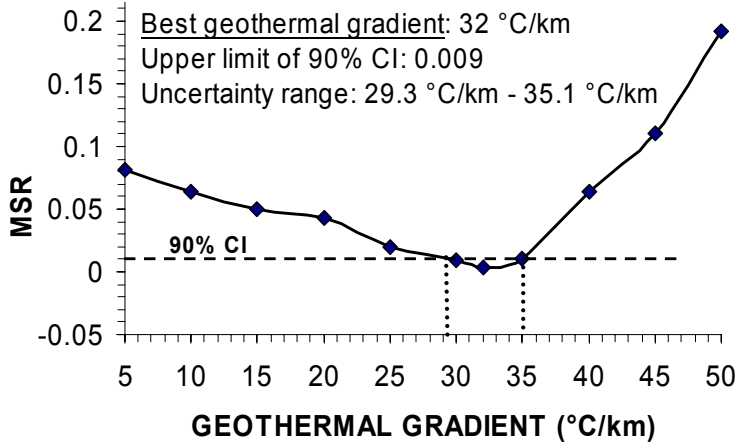
**Tatarköy-1**

TG (°C/km)	MSR
5	0.10202
10	0.08101
15	0.07805
20	0.04348
25	0.01999
30	0.00895
<b>35</b>	<b>0.00251</b>
40	0.11556
45	0.13854
50	0.24784



**Terzili-2**

TG (°C/km)	MSR
5	0.08120
10	0.06440
15	0.05005
20	0.04309
25	0.01987
30	0.00922
<b>32</b>	<b>0.00354</b>
35	0.01027
40	0.06367
45	0.11021
50	0.19208



**Turgutbey-1**

TG (°C/km)	MSR
5	0.14787
10	0.11441
15	0.10331
20	0.05590
25	0.02054
30	0.01859
<b>34</b>	<b>0.00254</b>
35	0.00312
40	0.01224
45	0.05557
50	0.22012

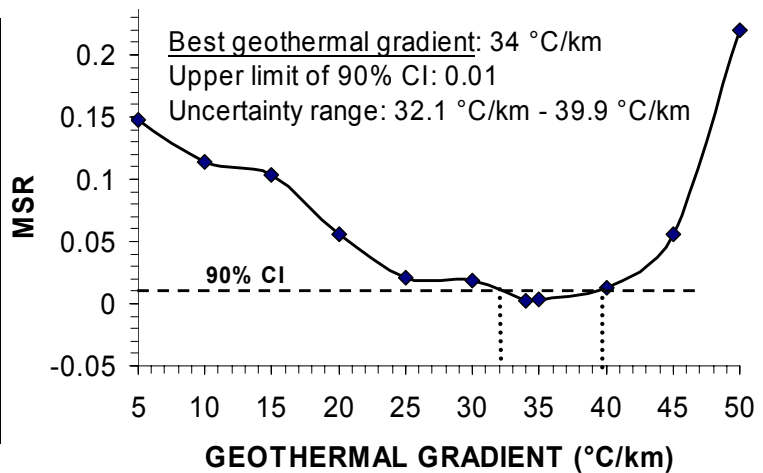
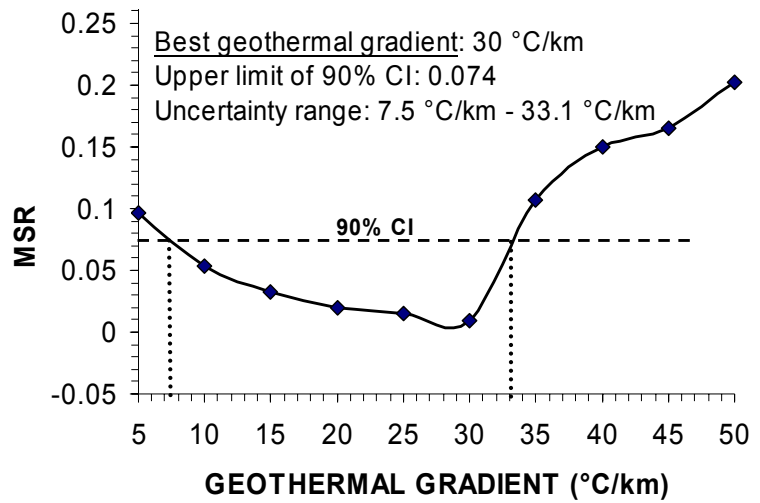


Figure C.1 cont'd.

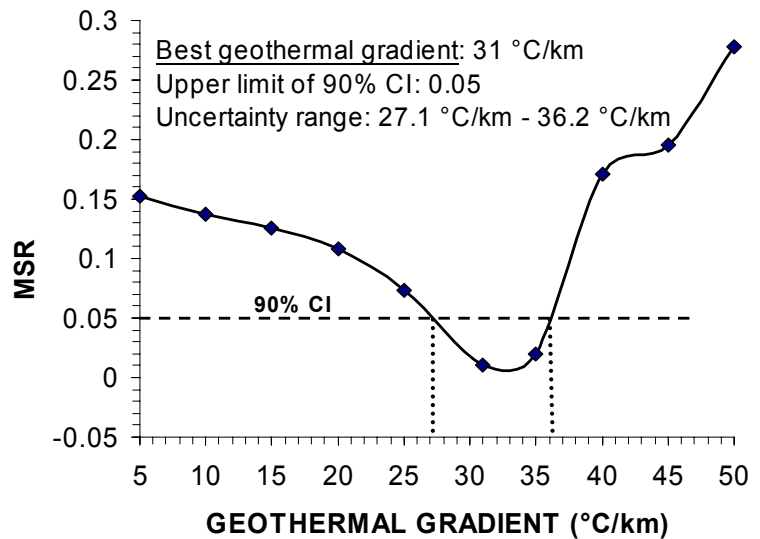
**Üçtepeler-1**

TG (°C/km)	MSR
5	0.09631
10	0.05346
15	0.03217
20	0.02012
25	0.01511
<b>30</b>	<b>0.00889</b>
35	0.10697
40	0.15004
45	0.16547
50	0.20226



**Umur-1**

TG (°C/km)	MSR
5	0.15254
10	0.13751
15	0.1255
20	0.10774
25	0.07304
<b>31</b>	<b>0.01007</b>
35	0.01931
40	0.17087
45	0.19547
50	0.27773



**Umurca-1**

TG (°C/km)	MSR
5	0.15373
10	0.13111
15	0.12808
20	0.10397
25	0.07452
30	0.01364
<b>33</b>	<b>0.01254</b>
35	0.01805
40	0.07773
45	0.16348
50	0.25801

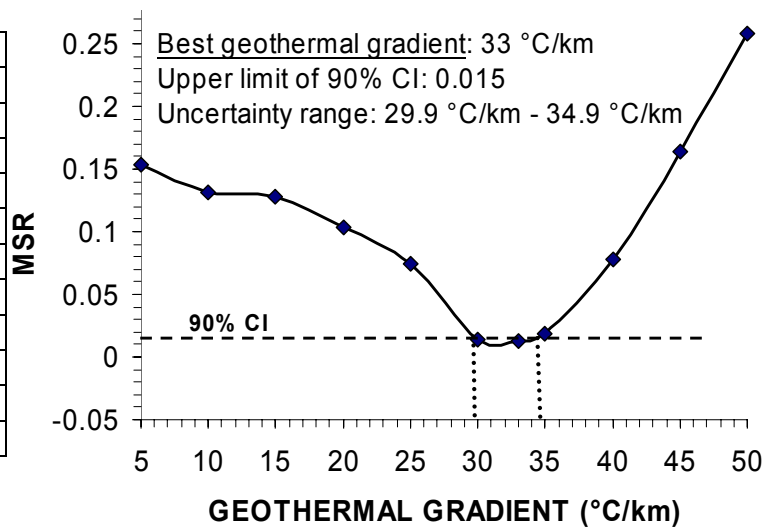
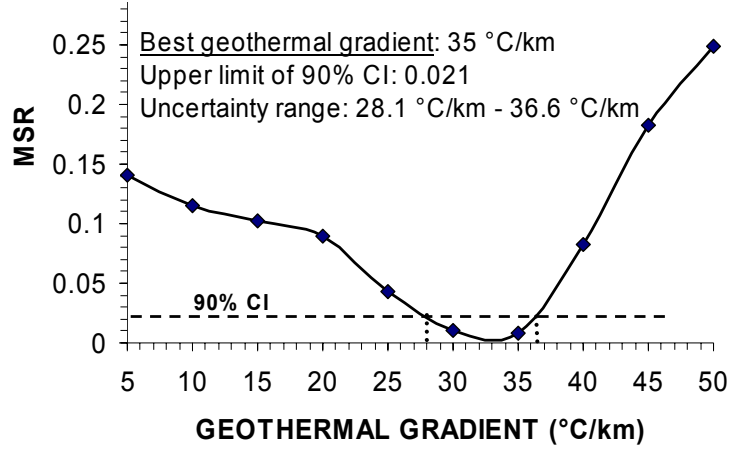


Figure C.1 cont'd.



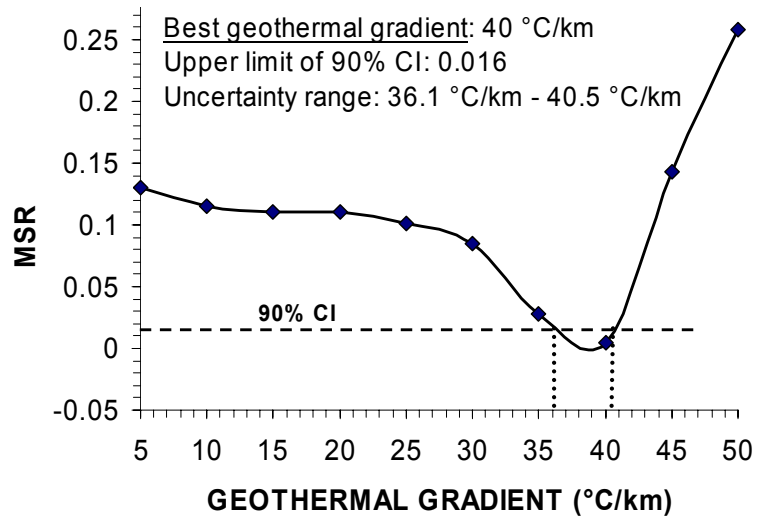
**Vakıflar -1**

TG (°C/km)	MSR
5	0.14114
10	0.11520
15	0.10207
20	0.08962
25	0.04258
<b>30</b>	<b>0.01025</b>
35	0.00864
40	0.08267
45	0.18228
50	0.24932



**Yancıklar-1**

TG (°C/km)	MSR
5	0.12999
10	0.11562
15	0.11050
20	0.11029
25	0.10112
30	0.08447
35	0.02785
<b>40</b>	<b>0.00424</b>
45	0.14263
50	0.25771



**Yaylaköy-1**

TG (°C/km)	MSR
5	0.10224
10	0.08384
15	0.04287
20	0.03601
25	0.03085
30	0.02557
35	0.01664
<b>36</b>	<b>0.01257</b>
40	0.07224
45	0.19859
50	0.28332

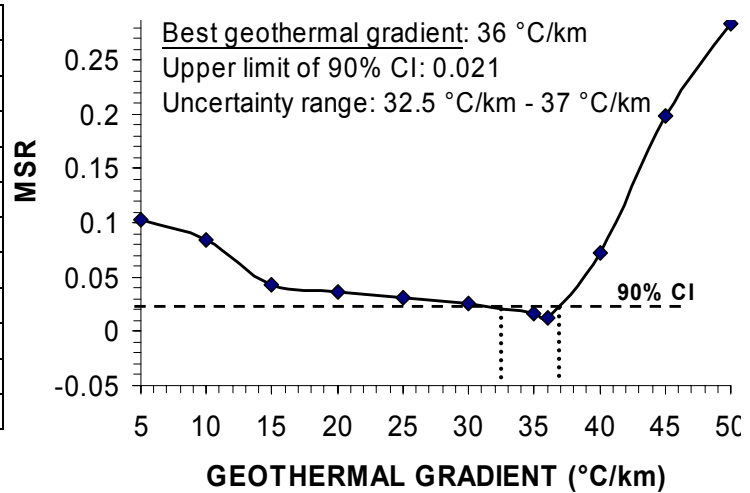


Figure C.1 cont'd.

**Yunus-1**

TG (°C/km)	MSR
5	0.11851
10	0.10943
15	0.10658
20	0.09558
25	0.07764
30	0.03557
35	0.01645
<b>40</b>	<b>0.01011</b>
45	0.19867
50	0.28252

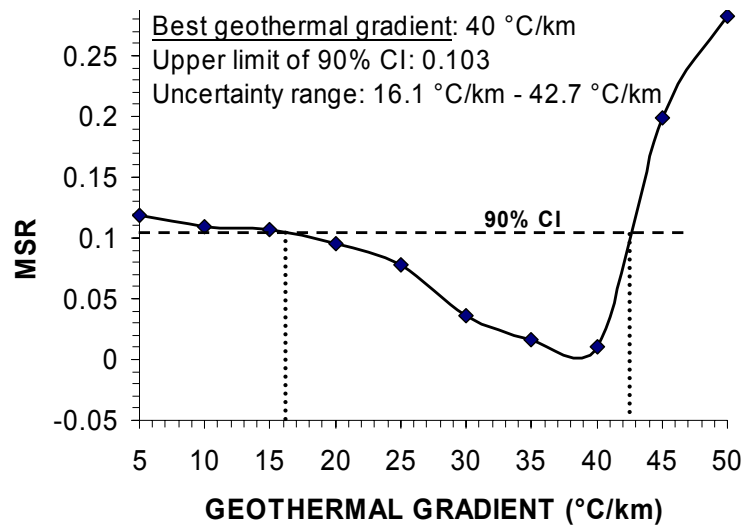


Figure C.1 cont'd.

## APPENDIX D

### PREDICTED AND CALCULATED MSR VALUES

Predicted paleo-thermal gradients from the MSR curves and calculated present day thermal gradients using BHT measurements and their comparison for each well location. The well locations where a variation more than 10% is observed between predicted and measured thermal gradient values are marked with bold characters.

Table D.1.

Well Name	Predicted TG (°C/km)	Calculated TG (°C/km)	TG <sub>p</sub> -TG <sub>c</sub> (°C/km)	Departure (%)	(TG <sub>p</sub> -TG <sub>c</sub> ) <sup>2</sup>
Abalar-1	32	29.0	-3.0	9.37	9.00
Akbaş-1	32	31.0	-1.0	3.12	1.00
Alipaşa-1	39	39.0	0.0	0.00	0.00
Ardıç-1	35	35.3	0.3	0.85	0.09
Arızbaba-1	31	32.4	1.4	4.51	1.96
Asilbeyli-1	36	35.5	-0.5	1.38	0.25
Babaeski-1	26	25.9	-0.1	0.38	0.01
Bahçedere-1	<b>38</b>	<b>42.6</b>	<b>4.6</b>	<b>12.10</b>	<b>21.16</b>
Ballı-1	35	35.1	0.1	0.28	0.01
Bayramdere-1	36	35.9	-0.1	0.27	0.01
Bayramlı-1	42	43.0	1.0	2.38	1.00
Çeltik-1	39	39.2	0.2	0.51	0.04
Ceylan-4	37	37.0	0.0	0.00	0.00
Çorlu-3A	35	34.8	-0.2	0.57	0.04
Çukuryurt-1	41	40.0	-1.0	2.43	1.00
Değirmencik-3	33	33.8	0.8	2.42	0.64
Değirmenköy-1	36	35.7	-0.3	0.83	0.09
Delen-1	32	32.1	0.1	0.31	0.01
Deveçatağı-9	31	31.0	0.0	0.00	0.00
Edirne-1	38	38.2	0.2	0.52	0.04
Ergene-1	30	30.0	0.0	0.00	0.00
Ertuğrul-1	36	35.9	-0.1	0.27	0.01
Gerdelli-1	38	39.8	1.8	4.73	3.24
Hamitabat-1	34	31.8	-2.2	6.47	4.84
Havsa-1	35	35.3	0.3	0.85	0.09
İnece-1	35	36.7	1.7	4.85	2.89
İpsala-1	26	26.5	0.5	1.92	0.25
Kandamış-1	31	31.0	0.0	0.00	0.00
Karaagac-1	35	35.5	0.5	1.42	0.25
Karacaoğlan-2	33	33.4	0.4	1.21	0.16
Karahıdır-1	34	35.4	1.4	4.11	1.96
Karakavak-1	36	36.4	0.4	1.11	0.16
Karıştıran-1	32	32.0	0.0	0.00	0.00

Table D.1 cont'd.

Kavakdere-3	37	38.5	1.5	4.05	2.25
Kaynarca-1	<b>31</b>	<b>24.6</b>	<b>-6.4</b>	<b>20.84</b>	<b>40.96</b>
Kepirtepe-1	<b>33</b>	<b>37.7</b>	<b>4.7</b>	<b>14.24</b>	<b>22.09</b>
Keşan-1	31	31.1	0.1	0.32	0.01
Korucu-1	27	27.3	0.3	1.11	0.09
Kuleli-3	33	32.0	-1.0	3.03	1.00
Kumburgaz-1	33	32.0	-1.0	3.03	1.00
Kumrular-1	34	33.2	-0.8	2.35	0.64
Kurtdere-1	36	36.0	0.0	0.00	0.00
K.Abalar-1	34	34.0	0.0	0.00	0.00
K.Çerkezköy-1	<b>35</b>	<b>39.4</b>	<b>4.4</b>	<b>12.57</b>	<b>19.36</b>
K. Marmara-3	43	42.0	-1.0	2.32	1.00
K. Osmancık-1	37	38.3	1.3	3.51	1.69
Meriç-2	42	43.0	1.0	2.38	1.00
Mezardere-1	30	30.2	0.2	0.66	0.04
Minnetler-1A	38	38.5	0.5	1.31	0.25
Mürefte-1	35	35.0	0.0	0.00	0.00
Ortaköy-1	27	27.9	0.9	3.33	0.81
Osmancık-2	37	36.0	-1.0	2.70	1.00
Pehlivan köy-1	<b>37</b>	<b>41.0</b>	<b>4.0</b>	<b>13.33</b>	<b>16.00</b>
Şahankaya-1	34	34.0	0.0	0.00	0.00
Şarkoy-1	26	26.3	0.3	0.88	0.09
Sevindik-1	30	30.5	0.5	1.92	0.25
Silivri-1	28	28.0	0.0	0.00	0.00
Soğucak-1	36	36.3	0.3	1.07	0.09
Süluoğlu-1	35	35.2	0.2	0.55	0.04
Sütlüce-3	34	33.3	-0.7	2.00	0.49
Tatarköy-1	35	35.9	0.9	2.64	0.81
Terzili-2	32	31.9	-0.1	0.28	0.01
Turgutbey-1	34	34.7	0.7	2.18	0.49
Üctepeler-1	30	30.4	0.4	1.17	0.16
Umur-1	31	31.9	0.9	3.00	0.81
Umurca-1	33	33.0	0.0	0.00	0.00
Vakıflar-1	30	29.2	-0.8	2.42	0.64
Yancıklar-1	<b>40</b>	<b>53.4</b>	<b>13.4</b>	<b>44.66</b>	<b>179.56</b>
Yaylaköy-1	36	36.7	0.7	1.79	0.49
Yunus-1	40	40.0	0.0	0.00	0.00
		$\sum_{i=1}^n (TG_p - TG_m)^2$			343.32
		$MSR = \frac{1}{n} \sum_{i=1}^n (TG_p - TG_m)^2$			4.9

## APENDIX E

### THERMAL CONDUCTIVITY MEASUREMENT WITH KEMTHERM QTM-D3

Conductivity measurement is performed using the probe method of Kemtherm QTM-D3 which measures thermal conductivity from a single sample or a surface (Kyoto Electronics Manufacturing Co. Ltd., 1987). Probe has an elastic base of with a known thermal conductivity which is accompanied by a hot-wire and a thermocouple embedded in the surface of the base unit. They establish a stable contact with the sample surface by means of spring loading system. Microprocessor of the thermal conductivity meter makes all of the calculations one minute after pressing down the probe on the sample. It has a thermal conductivity range of 0.023-11.63 W/mK and a temperature range of 10-200 °C. The measuring accuracy is  $\pm 5\%$  and the precision is  $\pm 3\%$ . Thermal conductivity ( $\lambda_p$ ) is calculated by the applied probe method using the following equation:

$$\lambda_p = K * \frac{I^2 * \ln(t_2 / t_1)}{V_2 - V_1} - H$$

where  $K$  and  $H$  are the constants of the probe, and they include a resistance of the heating wire, thermoelectric power of thermo couple and a thermal conductivity of the known heat insulated material.  $V_1$  and  $V_2$  are electromotive forces (voltage) at sampling times  $t_1$  and  $t_2$  (s) and  $I$  is the constant heating current (A).

## CURRICULUM VITAE

### PERSONAL INFORMATION

Surname, Name: Özkan, Huvaz  
Nationality: Turkish  
Date and Place of Birth: 26 March 1975 , İstanbul  
Marital Status: Married  
Phone: +90 312 286 91 00/2656  
email: huvaz@tpao.gov.tr

### EDUCATION

Degree	Institution	Year of Graduation
MS	Texas A&M University Geology&Geophysics	2000
BS	İstanbul Technical University Geological Engineering	1997
High School	Düzce Anatolian High School	1993

### WORK EXPERIENCE

Year	Place	Enrollment
2000- Present	Türkiye Petrolleri A.O.	Petroleum Systems

### FOREIGN LANGUAGES

Fluent English, Intermediate German

### SELECTED PUBLICATIONS

- Huvaz, O., Sarikaya, H., Nohut, O.M., in press, Nature of a regional dogleg pattern in maturity profiles of the Thrace Basin, Northwestern Turkey: A newly discovered unconformity or a thermal anomaly?, American Association of Petroleum Geologists Bulletin.
- Ediger, V.Ş., Huvaz, O., in press, Examining the sectoral energy use in Turkish economy (1980-2000) with the help of decomposition analysis, Energy Conversion and Management.
- Huvaz, O., Thomsen R.O., Noeth, S., 2005, A method for analyzing thermal gradient history using the statistical assessment of uncertainties in maturity models, Journal of Petroleum Geology, v.28, no. 2, p.3-14.
- Huvaz, O., 2003, An inverse method for determining various basin parameters using the basin modeling tools: thermal regime of the Thrace Basin: 14<sup>th</sup> International Petroleum and Natural Gas Congress and exhibition of Turkey, p. 150-157.
- Huvaz O., Vardar, M., 2001, Assessing the efficiency and applicability of contact grouting in the İstanbul Sub-way, Engineering Geology and the Environment Bulletin, v. 60, no. 1, p. 13-17.